CHARACTERIZATION OF THE SURFACE MORPHOLOGY OF *BACILLUS* SPORES BY ATOMIC FORCE MICROSCOPY

THESIS

Ruth A. Zolock, Captain, USMC

AFIT/GEE/ENV/02M-17

DEPARTMENT OF THE AIR FORCE
AIR UNIVERSITY

AIR FORCE INSTITUTE OF TECHNOLOGY

Wright-Patterson Air Force Base, Ohio

The views expressed in this thesis are those of the author and do not reflect the official policy or position of the United States Marine Corps, United States Air Force, Department of Defense, or the U. S. Government.

AFIT/GEE/ENV/02M-17

CHARACTERIZATION OF THE SURFACE MORPHOLOGY OF *BACILLUS* SPORES BY ATOMIC FORCE MICROSCOPY

THESIS

Presented to the Faculty

Department of Systems and Engineering Management

Graduate School of Engineering and Management

Air Force Institute of Technology

Air University

Air Education and Training Command

In Partial Fulfillment of the Requirements for the

Degree of Master of Science in Engineering and Environmental Management

Ruth A. Zolock, B.S.

Captain, USMC

March 2002

AFIT/GEE/ENV/02M-17

CHARACTERIZATION OF THE SURFACE MORPHOLOGY OF *BACILLUS* SPORES BY ATOMIC FORCE MICROSCOPY

Ruth A. Zolock, B.S.

Captain, USMC

Approved:

Dr. Charles A. Bleckmann (Chairman)	27 Feb 02 date
Dr. Larry W. Burggraf (Member)	27 Feb 02 date
Colonel Douglas C. Fuller, M.D. M.P.H. (Member)	28 Feb 02 date
Dr. Guangming Li (Member)	27 Feb 02 date

Acknowledgments

I would like to express my sincere appreciation to my faculty advisors, Dr. Bleckmann and Dr. Burggraf. Their guidance, support, and patience throughout the course of this thesis effort was prized more than they will ever know. I am profoundly grateful for the instruction on atomic force microscopy from Dr. Li, who was generous with his time and expertise. I am also very appreciative of the efforts and experience of Colonel Fuller.

I would also like to thank my sponsor, Dr. Eric Holwitt and the Air Force Research Laboratories Biomechanisms and Modeling Branch for support in this endeavor. I am indebted to the superior professionals from this lab who spent their valuable time teaching me and sharing their experiences with me. Special thanks goes to Dr. Johnathan Kiel, Dr. Jill Parker, Mr. John Alls, MSgt Homer Gifford, Mrs. Lucy Stribling, and Elizabeth Gutierrez.

This work would not have been possible without the efforts of Major LaPuma. Lacking his support and rapid development of a Laboratory Biosafety Protocol, the surface structure of *Bacillus* spores would still be a mystery.

I also owe thanks to the Department of Systems and Engineering Management and the Department of Physics here at the Air Force Institute of Technology. Without their financial and material support this work would never have been possible.

Finally, and most importantly, to my best friend and better half, thank you. Without your support and inspiration, this work could not have been done. This thesis is dedicated to you.

Table of Contents

Page

Page

Page

List of Figures

Page

Page

Page

Page

List of Tables

Page

Abstract

The surface morphology of *Bacillus* spores was resolved by atomic force microscopy in order to determine if characteristic surface features could be used to distinguish between closely related species. Four strains were studied: *Bacillus anthracis* Sterne strain, *Bacillus thuringiensis* var. *kurstaki*, *Bacillus cereus* strain 569, and *Bacillus globigii* var. *niger*. The spores were separated from a nutrient agar culture by filtering and centrifugation, suspended in deionized water, and immobilized on a graphite substrate by spin-coating. Atomic force microscopy imaging was done using intermittent contact mode, in air, under reduced humidity. Seven to ten spores of each species were fully characterized at three scan sizes: whole spore, $750nm^2$, and $500nm^2$. Images were captured with both height and phase information. Height images showed an irregular topography of subtle grooves, bumps, and steps across the curved upper surface of the spores. Phase images showed a superficial grain structure with different levels of phase contrast. Although some similarities were observed among spores of the same species, there was also significant variability within each species. The four species were not distinguished by observed surface morphology. Surface texture analysis (roughness, power spectral density, and bearing) did not establish quantitative differences between species based on surface topography. Overall, atomic force microscopy revealed a spore surface morphology rich with information. Additionally, it appears that further analysis and a larger sample size could provide sufficient information to allow identification and differentiation between *B. anthracis* and its close relatives based on spore surface morphology.

CHARACTERIZATION OF THE SURFACE MORPHOLOGY OF *BACILLUS* SPORES BY ATOMIC FORCE MICROSCOPY

I. Introduction

Overview

This work seeks to expand the fundamental knowledge of bacterial spores by characterizing the surface properties of *Bacillus* spores using atomic force microscopy. *Bacillus anthracis* Sterne strain, *Bacillus thuringiensis* var. *kurstaki*, *Bacillus cereus* strain 569, and *Bacillus globigii* var. *niger* were studied.

These four strains are significant for two reasons. First, each occupies a particular niche. *B. anthracis* is the causative agent of anthrax. *B. cereus* is of great concern in food and medical microbiology as a cause of food poisoning and infection. *B. thuringiensis* is a common bio-insecticide. *B. globigii* is employed as a research organism and as an anthrax simulant. Second, the three species *B. cereus*, *B. thuringiensis*, and *B. anthracis* are very closely related genetically. They are related so closely, that some believe they should be considered one species. A skilled microbiologist can identify these bacteria down to the level of a particular strain. However, the analysis requires significant time and sophisticated resources.

Until the fall of 2000, the use of anthrax as a weapon for bioterrorism was only a theoretical prospect. Now, with five Americans dead of inhalational anthrax, 12 sickened, and thousands exposed, the hypothetical has become reality. Moreover, the inherent difficulty of defending against bioterrorism has been made painfully clear.

The need for a rapid and accurate identification biological warfare agents has never been more apparent. For *Bacillus anthracis*, it is difficult to differentiate the pathogenic bacterium from its ubiquitous close relatives. It is more important now than ever to seek a novel and effective means to rapidly and accurately identify this deadly pathogen.

This thesis effort does not solve the problem of rapid and accurate detection. However, by expanding the fundamental knowledge of the structure of the *Bacillus* spore, more effective practical solutions may be found in the future.

Exploring the relationship between *Bacillus anthracis*, *Bacillus thuringiensis*, and *Bacillus cereus* opens a Pandora's box of taxonomic confusion and controversy. This research asks a fundamental, yet unanswered question. Is it possible to differentiate closely related microorganisms simply by looking at the surface morphology of their spores?

Purpose of Research

The purpose of this research is to characterize the surface morphology of four strains of *Bacillus* spores using atomic force microscopy: *B. anthracis* Sterne strain, *B. thuringiensis* var. *kurstaki*, *B. cereus* strain 569, and *B. globigii* var. *niger*.

Documented differences in the surface properties of the spores suggest that surface morphology could be a means for differentiating these four species. This morphology has

not been well characterized, and it was not clear, prior to this work, what the atomic force microscope would reveal. The outer surface of the bacterial spore consists of a thin membrane of protein, carbohydrate, and lipid called the exosporium. The function of this membrane remains a mystery and little is known of its structure and detailed biochemistry.

The atomic force microscope is a powerful and versatile tool, which under certain conditions can produce atomic scale images of surfaces in air or fluid. It is easily adapted to study the surface morphology of bacterial spores.

This thesis effort does not build directly on any prior research projects. As such, the experimental procedures applied to this work were developed through professional collaboration and thorough studies of the relevant literature. It is not intended to be an end in itself, but only a beginning.

Research Objectives

The three primary objectives of this research project were: 1) develop a simple yet effective methodology for characterizing bacterial spores with atomic force microscopy; 2) apply this protocol to characterize the morphology and exterior structure of spore surfaces of *B. anthracis* Sterne strain, *B. thuringiensis* var. *kurstaki*, *B. cereus* strain 569, and *B. globigii* var. *niger*; and 3) compare the surface characteristics of the spores in search of distinctive features that would differentiate the strains.

Although the application of atomic force microscopy (AFM) to biological systems is fairly well established, each successful use of the technology requires the development

of a system-specific protocol. The quality of images and data obtained from AFM directly reflects, and is significantly influenced by, the protocol used to generate the data.

Second, the chosen protocol must be applied uniformly in order to examine the spores of each of the four bacterial species that are the focus of this study. This goal assumes that the spores of each species possess a characteristic structure. This is a logical assumption. However, microorganisms are generally studied as colonies that consist of a vast population of individuals. In this work, the individual bacterial spore is the focus. Thus, drawing conclusions from a small sample of individuals from a vast population must be done in a limited and well-defined context.

Lastly, the Holy Grail sought by this thesis effort was the identification of one or more features that are characteristic of a particular species and capable of differentiating the spores of the four microorganisms examined in this work. It is reasonable that the structure and arrangement of the surface proteins on the outermost spore integument are distinctive.

Scope of Research

This research is limited in scope in several ways. First, only the spores of *B. anthracis* Sterne strain, *B. thuringiensis* var. *kurstaki*, *B. cereus* strain 569, and *B. globigii* var. *niger* will be examined. This decision was based on the availability of pure stocks of microorganisms and the importance of these organisms as simulants for biological warfare agents.

The bacterial spore is a dormant cell type that can withstand a barrage of environmental assaults that would destroy a vegetative cell (Driks, 1999:1). This

research focuses on the spore rather than the vegetative cell because the spore is the usual form of the bacteria in the environment (outside an insect or animal host).

Third, the application of AFM will focus on intermittent contact mode in a reduced humidity environment. Several alternative methods of imaging spores were explored, however, none produced more faithful, high-resolution images than the chosen configuration. Refinements in the techniques used here as well as applying completely different techniques have the potential to reveal vastly more information.

Finally, only a limited number of spores were characterized in detail for each species. This small sample size is far from ideal, but was necessitated by the lengthy data collection time required by experimental protocol.

II. Literature Review

Overview

This research effort looks for distinguishing characteristics on the surface of the spores of several closely related *Bacillus* species using atomic force microscopy. *Bacillus cereus*, *Bacillus thuringiensis*, and *Bacillus anthracis* are clearly distinct in their pathology, yet they are remarkably similar morphologically, genetically, and physiologically.

The knowledge of several scientific disciplines will be brought together to frame the research in this work in the context of the available literature. This chapter is divided into two parts. The first half reviews the microbiological aspects of this work – the bacteria, the characteristics and construction of their spores, and the principles of bacterial identification and categorization. The second half of the chapter discusses atomic force microscopy – principles behind the technology, issues associated with image interpretation, and applications of atomic force microscopy to biological research.

The Genus *Bacillus*

The bacterial genus *Bacillus* consists of rod-shaped, spore-forming aerobes and facultative anaerobes (Rosovitz and others, 1998:709). This genus is part of the larger bacterial family *Bacillaceae* which is comprised of several genera of bacteria that form heat-resistant endospores (Priest and others, 1988:847).

The genus *Bacillus* is historically important from both economic and experimental perspectives. Commercially, the genus is used worldwide for fermentation, as an insecticide, and for enzyme, antibiotic, and biochemical production (Harwood, 1989:1). The academic knowledge of the genetics and physiology of *Bacillus subtilis* is second only to that of *Escherichia coli* (Harwood, 1989:2).

The taxonomy and organization of this genus will be discussed in a later section. First, *B. cereus*, *B. thuringiensis*, *B. anthracis*, and *B. globigii* will be described.

Description of *Bacillus cereus*. *B. cereus* (from the Latin *cereus* meaning wax-like) is a ubiquitous microorganism and a causative agent of food poisoning and other human infections (Sneath, 1986:1108, 1131; Rosovitz and others, 1998:722). First isolated in 1887, *B. cereus* is a gram-positive, straight, rod-shaped bacteria 3 to 5 μm in length and 1 to 1.2 μm in width (Sneath, 1986:1108, 1131). It is motile and not susceptible to penicillin or γ-phage (which distinguishes it from *B. anthracis*) (Willett, 1992a:618).

Several strains of *B. cereus* are pathogens. Pathogenic *B. cereus* can produce a necrotizing enterotoxin, emetic toxin, phospholipases, proteases, and hemolysins during growth (Drobniewski, 1993:324, 332). *B. cereus* is medically significant and has been implicated in six types of clinical infections: "(i) local infections, particularly of burns, traumatic or postsurgical wounds, and the eye; (ii) bacteremia and septicemia; (iii) central nervous system infections, including meningitis, abscesses, and shunt-associated infections; (iv) respiratory infections; (v) endocarditis and pericarditis; and (vi) food poisoning" (Drobniewski, 1993:324).

Because *B. cereus* is common in gastrointestinal disease where it "is a significant cause of food-related disease", and has been a focus of study for the food industry (Drobniewski, 1993:331,333). *B. cereus* spores are ubiquitous and can survive heat treatment and disinfection (Mäntyen and Lindström, 1998:1634).

Physical maps of the genome of several *B. cereus* strains have been constructed (Carlson and others, 1992; Kolstø and others, 1990; Léonard and others, 1998:2163). Overall, the structure of the *B. cereus* genome is considered complex because of variations in the size of its chromosome and the presence of large plasmids (Leonard and others, 1998:2163). The presence of extrachromosomal DNA among certain *B. cereus* strains has been demonstrated although the function of the plasmids is not known (Helgason and others, 2000a:1620).

Description of *Bacillus thuringiensis*. *B. thuringiensis* (named for Thuringia, a German province) was first isolated in 1915 (Sneath, 1986:1131, 1135). This species is distinguished by its production of an insecticidal parasporal protein crystal (Sneath, 1986:1131, 1135). *B. thuringiensis* is generally not considered a human pathogen (Rosovitz and others, 1998:723).

The insecticidal action of *B. thuringiensis* comes from the production of a parasporal protein crystal formed during the sporulation process. Several different insecticidal proteins can be produced during sporulation (by different strains and by bacteria of the same strain) (Agaisse and Lereclus, 1995:6027). These δ-endotoxin protein molecules termed "Cry" protoxins accumulate to form a single large crystal that can account for 20% to 30% of the dry weight of the spore (Schnepf and others, 1998:777). Different toxins crystallize in different forms. For example, Cry1 forms

bipyramidal crystals, Cry2 forms cuboidal crystals, and Cry3A forms flat, rectangular crystals (Agaisse and Lereclus, 1995:6030, Schnepf and others, 1998:779). The toxin crystal is resistant to proteolytic enzymes (often produced by *Bacillus* species, yet is easily solubilized in the gut of insect larvae (Agaisse and Lereclus, 1995:6030).

This work uses *B. thuringiensis* var. *kurstaki* derived from a commercial insecticide. This strain produces up to three different types of Cry1 protoxons (Cry1A, Cry1B, and Cry1C) (Aronson, 1993:955). During sporulation, different amounts of each protoxin form a single bipyramidal inclusion (Aronson, 1993:955). The literature also indicates that this strain can produce Cry2 toxin (Aronson, 1993:954).

Insect larvae consume the spores, which, when digested, move to the midgut region. Here, enzymes in the highly alkaline environment dissolve the protein crystal releasing the Cry toxins (Sneath, 1986:1131, 1135). The toxin then binds to a midgut receptor, becomes inserted into the apical membrane (epithelium), and creates ion channels or pores (Schnepf and others, 1998:783). This disruption of the digestive tract causes the insect to stop eating and eventually starve to death.

The proteinaceous protoxin crystals possess varied toxicity and generally act in a specific manner for different insect species (Rosovitz and others, 1998: 723; Aronson, 1993:953). There is great variety (greater than 20 serotypes) within the *B. thuringiensis* species (Aronson, 1993:953). Over 50 proteinaceous protoxins have been "well-characterized" from *B. thuringiensis* strains. Further, novel strains of *B. thuringiensis* have been characterized that form parasporal crystals with no known insecticidal toxicity (Lopez-Meza and Ibarra, 1996:1306).

B. thuringiensis is widely used as a bioinsecticide against insects of the orders Lepidopteran (caterpillars), Diptera (mosquitos and blackflies), and Coleoptera (beetles) (Lopez-Meza and Ibarra, 1996:1306). The genes encoding the various toxins produced by *B. thuringiensis* species have also been introduced to a variety of other vectors including plants and epiphyte bacteria (Aronson, 1993:960).

Description of *Bacillus anthracis*. *B. anthracis* (of Greek origin, meaning coal or carbuncle) was first isolated by Robert Koch in 1877 and is the pathogenic cause of the disease anthrax (Willett, 1992a:615). *B. anthracis* is a gram-positive, straight, rod-shaped bacteria 3 to 5 μm in length and 1 to 1.2 μm in width (Willett, 1992a:616). The bacilli are non-motile and virulent strains are encapsulated during growth (Willett, 1992a:616). *B. anthracis* sporulates in culture, in soil, and in the remains of dead animals (but not in the blood or tissues of live animals) forming centrally located oval or ellipsoidal spores (Willett, 1992a:616).

B. anthracis pathogenicity depends on two factors causing virulence: a polypeptide capsule of poly-D-glutamic acid and a toxin. The capsule is necessary for disease because it interferes with phagocytosis (Willett, 1992a:617). The anthrax toxin "is a complex exotoxin consisting of three protein components: protective antigen, lethal factor, and edema factor" (Willett, 1992a:617). Individually, these three proteins exhibit no known toxic activity; however, when collectively present they act synergistically to produce the characteristic symptoms of anthrax (Willett, 1992a:617). The combination of protective antigen and edema factor produce the edema toxin (Iacono-Connors and others, 1990:366). Together, protective antigen and lethal factor combine to produce the lethal toxin (Iacono-Connors and others, 1990:366).

The two virulence factors of *B. anthracis* are located on two plasmids: pX01 encodes for the two binary exotoxins and pX02 encodes for the poly-D-glutamic acid capsule (Iacono-Connors and others, 1990:366). Both plasmids are considered large, pX01 is 60 MDa and pX02 is 110 MDa (Okinaka and others, 1999:6509).

Pasteur developed the first anthrax vaccine in 1881 by attenuating a living strain (with only the pX02 plasmid) by passing the bacilli through chickens (who have an elevated body temperature compared to humans) (Rosovitz and others, 1998:721). Currently, a living spore vaccine derived from the non-encapsulated Sterne strain is used for veterinary applications (Willett, 1992a:617). The human protective antigen-based vaccine consists of supernatant material from fermented cultures of another toxigenic but non-encapsulated strain adsorbed to aluminum hydroxide (Cohen and others, 2000:4549).

The number of strains of *B. anthracis* isolated globally is unknown. Studies of the variable-number tandem repeat loci have identified seven major clones split into two groups (Keim and others, 1999:217). Overall, there is low diversity among the clonal lineages, which "is consistent with a slowly evolving organism or one that recently derived from a common ancestor" (Smith and others, 2000:3780). Several studies have characterized strains based on phenotypic, biochemical, and genetic factors. A study of a French outbreak of anthrax in 1997 identified 11 strains (Patra and others, 1998:2412). A Chinese project establishing a reference strain collection distinguished 84 strains (Liang and Yu, 1999:200). A study of the 1979 Sverdlovsk anthrax outbreak, caused by the release of spores from a military microbiology facility, indicated the likelihood of greater than four different strains of *B. anthracis* were present in victim's tissues (Jackson and others, 1998:1229). A study in South Africa's Kruger National Park identified 98 isolates

and demonstrated a probable environmental association with specific genotypic groups (Smith and others, 2000:3780).

Description of *Bacillus globigii*. *B. globigii* was originally described by W. Migula in 1900 (in System Der Bakterien. V. 2, 1068 pp. Gustav Fiscer. Jena.). The origin of the name is unknown. In 1952, strains originally classified as *B. globigii* were reclassified as *B. licheniformis*, *B. circulans*, *B. pumilus*, and *B. subtilis* var. *niger* (Smith, 1952:70, 88, 84, 110). In 1973, the name *B. globigii* was labeled "meaningless" because it could refer to any of four species of *Bacillus* (Gordon and others, 1973:34). In 1989, strains of *B. subtilis* (DSM 675 and DSM 2277) which were synonymously named *B. globigii* var *niger* "red strain" and *B. globigii* were re-classified as *B. atrophaeus* (Nakamura, 1989).

B. globigii is considered harmless to humans (Regis, 1999:53). *B. globigii* has been used extensively as simulant material by American and many foreign biological warfare programs (Regis, 1999:73, 77, 92, 118, 197, and 204). For example, in 1950, clouds of *B. globigii* spores were released by navy minesweepers positioned outside the Golden Gate Bridge to study the impact on the citizens of San Francisco (Barnaby, 2000:89). This was one test of 239 open-air tests that were conducted by the army between 1949 and 1969 over U.S. cities (Barnaby, 2000:89).

Although *B. globigii* does not have officially recognized standing in taxonomy, it is not uncommon to see this species used experimentally or referred to in the literature (Weimer and others, 2001; Hathout and others, 1999; Beverly and others, 2000).

The *Bacillus* Spore

The bacterial spore is the dormant state for the *Bacillus* bacterium. It represents the culmination of vegetative growth. However, it also represents a beginning, with an embryonic function and a capacity for "rapid and sustained growth" (Sussman and Halvorson, 1966:2). Far from static, the spore retains "an alert sensory mechanism which is able to respond to specific germinants within minutes and triggers a series of sequentially degradative events known as germination" (Leuschner and Lillford, 2001:36). Thus, the spore is much more than the seemingly inert structure one sees upon initial inspection. Instead, it is a versatile, powerful structure fundamental to the life of the *Bacillus*.

The Structure of a *Bacillus* Spore. The spores of Bacillus consist of several layers of protective coatings surrounding a core of DNA and enzymes. Figure 1 illustrates the compartmentalized and layered structure of the spore.

The spores of *Bacillus* vary by species and can even exhibit differing properties among strains of the same species. Further, environmental factors such as temperature and available metabolites (amino acids, growth factors, etc.) have been shown to affect sporulation and the resulting spore structure (Ellar and Lundgren, 1966:752).

The external surface of spores of *B. anthacis*, *B. cereus*, and *B. thuringiensis* is the exosporium (Sussman and Halvorson, 1966:14). It is not known whether or not the spores of *B. globigii* have an exosporium. As the outermost external structure of the spore, the exosporium will be the focus this work. The next section discusses the external properties of the spore in detail.

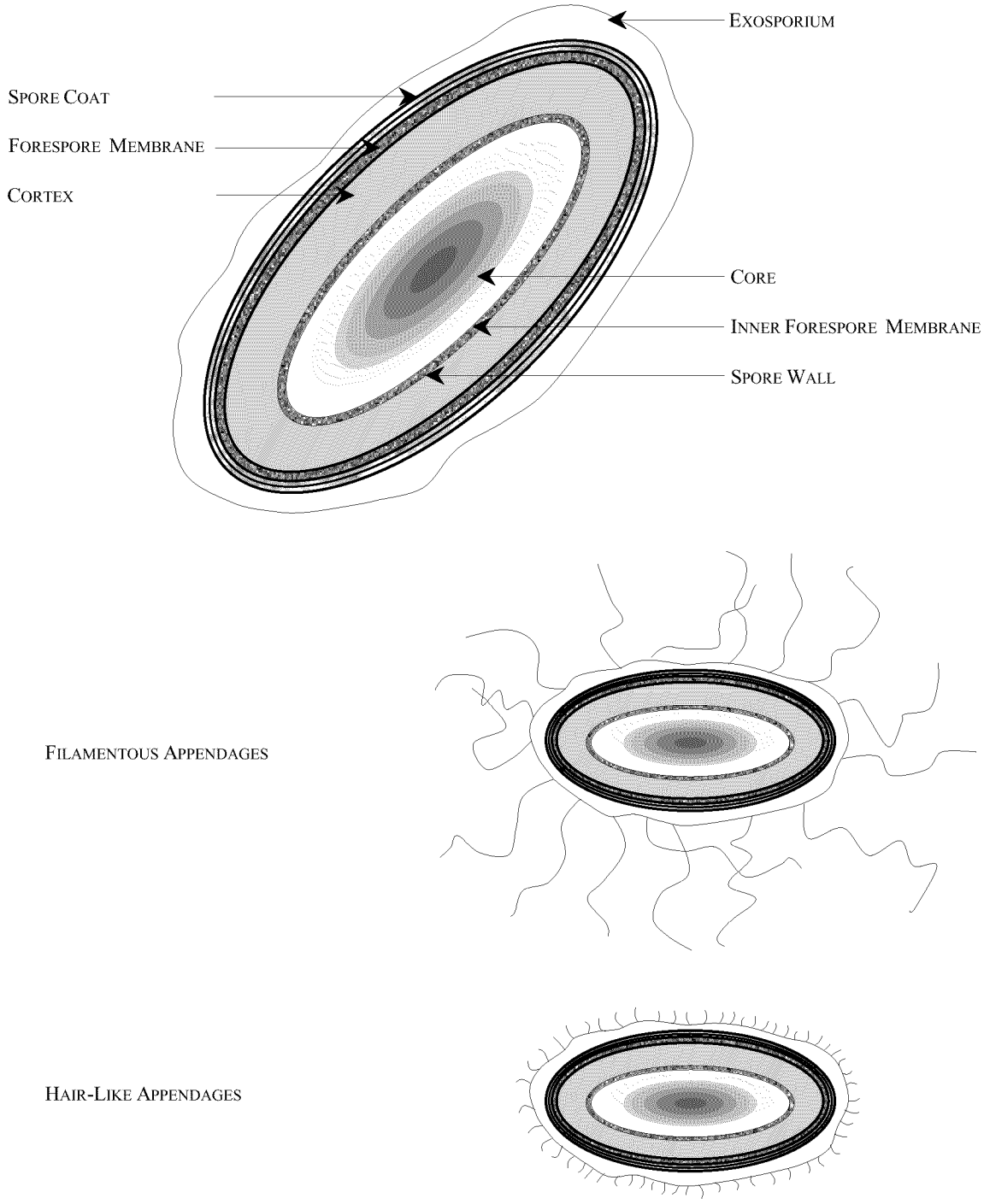

Figure 1. Structure of a *Bacillus* Spore

Beneath the exosporium is the multilayered proteinaceous spore coat (Driks and Setlow, 2000:193). In *B. subtilis* species, the spore coat is the external spore structure. The spore coat may have one or more layers. Each layer itself could have a laminated structure (Sussman and Halvorson, 1966:15-16). This multi-layered structure is been divided into an electron-opaque outer coat and a laminated inner spore coat (Warth and others, 1963:581). The outer spore coat can have a "uniform fine-grained appearance" or a layered structure (Warth and others, 1963:581,584). Although the inner coat is generally composed of a laminar structure, the layers may not be so well resolved in certain species (Warth and others, 1963:589). The construction of the spore coat varies with species, in terms of number of coats, number of layers, lamellae thickness, adhesion between layers, and pattern of the spore coat surface (grooves, ridges, or dimples) (Sussman and Halvorson, 1966:15-16; Warth and others, 1963:589). The spore coat appears to play an important role in resistance to mechanical disruption, chemicals, and enzymes (Driks and Setlow, 2000:193). The spore coats are composed primarily of protein (Popham and Setlow, 1993:2767).

Underlying the spore coat is the little understood forespore membrane (Driks and Setlow, 2000:193). Below the forespore membrane is the cortex, which is composed of peptidoglycan, thought to be essential for establishing relative dehydration in the central part of the spore (Driks and Setlow, 2000:193). The cortex consists of concentric layers of "fine fiberlike bundles" (Sussman and Halvorson, 1966:16). The cortex peptidoglycan has a low to moderate degree of cross-linking (Popham and Setlow, 1993:2767). The cortex is flexible and can shrink or swell in response to pH or ionic strength, and may play a role in attaining and maintaining the dehydration of the spore core, which results in

heat resistance and dormancy (Popham and Setlow, 1993:2767,2769; Popham and others, 1999:6205). It has been shown that if the cortex peptidoglycan is degraded, rapid rehydration of the protoplast results as well as a loss of spore heat resistance and dormancy (Popham and others, 1996a:6451).

Beneath the thick cortical peptidoglycan layer is a thin layer of structurally distinct peptidoglycan termed the spore wall (or germ cell wall) (Driks and Setlow, 2000:193). The spore wall will become the initial vegetative cell wall upon germination (Sussman and Halvorson, 1966:17) and (Popham and others, 1996b:15405). The thin inner forespore membrane is the final barrier to the core of the spore.

The spore core (or protoplasm) is significantly dehydrated and contains the nucleoid, enzymes, and ribosomes (Driks and Setlow, 2000:193). Although it does vary with species, the protoplast volume has been estimated to be 42% of total spore volume for *B. cereus* (Marshall and Murrell, 1970:124). The nucleoid has a "doughnut-like structure" with a group of small, α/β type acid-soluble proteins bound to its surface which appear to be important in protecting the DNA from heat and UV radiation (Ragkouski and others, 2000:5556).

Overall, the structure of the spore is unique and complex. Spores form slowly (6-10 hours) and can accumulate metabolic byproducts from the culture media (Murrell, 1969:216). This complicates analysis. Because environmental conditions affect the chemical composition of the spore, the structure of the spore should not be considered as absolutely fixed. The spore forms as a result of environmental conditions and reflects these conditions in its structure.

Sporulation. *Bacillus* bacteria form spores as a final response to depletion of a readily metabolized carbon or nitrogen source (Setlow and Johnson, 2001:34). Bacterial cells may initially attempt to overcome a nutrient deficit by mobilizing chemotaxis systems (synthesis of flagella, increased mobility, production of intracellular and extracellular enzymes) (Doi, 1989:202). In addition to nutrient deprivation, the initiation of sporulation also requires high bacterial cell density and ability to synthesize DNA. (Marahiel and Zuber, 1999:588).

Bacillus subtilis has been used as a model organism for studying bacterial sporulation. The information presented here primarily reflects knowledge of this species. However, the fundamental mechanisms involved in sporulation appear consistent and sequences of sporulation specific genes appear to be conserved between *B. subtilis* and not only other *Bacillus* species, but other gram-positive sporeformers as well (Setlow and Johnson, 2001:34).

The morphological events that occur during sporulation are used to divide the process into eight stages (0 through VII). From initiation to complete sporulation, the process may take as little as eight hours (Setlow and Johnson, 2001:35). The *Bacillus* spore is termed an endospore because it forms within a mother cell (Setlow and Johnson, 2001:33). The sporulation process is outlined in Figure 2 – from information in (Driks and Setlow, 2000:191-210; Marahiel and Zuber, 1999:597; Setlow and Johnson, 2001:35).

Some references do not consider Stage I to be a distinct stage of sporulation – the formation of axial filaments may not be specific to sporulation (Doi, 1989:172; Sporulation, 1999:586). Stage I is described here for information only.

STAGE 0		SPORULATION INITIATED. CHROMOSOME REPLICATION RESULTS IN TWO IDENTICAL NUCLEOIDS.
STAGE I	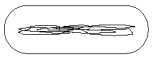	TWO NUCLEOIDS FORM AN AXIAL FILAMENT
STAGE II		A DOUBLE MEMBRANE SEPTUM FORMS WHICH DIVIDES THE CELL INTO A MOTHER CELL AND A FORESPORE. THE FORESPORE NUCLEOID CONDENSES.
STAGE III		THE MOTHER CELL ENGULFS THE FORESPORE. THE CELL IS COMMITTED TO SPORULATION.
STAGE IV		THE SPORE CORTEX FORMS WHEN PEPDIDOGLYCAN IS DEPOSITED BETWEEN THE TWO MEMBRANES.
STAGE V		AN INNER SPORE COAT PROTEIN IS DEPOSITED ON THE SURFACE OF THE OUTER FORESPORE MEMBRANE.
STAGE VI		THE OUTER SPORE COAT IS DEPOSITED ON THE SURFACE OF THE INNER SPORE COAT. THE SPORE BECOMES INCREASINGLY RESISTANT TO CHEMICALS AND HEAT. THE SPORE MATURES.
STAGE VII		THE MOTHER CELL PRODUCES AUTOLYSINS AND THE MATURE SPORE IS RELEASED.

Figure 2. Stages of Sporulaton

In stage 0 of sporulation, growing bacterial cells undergo a complete chromosome replication (Setlow and Johnson, 2001:36). The two nucleoids form into an axial filament in stage I (Setlow and Johnson, 2001:36). The process of sporulation begins when a double-membrane septum forms asymmetrically dividing the cell into a larger mother cell and a smaller forespore (Setlow and Johnson, 2001:36; Driks and Setlow, 2000:194; Rosovitz and others, 1998:717-718). The septum forms before the chromosomes are completely separated and "closes around one of the pair of replicating chromosomes, pinching it into a larger and smaller lobe" (Bath and others, 2000:995). "The larger chromosome lobe is then transported from the mother cell into the prespore, presumably through a small pore in the septum" (Bath and others, 2000:995). The

forespore will ultimately become the mature endospore and the mother cell will ultimately lyse releasing the mature endospore (Rosovitz and others, 1998:717).

In stage III, the mother cell "grows around and eventually engulfs the forespore" (Setlow and Johnson, 2001:36). The inner and outer forespore membranes now surround the forespore (Setlow and Johnson, 2001:36). These two membranes have opposite polarities (Setlow and Johnson, 2001:36).

The spore cortex forms between the inner and outer forespore membranes in stage IV (Setlow and Johnson, 2001:36). The cortex is a large, peptidoglycan structure (Setlow and Johnson, 2001:36). Also, the spore's germ cell wall forms between the cortex and the inner forespore membrane. The germ cell wall "appears to have the same structure as cell wall peptidoglycan" (Setlow and Johnson, 2001:36). During this stage the forespore synthesizes glucose dehydrogenase and small, acid-soluble proteins (SASP) (Setlow and Johnson, 2001:36). The forespore now has full resistance to ultra violet light and partial chemical resistance (Setlow and Johnson, 2001:36). The pH of the forespore falls slightly and dehydration begins (Setlow and Johnson, 2001:36).

In stage V several "proteinaceous coat layers" (the inner spore coat) form outside of the outer forespore membrane (Setlow and Johnson, 2001:36). The number and type of these layers vary within *Bacillus* species ranging from the simple to the highly complex (Setlow and Johnson, 2001:37). The forespore begins to acquire γ-radiation resistance and continues to develop chemical resistance (Setlow and Johnson, 2001:37). The forespore also continues to dehydrate (Setlow and Johnson, 2001:37).

By stage VI, the spore central region has accumulated dipicolinic acid (pyridine-2,6-dicarboxylic acid or DPA) synthesized by the mother cell (Setlow and Johnson,

2001:33,37). Also, large amounts of divalent cations (Ca^{+2}, Mg^{+2}, Mn^{+2}) are absorbed in parallel with the DPA (Setlow and Johnson, 2001:37). Finally, the spores central region (or core) undergoes the final process of dehydration (Setlow and Johnson, 2001:37). Permeability changes within the spore's membranes result in poor staining by common bacteriological stains (Setlow and Johnson, 2001:37). The forespore acquires additional γ-radiation and chemical resistance (Setlow and Johnson, 2001:37). The outer spore coat is deposited on the surface of the inner spore coat (Doi, 1989:172). The spore becomes metabolically dormant (Setlow and Johnson, 2001:37).

The final stage of sporulation involves the production of one or more autolysins in the mother cell resulting "in its lysis and release of the spore" (Setlow and Johnson, 2001:37). Stage VII concludes the sporulation process.

The control of gene expression during sporulation is "striking not only in its complexity but also in the redundancy of its control mechanisms" (Setlow and Johnson, 2001:37-38). A "defined pattern" of gene expression controls sporulation, which is "ordered not only temporally but also spatially, as some genes are expressed only in the mother cell or forespore (Setlow and Johnson, 2001:33). Overall, a cascade of transcriptional regulatory processes control sporulation – synthesis and control of RNA polymerase σ factors, transcription activators and repressors, modulation of transcription factors by phosphorylation, and mechanisms that couple the activities in each cell compartment– (Rosovitz and others, 1998:717-718; Setlow and Johnson, 2001:37). Over 125 genes govern sporulation and over 500 genes can be expressed during the sporulation process (Fawcett and others, 2000:8063,8068).

Germination

Germination is the process of transforming a dormant, resistant spore into a metabolically active vegetative cell (Willett, 1992b:72; Atrih and other 1998:4603). In spite of their extreme dormancy, spores "retain an alert sensory mechanism enabling them to respond within minutes to the presence of specific germinants" (Atrih and other 1998:4603).

The three stages of spore germination are: activation, germination, and outgrowth (Willett, 1992b:72). Overall, the process "is characterized by sequential, interrelated biochemical events" (Atrih and other 1998:4603). Activation is a reversible process triggered by heat or certain chemical treatments (Willett, 1992b:72). Germination is non-reversible. This stage requires the spore to be exposed to "a wide range of nutrient and non-nutrient stimulants" (Willett, 1992b:72). Spore outgrowth consists of the "de novo synthesis of proteins and structural components that are characteristic of vegetative cells" (Willett, 1992b:72).

The process of germination must be considered in the context of the larger population of bacteria as well as a single event. A high degree of synchrony can occur in a population of germinating spores (Willett, 1992b:72). Also, germinating spores have been shown to excrete a substance (or substances) that inhibits the germination of the remainder of the population (Stedman and others, 1956:404).

The biochemical complexity of germination rivals that of sporulation. A more detailed treatment of the germination process is beyond the scope of this work. It is important to recognize, however, the role of the spore as one stage of the complex life cycle of the bacterium.

The Exterior Structure of *Bacillus* Spores

The primary physical barrier between the spore and its environment is the exosporium. This structure is not a remnant of the sporulation process, but rather a specific component of the bacterial spore. The formation of the exosporium begins during stage III of sporulation at the time of forespore engulfment (Desrosier and Lara, 1984:939). It is believed, however, that the production of exosporium components begins during stages I and II and that the exosporium synthesis is intimately associated with the forespore membrane (Desrosier and Lara, 1984:939).

Robert Koch first identified the exosporium as a "round transparent mass which appeared like a small, light ring surrounding the spore" during his studies of *B. anthracis* in 1877 (Gerhardt and Ribi, 1964:1774). C. Flügge named the structure in 1886 (Gerhardt and Ribi, 1964:1774).

The exosporium is a thin, delicate membrane (Sussman and Halvorson, 1966:14). Its thickness has been measured as approximately 500Å (Gerhardt and Ribi, 1964:1780).

The exosporium has been described as a "large balloon-like structure that is not attached to the rest of the spore" (Desrosier and Lara, 1984:935). Another author describes the exosporium of *B. cereus* as "a loose covering that is closely connected to the sides of the spore but extends beyond the poles (Sussman and Halvorson, 1966:14)

It is suspected that the presence of an exosporium in *B. cereus*, *B. thuringiensis*, and *B. anthracis* contributes to their pathogenicity (Charlton and others, 1999:241). However, the true function of the exosporium is not known (Charlton and others, 1999:241).

Chemical Composition of the Exosporium. Estimates of the chemical composition of the exosporium vary. The first studies of the biochemistry of the exosporium were done in 1964 and 1965. These studies were corrected and improved in 1970 (Matz and others, 1970:200). The 1970 work concluded the exosporium was composed of protein (~50%), polysaccharide (~20%), and lipid (~18%) with smaller amounts of calcium, phosphate, and magnesium ash, teichoic acids, RNA, and dipicolinic acid (Matz and others, 1970:198). A study published in 1985 concluded the exosporium is predominantly composed of protein (~50%), carbohydrate (~12%), and lipid (~7%) (Kozuka and Tochikubo, 1985:28). It has been estimated that the exosporium constitutes only about 2% of the dry weight of a spore (Matz and others, 1970:197).

Only about 70% of the exosporial components are soluble in buffers and have been characterized (Charlton and others, 1999:242). The proteins that comprise the structural framework of the exosporium have yet to be identified (Charlton and others, 1999:243). Further, the exosporium can harbor proteins that are not truly components, but products of mother cell lysis, secretions, or adsorbtions from the spore's surroundings (Charlton and others, 1999:243). These factors complicate exosporium studies.

The most recent work done to characterize the biochemical structure of the exosporium occurred in 1999 (Charlton and others, 1999). Exosporium components of *B. cereus* were purified and separated by gel electrophoresis. N-terminal sequences were identified and several were matched to homologues in known protein databases (Charlton and others, 1999:242). The matches included: immune inhibitor A (InA), molecular chaperone GroEL, and the proteins RocA and YcgN (Charlton and others, 1999:243). InA is a zinc metalloprotease from *B. thuringiensis* "thought to specifically degrade two

proteins of the insect immune system" (Charlton and others, 1999:242). GroEL has been observed on the cell surfaces of several species pathogenic bacteria (although its role in pathogenicity is not known) (Charlton and others, 1999:242). The proteins RocA and YcgN are produced by *B. subtilis* and have functions associated with degradation of amino acids (Charlton and others, 1999:243). None of the proteins identified were likely inherent to the structure of the exosporium, and it is possible the proteins were simply associated with the exosporium or adsorbed to its surface as a result of sporulation (Charlton and others, 1999:244)

Synthesis of the Exosporium. The exosporium begins to form during stage III of sporulation (Desrosier and Lara, 1984:935). It is not physically observed until stage IV (Ohye and Murrell, 1973:1180). Exosporium formation proceeds independently of the formation of the outer forespore membrane and the mother cell plasma membrane (Ohye and Murrell, 1973:1185). Exosporium formation begins at one pole of the forespore (the end nearest the center of the mother cell) and proceeds concurrently with other spore-forming processes until stage VI, where the exosporium completely surrounds the forespore (Ohye and Murrell, 1973:1180). During the later stages of development, the exosporium has been shown to extend irregularly into the cytoplasm suggesting it is "flexible and extensible" (Ohye and Murrell, 1973:1180). The lysis of the mother cell cytoplasm begins in a region adjacent to the exosporium suggests that the exosporium is a site for the synthesis of autolytic enzymes (Ohye and Murrell, 1973:1189). The cytoplasm between the exosporium and the spore coat is also lysed during the last stage of sporulation leaving the exosporium as a "loose sac around the spore" (Ohye and Murrell, 1973:1189).

Morphology of the Exosporium. The topography of the exosporium has been studied using electron microscopy of carbon replicas (Bradley and Franklin, 1958:618; Bradley and Williams, 1957:75). This technique resulted in "striking and unexpected" results showing the spores showed a complex, "deep sculpturing" on the spore surface that widely varied among species (Bradley and Franklin, 1958:618; Bradley and Williams, 1957:75). It should be noted that the thinness of the exosporium suggests that the structures observed on the surface of spores arise from features internal to the spore rather than on its surface.

Comparisons of spores of *B. anthracis* and *B. cereus* have suggested very similar structures, with differences in the tightness of the fit of the exosporium and the depth of the nap covering the exosporium (Moberly and others, 1966:228).

The exosporium of *B. cereus* (examined by electron microscopy) is composed of an inner paracrystalline basal layer and a hairlike outer layer (Gerhardt and Ribi, 1964:1784). Isolates of *B. cereus* exosporium have been shown to have a characteristic hexagonal lattice structure (Kozuka and Tochikubo, 1985:28). In the first study, the exosporium was removed by extruding a spore suspension through a refrigerated pressure unit and isolated by centrifugation in linear gradient of glycerol (Gerhardt and Ribi, 1964:1775). In the latter study, the exosporium was removed by sonication and isolated with centrifugation of differential sucrose gradients (Kozuka and Tochikubo, 1985:22-23).

X-ray diffraction of exosporium basal layer isolates indicated a hexagonal close-packed crystal structure (Gerhardt and Ribi, 1964:1784). High-resolution electron microscopy (resolving at approximately 10 Å) confirmed a hexagonally perforate pattern (Gerhardt and Ribi, 1964:1784).

Several studies have suggested using the presence (or absence) of filamentous appendages on the spores as a diagnostic indication of bacterial species (Hachisuka and Kozuka, 1981:1203; Hachisuka and others, 1984:619). However, not all strains of a species have been shown to produce appendages. The character of the strains used in this work in regard to filament production is not known.

Several strains of *B. cereus* form filamentous appendages on their exosporium – *B. cereus* 9373 (called pili in this case) and *B. cereus* IAM 1110 (Kozuka and Tochikubo, 1985:35). Representations of the variety of appendages that have been observed are shown in Figure 1. It has been reported that the appendages are primarily composed of protein (> 70%) (Kozuka and Tochikubo, 1985:28). Although their structure and location can vary, Mizuki and others report "sword-like appendages" extending from a swelling on the basal part of the exosporium giving the spore a "jellyfish-like appearance" (Mizuki and others, 1998:37). These appendages were reportedly 0.03 to 0.6 μm wide and 1.5 to 2.8 μm long (Mizuki and others, 1998:37). Kozuka and others report 11 *B. cereus* strains with approximately 10 tubular appendages (averaging 6 nm in diameter and 2.5 μm in length) originating from the exosporium in locations all around the spore (Kozuka and Tochikubo, 1985:26).

Electron microscopy of *B. anthracis* AKASHI showed "a nap of fine filamentous structures," approximately 720 Å long and 100 Å in diameter on the exterior of the exosporium (Hachisuka and others, 1966:2382). Electron microscopy of *B. anthracis* Sterne strain also showed a fringe of hair-like projections of the outer surface of the exosporium basal layer constituting a "deep nap" (Moberly and others, 1966:223,228).

Another study of 14 strains of *B. anthracis s*howed no filamentous appendages on any of the spores (Hachisuka and Kozuka, 1981:1201).

B. thuringiensis spores have been shown to develop fimbrial appendages (Smirnova and others, 1991:1). Further, just as strains of *B. thuringiensis* produce distinct crystalline toxins, they also produce distinct fimbriation patterns that can result in significant variation in adhesive properties and hydrophobicity (Smirnova and others, 1991:1). The presence of fimbriation varies with *B. thuringiensis* subspecies. The strain used in this work (*B. thuringiensis* var. *kurstaki*) has been shown to develop tubular and filamentous appendages about 2nm in diameter and several hundred nanometers in length when grown on nutrient agar (Smirnova and others, 1991:3).

Surface Properties of *Bacillus* Spores. The hydrophobicity of *Bacillus* spores is an important factor in the adhesion of the spores to a surface. A study using a hexadecane aqueous partition system of 12 strains of *Bacillus* concluded that spores possessing an exosporium were significantly more hydrophobic than spores lacking an exosporium with only a spore coat exterior (Koshikawa and others, 1989:2721). A more recent work based on the affinity for spores to hexadecane and other hydrophobic solvents confirmed that *B. cereus* is the most hydrophobic of the *Bacillus* spores followed by *B. thuringiensis*, *B. anthracis*, and *B. subtilis* (Doyle and others, 1984:330).

The expected structure of spores of the strain of *B. globigii* used in this work is not known. Although *B. subtilis* species typically do not posess an exosporium (the spore coat constitutes the exterior structure (Driks and Setlow, 2000:193), a study of bacterial spore heat resistance presented an electron micrograph of *B. subtilis* var. *niger* that showed an exosporium (Beaman and others, 1982:874). In this work, *B. globigii* is a

negative control where the spore exterior should appear structurally different than the exosporium present in spores of the more closely related *B. anthracis*, *B. cereus*, and *B. thuringiensis*.

It has been hypothesized that the appearance of appendages on the spores may facilitate the attachment of spores to a substrate, similar to a mechanism employed by fungal spores (Mizuki and others, 1998:38). It has been demonstrated the removing appendages by ultrasonication significantly decreases their adhesion to surfaces (Husmark and Ronner, 1992).

The surface properties of the *Bacillus* spores have significant implications for the development of a method for adhering the spores to a substrate in preparation for imaging with atomic force microscopy. In general, spores of *Bacillus* are considered highly adhesive (Husmark, 1993). The hydrophobic nature of the spores can cause significant clumping in deionized water (Husmark and Ronner, 1990:568). Introducing dyes, fixatives, or other chemicals can alter the surface properties of the spores. This work seeks to avoid these alterations in order to see the spore as it appears as a direct result of sporulation.

One of the most significant implications of this review of the literature on *Bacillus* and its spores is that in spite of decades of work, there is no indication of what the surface morphology of a spore looks like. Although extensive work has been done using sections of spores, there has been no known work that has looked directly at the surface properties of the spores as they appear in nature. It is not at all clear from the literature if the surface structure of a spore is a useful marker that could be used to differentiate the spores of closely related species. However, studies showing that even closely related *Bacillus*

species exhibit different surface properties suggest that spore surface structure could be a promising tool for differentiation.

Organization of the Genus *Bacillus*

The taxonomy of *Bacillus* was systematized in 1952 and updated in 1973, based on morphological, physiological, and ecological characteristics, and more specifically by the "shape of the spores, swelling of the sporangium by the spore, and … by the diameter of the rod and the appearance of the protoplasm" (Smith and others, 1952:2; Gordon and others, 1973:16). In 1952, the United States Department of Agriculture examined 1,134 cultures of aerobic, spore forming bacteria and divided them into three groups of 19 species and 1,119 strains, subspecies, or variants by (Smith and others, 1952:46). The International Journal of Systematic and Evolutionary Microbiology (the official journal of record for bacterial taxa nomenclature, published by the Society for General Microbiology on behalf of the International Union of Microbiological Societies) currently recognizes 125 species of *Bacillus* (Euzeby, 2001). There are countless strains, subspecies, or variants housed in hundreds of culture collections around the world.

Many factors contribute to the complexity of *Bacillus* taxonomy. Early taxonomy of the genus *Bacillus* was based on physiological, ecological, or morphological characteristics (Priest and others, 1988:1847). Several efforts have presented revised classification systems based on numerical methods or genetics, however, the results of these works have highlighted the diverse assemblage of organisms classified as *Bacillus* and the overall unsatisfactory state of the genus' taxonomy (Priest and others, 1988:1847-1848; Ash and others, 1991b:202). Transposable genetic elements and extra-

chromosomal DNA contribute to instability (Staley and Krieg, 1984:1). Further, the entire classification scheme seems to be undergoing a shift from taxonomy based on "practical" or phenotypic characteristics to an organization based on phylogenetic or evolutionary evidence through genetic-relatedness (Staley and Krieg, 1984:3).

The *Bacillus cereus* Group. Within the genus *Bacillus* is a group of bacteria termed *B. cereus sensu lato* which includes the four species: *B. cereus*, *B. thuringiensis*, *B. anthracis*, and *B. mycoides* (Leonard and others, 1998:2163). Recently, the species *B. pseudomycoides* and *B. weihenstephanensis* have also been added to the *B. cereus* group (these two species were not studied in this work) (Granum, 2001:373). *B. weihenstephanensis* is distinct due to its psychotolerant but not mesophilic character (Lechner and others, 1998:1380). *B. pseudomycoides* is only distinguishable from *B. mycoides* based on fatty acid composition and 16S RNA sequences (Granum, 2001:374).

The original taxonomy differentiated the four species based on physiological parameters. *B. thuringiensis* produces parasporal crystals of an insecticidal toxin (Sneath, 1986:1135). *B. cereus* is ubiquitous in soil and is the causative agent in several types of food poisoning and opportunistic infections (Leonard and others, 1998:2163). *B. anthracis* is the causative agent of anthrax (Sneath, 1986:1130). *B. mycoides* forms distinctive rhizoid colonies on agar and is recognized as a plant growth-promoting bacterium associated with conifer roots (Sneath, 1986:1133; Daffonchio and others, 1999:1298). The three species *B. cereus*, *B. thuringiensis*, and *B. anthracis* are very closely related and are the focus of this research effort.

In the earliest attempt at establishing an organized taxonomy for *Bacillus*, *B. anthracis* and *B. thuringiensis* were considered variants of *B. cereus* (Smith and others,

1952:56). Although they acknowledged the controversy in this approach and the desire by some to elevate *B. anthracis* and *B. thuringiensis* to species status, in 1973 Gordon (and others) retained Smith's 1952 nomenclature and again referred to them as subspecies of *B. cereus* (Gordon and others, 1973:23). In 1980, both *B. anthracis* and *B. thuringiensis* were accepted as a recognized species distinct from *B. cereus* (Euzeby, 2001). However, this has done little to quell the controversy. Because of their high degree of similarity, it has again been proposed that all of the species in the *B. cereus* group be merged into a single group (Ash and Collins, 1992:75). Overall, the taxonomic interrelationship between *B. cereus*, *B. thuringiensis*, and *B. anthracis* remains controversial and unresolved.

Principles of Taxonomy. The concepts of identification and differentiation of bacterial species are important parts of this work. The diversity of life seen among prokaryotic organisms is enormous. Taxonomy seeks to bring order and organization to the ostensible chaos of the natural world. It is a valuable tool used by researchers and represents a common language across a broad spectrum of scientific disciplines. To that end, a brief review of bacterial taxonomy is presented.

Bacterial taxonomy consists of the classification, nomenclature, and identification of microorganisms (Staley and Krieg, 1984:1). Classification refers to arrangement into groups based on similarities. Nomenclature is the assignment of names based on international rules. Identification is the process of determining that an isolate belongs to an established group.

Several phenotypic and genotypic methods are used for microbial identification and classification. Taxonomy can be based on similarities or phylogeny (Sneath, 1984:5).

The similarities approach studies attributes of an organism presently seen without regard to their origin. Phylogeny looks for apparent evolutionary relationship without regard to present attributes.

Bacterial taxonomy is formal and hierarchical, but never static (Staley and Krieg, 1984:1). It has been clearly acknowledged that bacterial taxonomy will always be a progressive effort (Gordon and others, 1973:3). The world of bacterial taxonomy, described by Cowan and Steel in their 1965 *Manual for the Identification of Medical Bacteria* as, "The different kinds of bacteria are not separated by sharp divisions but by slight and subtle differences in characters so that they seem to blend into each other and resemble a spectrum." – quoted in (Gordon and others, 1973:16).

Further, there is no "official" classification of bacteria (Staley and Krieg, 1984:3). The nomenclature of bacterial taxonomy is governed by internationally agreed-upon rules. However, "bacterial classifications are devised for microbiologists, not for the entities being classified" and the only "official" classification is wide acceptance by the community of microbiologists (Staley and Krieg, 1984:3).

A bacterial species is defined as "a collection of strains that share many features in common and differ considerably from other strains" (Staley and Krieg, 1984:1). The International Journal of Systematic and Evolutionary Microbiology considers a phylogenetic species to be one which would include strains with approximately 70% or greater DNA-DNA relatedness and divergency within related nucleotide sequences of 5% or less (Euzeby, 2001). A bacterial species can be divided into multiple subspecies "based on minor but consistent phenotypic variations within the species or on genetically determined clusters of strains within the species" (Staley and Krieg, 1984:2). The

subspecies (synonyms: variety, variant, or strain) is the lowest taxonomic rank with official standing in nomenclature (Staley and Krieg, 1984:2).

Bacterial classification is based on studies from four sources: numerical taxonomy, nucleic acids, serology and chemotaxonomy, and genetic methods. Numerical taxonomy uses multivariate analysis to examine physiological, biochemical, and other properties to sort individual strains of bacteria into homologous groups (Sneath, 1984:5). Nucleic acid studies use properties of DNA and RNA to establish levels of genetic homology/heterogeneity and to correlate these results with phenotypic observations Johnson, 1984:11). Serology and chemotaxonomy use chemical and physical techniques to investigate the molecular architecture of bacterial cells (Jones and Krieg, 1984:15). The genetic approach to taxonomy includes sophisticated physicochemical methods for the analysis of bacterial genomes and methods based on the transfer of genes between bacteria (Jones, 1984:12).

Differentiation Based on Phenotypic Characteristics. Although officially separated into three taxa, *B. cereus*, *B. thuringiensis*, and *B. anthracis* share many common phenotypic properties and are difficult to distinguish using common biochemical and serological tests. However, as C. D. Stein noted in 1943, it is the effects of the organisms rather than any morphological characteristic that definitively differentiates these organisms. He stated, "Pathogenicity constitutes the principal point of difference between typical strains of *B. anthracis* and those of anthrax-like organisms" (Stein, 1943). Along these same lines, it is the presence of the Cry protein or δ-endotoxin that "defines" *B. thuringiensis*. "The loss of the relevant plasmid(s) makes the bacterium indistinguishable from *B. cereus*" (Granum, 2001:374).

Table 1 summarizes some of the work done on establishing differential tests based on classical microbiological methods. Table 2 illustrates the response of the three species in the group to standard microbiological differentiation methods (Sneath, 1986:1108, 1122-1123). Note that on all tables the following abbreviations will be used: *B. a.* for *B. anthracis*, *B. c.* for *B. cereus*, and *B. t.* for *B. thuringiensis*.

Table 1. Distinguishing Species of the Group *B. cereus*

B. c. (Number of strains)	*B. t.* (Number of strains)	*B. a.* (Number of strains)	*Experimental Method*	*Conclusions*	*Reference*
44	15	23	30 morphological and physiological characters	"We are bound by our data" that there is no "basis for separation" into more than one species. *B. a.* and *B. t.* considered varieties of *B. c.*	(Gordon and others, 1973:23)
35	137	-	99 phenotypic traits	"Strains of *B. t.* were indistinguishable from *B. cereus*"	1a
39	12	-	329 physiological tests	Strains clustered in one main group, distinct from the other *Bacillus* species tested	1b
149	55	37	API test strips	Virulent *B. a.* strains distinguished. Members of the *B. c.* group very closely related.	(Logan and others, 1985)
17	35	-	118 morphological and physiological tests	"The numerical phenetic data underline the close relationship between *B. c.* and *B. t.*	(Priest and others, 1988:
33	9	-	Fatty acid analysis	All strains clustered together, distinct from the other *Bacillus* species tested	1c
3	3	3	Phospholipid analysis	The three "species" tested clustered into a "*B. cereus* group" readily distinguishable from *B. subtilis*	(Black and others 1997;198)

[1a] Baumann, L., K. Okamato, B. M. Unterman, M. J. Lynch and P. Baumann. *J. Invertebr. Pathol.*, 44:329-341 (1984). Referenced in (Zeigler, 1999:54).
[1b] Kampfer, P. *J. Gen. Appl. Microbiol.*, 37:225-247 (1991). Referenced in (Zeigler, 1999:54).
[1c] Kampfer, P. *System. Appl. Microbiol.*, 17:86-98 (1994). Referenced in (Zeigler, 1999:54).

Table 2. Summary of Differential Characteristics for the *B. cereus* Group

Characteristic	*B. cereus*	*B. thuringiensis*	*B. anthracis*
Colony morphology	white	white/gray	white
Hemolysis	+	+	-
Motility	+	+	-
Susceptible to penicillin	-	-	+
Parasporal crystal inclusion	-	+	-
Capsule formation	-	-	+

For decades, a *B. anthracis* isolate has been identified based on its characteristic colony morphology: matt appearance, fairly flat, markedly tacky, white or gray-white, non-hemolytic on blood agar, sensitive to penicillin and the diagnostic γ-phage, and often having curly tailings at the edges (Turnbull, 1999:238). Further, pathogenicity for anthrax constitutes definitive identification of *B. anthracis* (Turnbull and others, 1992: 21). Polymerase chain reaction (PCR) methods are available to confirm the presence of specific genes (e.g. for capsule or toxin) (Turnbull, 1999:238). Strains of *B. anthracis* do exist that lack the ability to produce capsule or toxin, however.

Differentiation Based on Genetic Characteristics. The close relationship among species of the *B. cereus* group indicated by phenotypic observations was confirmed in the 1970's with studies which showed that *B. cereus*, *B. thuringiensis*, and *B. anthracis* have a high degree of DNA homology (Sneath, 1986:1112).

Recently, techniques been developed to take the "genetic fingerprint" of *B. anthracis* (Enserink, 2001:1810). The state of the art uses genetic markers called variable-number tandem repeats (recurring short sequences of DNA). The laboratories of Paul Keim (Northern Arizona University) and Martin Hugh-Jones (Louisiana State University) have studied over 1,200 isolates and have painstakingly developed a "genetic family tree: for all known forms of anthrax (Enserink, 2001:1810; Regaldo, 2001:1).

Overall, the molecular basis for speciation in the *B. cereus* group is not clear (Turnbull, 1999:239). However, although the majority of studies have highlighted the similarities of the three genomes, certain differences do exist and can be used in differential tests to clearly identify species in the *B. cereus* group. Table 3 presents a summary a few of the genetics-focused investigations on these three bacteria.

Table 3. Genetics Studies Distinguishing Species of the *B. cereus* Group

B. c. (Number of strains)	*B. t.* (Number of strains)	*B. a.* (Number of strains)	*Experimental Method*	*Conclusions*	*Reference*
2	6	2	DNA reassociation	"The available DNA reassociation data indicate a single species	3a
2	1	1	16S rRNA sequencing	"These 'species' form a genealogically tight group" comparable to "other Gram-positive species."	(Ash, C. and others, 1991a)
24	12	-	*Not1* profiles, multilocus enzyme electrophoresis	"On the basis of these results … we conclude that strains typed as *B. c.* and *B. t.* belong to the same species	(Carlson and others, 1994)
1	-	3	Comparison of arbitrarily primed (AP) – PCR "fingerprints"	"The *vrrA* locus appears to be an excellent candidate for the differentiation of isolates of *Bacillus*."	(Andersen and others, 1996)
4	3	-	Physical mapping of chromosomes	Some *B. c.* genomes are more similar to *B. t.* genomes than to those of other *B. c.* strains	(Carlson and others, 1996)
1	2	78	Amplification fragment length polymorphism	"AFLP similarities are consistent with … close relationships, though *B. cereus* and *B. thuringiengsis* seem to be more closely related to each other than to *B. anthracis*."	(Keim and others, 1997)
85	10	1	Molecular diagnostic marker for *gyrB*	The use of a *B. cereus* specific PCR primer was able to distinguish *B. cereus* from *B. thuringiengsis* and *B. anthracis*.	(Yamada and others, 1999)
number of strains not listed			Amplification fragment length polymorphism and polymerase chain reaction analysis	"AFLP rapidly differentiates among all species so far tested and among different strains of even *B. anthracis*, the most genetically monomorphic species so far characterized."	(Jackson and others, 1999)
3	12	47	Distribution of Ba813 chromosomal DNA sequence	"The question of species delineation within the '*B. cereus* group' is still unanswered and may not be answerable."	(Ramisse and others, 1999)
23	4	27	Randomly amplified polymorphic DNA fingerprinting	"The restriction analysis … distringuished *B. anthracis* from from the other species of the *B. cereus* group."	(Daffonchio and others, 1999)
227 *B.c.* and *B.t.*		13	Multilocus enzyme electrophoresis and sequence analysis	"*B. anthracis* appears to be genetically indistinguishable from … the *B. cereus* and *B. thuringiengis* group"	(Helgason and others, 2000b)
65 *B.c.* and *B.t.*		-	Multilocus enzyme electrophoresis	There was a high degree of heterogeneity among strains isolated from dairies and high similarity among strains isolated from human infections.	(Helgason and others, 2000a)
23	58	27	homoduplex and heteroduplex polymorphisms of 16S-23S internal transcribed spacers	"The genetic relationships within the *B. cereus* group … further support the idea that *B. cereus*, *B. thuringiengis* and *B. anthracis* are members of a single species (*B. cereus* sensu lato) …"	(Daffonchio and others, 2000)
8	2	2	Fluorescent amplified fragment length polymorphism	"Since *B. anthracis* is very monomorphic in comparison to *B. cereus* and *B. thuringiensis* isolates, *B. anthracis* should probably be considered as a distinct species…"	(Ticknor and others, 2001)

[3a] Priest, F. G. "DNA homology in the genus *Bacillus*," in *The Aerobic Endospore-forming Bacteria*. Ed. R. C. W. Berkely and M. Goodfellow. London: Academic Press, 1981. Referenced in (Zeigler, 1999:54).

Studies of the 16S rRNA has been shown to have greater than 99% sequence similarity between the three species (Ash and others, 1991a:436). *Bacillus cereus*, and *Bacillus anthracis* showed only two differences (out of over 2900 base pairs) in the structure of their 23S rRNA (Ash and Collins, 1992:75). Similarity in 16S and 23SrRNA sequences indicates that the species "have diverged from a common evolutionary line relatively recently" (Granum, 2001:374).

The evolutionary lineage of the *B. cereus* group is important (Turnbull, 1999:239). It is hypothesized that *B. anthracis*, *B. cereus*, and *B. thuringiensis* descended from a common ancestor (Turnbull, 1999:239). *B. anthracis*, as an obligate pathogen of warm-blooded animal species, has exploited the animal niche. *B. thuringiensis*, an insect pathogen, has exploited the insect niche. *B. cereus* has exploited the environmental niche but also possesses the ability to cause infections in warm-blooded animals. A clear understanding of chromosomally based genes is important to understand certain aspects of each organism's pathogenicity and distinct phenotypic features (Turnbull, 1999:239).

Implications. The morphologic, phenotypic, genetic, and chemotaxonomic similarities between *B. anthracis*, *B. cereus*, and *B. thuringiensis* have led many microbiologists to consider them members of the same species (Black and others, 1997:197). These similarities make rapid and reliable identification of pathogenic *B. anthracis* inherently problematic. The rapid detection and clear identification of *B. anthracis* must be considered in the context of a large environmental population of ubiquitous *B. cereus* (Turnbull and others, 1992:22). In spite of the vast amounts of genetic information, it is not clear how *B. anthracis*, *B. cereus*, and *B. thuringiensis*, differ in regards to their specific surface properties. The link is not complete.

Atomic Force Microscopy

The tool used in this work to study *Bacillus* spores was the atomic force microscope (AFM). Rather than "looking" at a surface with a photon or an electron, atomic force microscopy visualizes a surface by "feeling" it with a sharp probe. Atomic force microscopes have the ability to achieve atomic-level resolution of sample surfaces under natural conditions (in gaseous or liquid environments) –an ability unrivaled by radiation-based microscopes (Morris and others, 1999:2).

Gerd Binnig and Heinrich Rohrer developed scanning tunneling microscopy in the early 1980's at the IBM Research Laboratories in Zürich, Switzerland (Morris and others, 1999:1; 1986 Nobel Prize, 2000). In 1986, they were awarded the Nobel Prize in physics for their work (Morris and others, 1999:1). Scanning tunneling microscopy (STM) uses an electric current sent through a sharpened tip maintained at a small distance from a surface (Multimode Manual, 1997:2-13). Tunneling is a phenomenon of quantum mechanics where an electron penetrates a potential barrier (in this case a non-conducting gap between the probe tip and a surface) by apparently digging a tunnel through the barrier (Binnig and others, 1986:52). In STM, a "tunneling" current flows from the end of the tip to the conducting surface of the sample. The magnitude of this current is a function of the distance from the tip to the surface. The requirement for a conductive sample in STM makes it a poor tool for most biological applications

In 1985, the first atomic force microscope was built by Binnig, Calvin Quate, and Christopher Gerber (Binnig and others, 1986:930). Their pioneering design was only the beginning. Significant advances, refinements and creative innovations have occurred in the past sixteen years. The field of scanning probe microscopy (SPM) has gained

widespread acceptance and use in a variety of scientific disciplines for its ability to create three-dimensional images down to the atomic scale of samples in ambient conditions. Over a dozen SPM technologies have been developed and commercialized (Miles, 1997:1845). AFM is the most widely used of these technologies (Miles, 1997:1845). The atomic force microscope described here is the Nanoscope IIIa produced by Digital Instruments, Inc. of Santa Barbara, California. Gerhard Meyer and Nabil Amer of the IBM Thomas J. Watson Research Center developed the original design for this AFM in 1988 (Bhushan, 1995:23; Meyer and Amer, 1988:1045).

Overview of the Atomic Force Microscope. The principal of atomic force microscopy is elegantly simple. A sharp stylus that sits on the end of a cantilever beam (of length ~ 100μm) acts as the probe. The topography of the specimen's surface is imaged by recording the deflection of the cantilever as the probe is raster scanned over the sample's surface.

Figure 3 shows a simplified schematic of the AFM system. The piezoelectric crystal controls the movement and position of the sample. The position of the probe is monitored by a laser, which reflects off of the surface of the probe and onto a dual element photodetector. A computer, using sophisticated software, records the three-dimensional position of the probe and uses this information to generate an image of the surface.

AFM can image the three-dimensional topography of a specimen in a variety of ways. The two imaging methods used in this research are contact and intermittent contact modes. In contact mode, the probe is simply scanned across the sample surface and an image is produced by monitoring the deflection of the cantilever. In intermittent contact

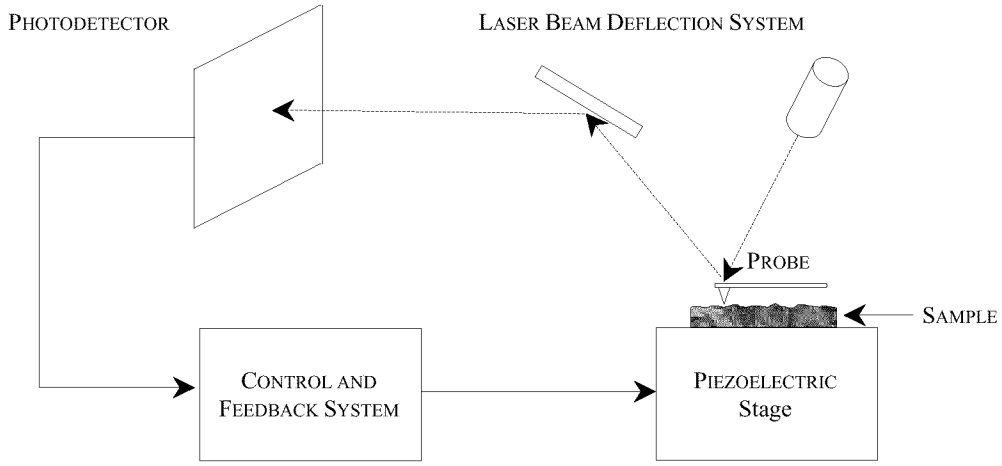

Figure 3. The Atomic Force Microscope

mode (or TappingMode®), the cantilever probe is oscillated at or near resonant frequency (200-500kHz). This significantly reduces the lateral forces exerted on the sample surface during scanning (Hansma, 1999:14678).

The Piezoelectric Stage. In the atomic force microscope used for this work the probe position is fixed and a piezoelectric scanner moves the sample.

The scanner consists of a tube of piezoelectric ceramic, capable of extremely precise positioning, held in a cylinder of Invar (an iron-nickel alloy) (Bhushan, 1995:25). A magnetic cap located on the top of the tube is used to hold the steel sample puck (Bhushan, 1995:25). The scanner sits atop a stepper motor that is built into the base of the microscope (Bhushan, 1995:25). This motor is used by the computer to engage and withdraw the tip and by the user to adjust the vertical position of the sample with respect to the cantilever mount.

The piezoelectric stage changes dimensions (by expanding and contracting) in proportion to an applied voltage. Figure 4 illustrates the construction and electrical

configuration of the piezoelectric stage (based on Multimode Manual, 1997:2-7). Electrodes are attached to the outside of the tube, electrically segmenting it into four vertical quarters (for $\pm x$ and $\pm y$ travel). Another electrode is attached to the center of the tube to provide motion in the z direction. Alternating current voltages applied to the x- and y- axes move the sample in a raster scan pattern. Applying current across the z-axis also controls the vertical distance of the probe above the sample. Controlling the vertical displacement of the probe through a feedback circuit allows the maintenance of a constant force on the probe.

A schematic of the scanner's movement to produce the raster scan is also shown in Figure 4. Images can be obtained in the trace (forward) or retrace (reverse) direction. Additionally, the scan direction can be rotated up to 359°.

The physical properties of the scanner determine its operating characteristics (length, diameter, wall thickness, strain coefficient, ceramic, etc.). These properties determine the maximum scan size (0.4 – 200 μm square) and maximum vertical range (0.4 – 8.0 μm) (Multimode Manual, 1997:2-6). The AFM used for this work uses an AS-130V (vertical "J") scanner. This particular scanner has a maximum scan size of 125 μm × 125 μm and a maximum vertical range of 5.0 μm (Multimode Manual, 1997:2-6).

In practice, piezoelectric scanners can diverge from ideal linear behavior through several avenues: intrinsic nonlinearity; aging; hysteresis; creep; and cross coupling (Howland and Benatar, 2000). Figure 5 illustrates these issues and some of the effects on the trace of the probe (and the resulting image) that can occur as a result of scanner nonlinearities (Howland and Benatar, 2000).

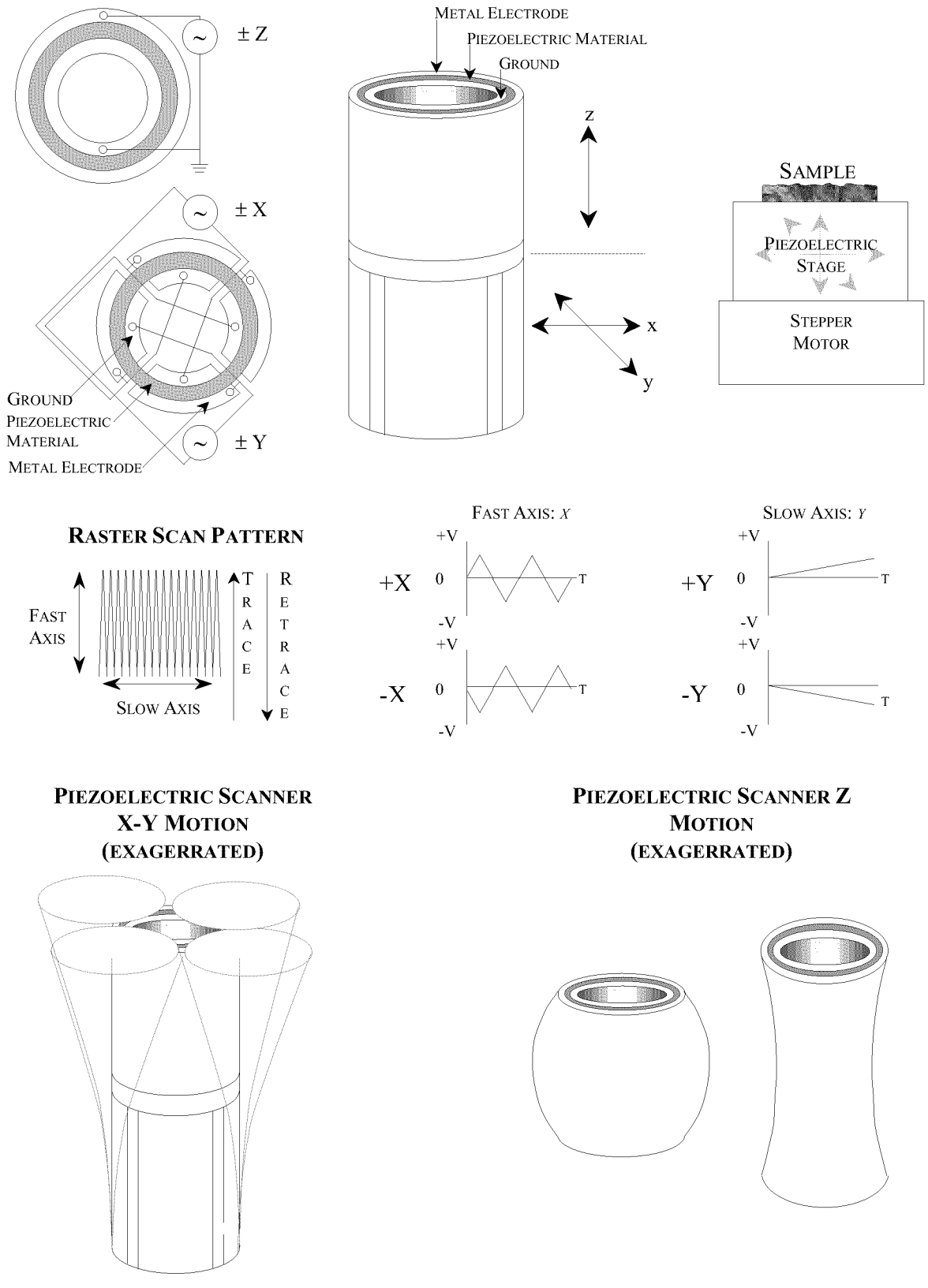

Figure 4. The Piezoelectric Scanner

The intrinsic nonlinearity is a material property representing the deviation from the ideal linear extension of the material at a given voltage. Expressed as a percentage, it can range from 2 – 25% in the materials used for AFM scanners (Howland and Benatar, 2000). Non-linearity can distort features on AFM images. However, a proprietary calibration routine (Digital Instruments U.S. Pat. #5,051,646) corrects for nonlinearities by "applying a nonlinear voltage in real-time to produce a linear scan in x and y in both trace and retrace scan directions" (DI Training Notebook, 1998:13).

Aging is the change in a material's strain coefficient over a long period of time. It is caused by changes in the alignment of the dipole moments within the polycrystalline ceramic comprising the piezoelectric tube. When a scanner is not used, a given voltage results in a decreasing deflection over time and with use. When a scanner is used regularly, a given voltage results in a slowly increasing deflection with use and time. Aging can result in erroneous length measurements taken from AFM images (Howland and Benatar, 2000).

Piezoelectric ceramics naturally display hysteretic behavior. AFM data are usually collected in one direction in order to avoid errors due to this hysteresis (Howland and Benatar, 2000). However, it is still possible to see errors caused by hysteresis in the z-direction because the extension and the contraction require different voltages. Figure 5 illustrates the type of error that can be caused by material hysteresis.

The change in the dimensions of a piezoelectric material in reaction to an abrupt voltage change is not an instantaneous process. Creep is "the drift of the piezo displacement after a DC offset voltage is applied to the piezo" (DI Training Notebook, 1998:17). As Figure 5 shows, the scanner immediately expands to nearly the full height

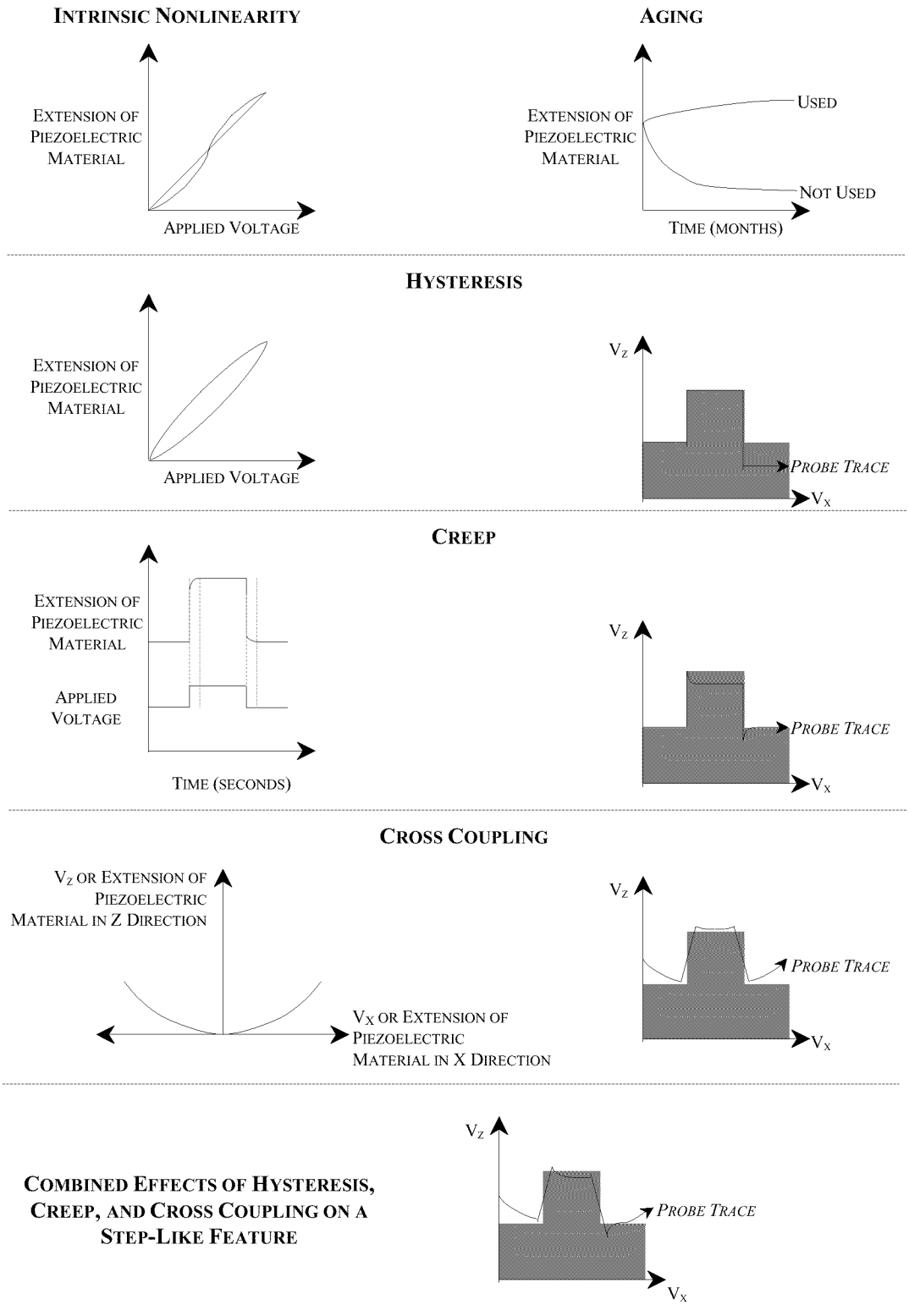

Figure 5. Piezoelectric Scanner Deviations from Ideal Linear Behavior

of the step as the voltage is applied, then slowly moves the remainder of the distance. As the scanner moves through the last part of the offset distance, creep occurs. In order to keep the tip in contact with the sample, a voltage must be applied in the other direction, which counteracts the creep. Creep can cause the display magnification to change with the speed of the scan, or an elongation of features in the direction of the offset. Also, zooming in on features over long ranges must be accomplished in a step-wise fashion.

Cross coupling refers to the tendency of *x*-axis or *y*-axis scanner movement to have a spurious *z*-axis component (Howland and Benatar, 2000). The *x*-*y* motion of the scanner tube is produced when one side of the tube shrinks and the other side expands (Howland and Benatar, 2000). As a result, a piezoelectric tube scans in an arc, not in a plane (Howland and Benatar, 2000). A voltage applied to move the piezoelectric tube along the *x*- or *y*-axis (parallel to the surface of the sample) necessitates that the scanner extend and contract along the *z*-axis (perpendicular to the surface of the sample) to keep the tip in contact with the sample (Howland and Benatar, 2000). Cross coupling can cause an AFM to produce a bowl-shaped image of a flat sample (Howland and Benatar, 2000).

Overall, deviations from non-linearity in scanner behavior can result in distortions in the resulting image (shown in Figure 5 for the vertical direction). Calibration and software are used to address these problems. Moreover, the non-linearity is negligible for small displacements and is usually only a problem for large scans (> 70% of the full scale displacement of the scanner) (Morris and others, 1999:31).

The Probe. The atomic force microscope probe consists of a sharp, pyramidal tip attached to a thin cantilever. The low force constant of the cantilever allows the AFM to control the force between the tip and the sample with great precision (Mueller and others, 1999:1078). Probe tips are commercially micro-fabricated and can vary in materials and shape. Figure 6 illustrates the AFM probe.

The aspect ratio is an important parameter for AFM tips. The aspect ratio affects the resolution of an image and limits the suitability of a tip for a given sample's depth of field (Mueller and others, 1999:1078). The "opening angle" refers to the aspect ratio at the sharpened end of the tip. The sharpness of a tip is given by its radius of curvature at the apex of the tip. Tips are commonly manufactured of silicon or silicon nitride. In the system used in this work, the probe remains stationary and the sample is scanned beneath. The probe is mounted in a metal block tipholder. It is held by a metal clip at an 11° downward tilt (with respect to the horizontal) (Bhushan, 1995:23).

The contact probe used in this work was a commercially manufactured (Digital Instruments, Santa Clara, California) Model NP silicon nitride (Si_3N_4) probe. This triangular (V-shaped) cantilever probe was microfabricated using a photolithographic technique, plasma-etched chemical vapor deposition (Bhushan, 1995:33; Albrecht and other, 1990: 3390). As Figure 6 shows, four probes are fabricated on a substrate of borosilicate glass (Pyrex®). Each probe has a different spring constant. The cantilevers are approximately 0.6μm thick. There is a 15nm thick gold reflective coating on top of the cantilever (and one side of the substrate) (Bhushan, 1995:34). At the end of the cantilever is a symmetric, pyramidal tip with a radius of curvature of 20-50 nm (Bhushan, 1995:34). The shape of the tip is formed in a "mold" of a (100) silicon

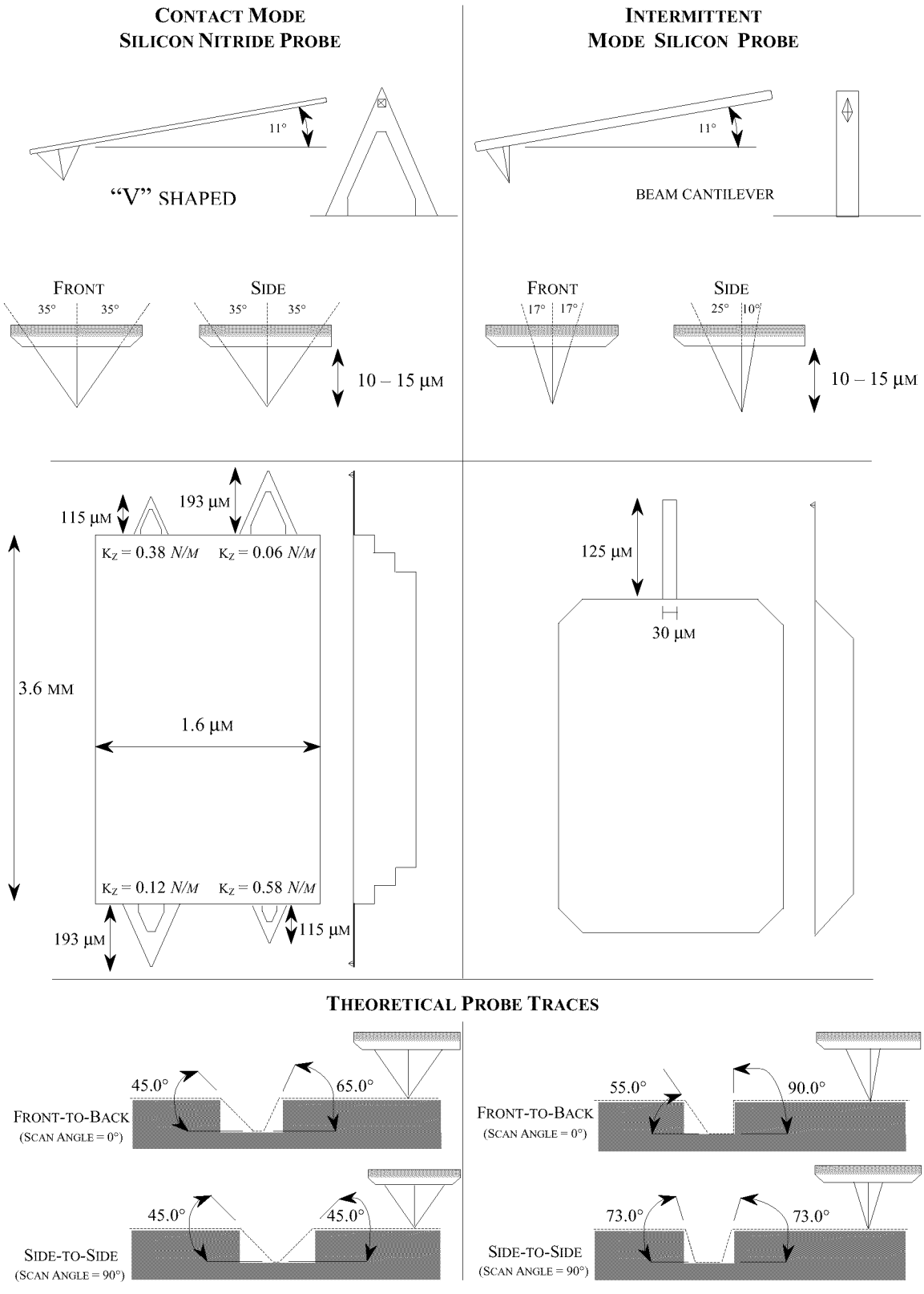

Figure 6. The AFM Probe

wafer etched to reveal intersecting (111) planes (Albrecht and others, 1990:3390). In contact mode, the flexible cantilever extends from a rigid substrate and acts as a "nanometric spring" that allows the tip to measure surface forces (Multimode Manual, 1997:2-11). The interaction between the tip and the sample is repulsive in nature (Morris and others, 1999:50).

The spring constant is a measure of the force required to generate a given cantilever deflection (in units of force per unit deflection, usually *N/m*). The vertical spring constant of an AFM probe, k_z, is approximated by the manufacturer. These are the values listed in Figure 6. However, the actual spring constant can significantly vary from cantilever to cantilever and is a function of geometry (length, width, and thickness) and material (elastic modulus).

In intermittent contact mode, the probe is an etched single-crystal, n-type silicon rectangular cantilever with a pyramidal tip. This probe is also commercially manufactured by Digital Instruments, Santa Clara, California (Model TESP). The resonant frequency of this probe is 200-400 kHz. The spring constant can vary from 20-100 N/m. The geometry of the tip is shown in Figure 6. When engaged, a piezoelectric driver oscillates the probe vertically at resonant frequency. The amplitude and phase are monitored in order to generate images.

The interaction between the probe and the surface is the heart of atomic force microscopy. In order to understand the resulting images, several issues will be discussed involving image artifacts that are not are not representative of "real" surface features, but are a result of the state of the probe and its interaction with the surface. Tip convolution,

probe broadening, sample compression, tip contamination, and potential tip shape artifacts will be addressed. These are all illustrated in Figure 7.

One of the most common artifacts on an AFM image is caused by tip convolution. The image resulting from an AFM scan is a "convolution" of both the shape of the tip and the feature on the sample surface. The geometry of the tip is important to consider as AFM tips can be non-symmetrical or much more complicated forms. The probe is "blind" to surface features with angles steeper than those of the tip. Inherently problematic surface features include deep recesses, shear walls, and undercuts.

Although the tip appears macroscopically sharp and pointed, the apex of an AFM tip has a radius of curvature that can figure prominently into the form of a resulting image. As Figure 7 shows, broadening of the tip can cause the probe to miss small features and falsely represent the sample surface. "Probe-broadening will always occur" and must be considered in analyzing an AFM image (Morris and others, 1999:33).

Other issues that must be considered when working with biological samples are the compression of a soft sample by the AFM tip and the contamination of the tip by surface debris. As Figure 7 shows, compression of the sample by the AFM tip distorts the image and affects the measurement of sample dimensions in the *z*-direction (Morris and others, 1999:33). A contaminated tip "imposes its own geometry" to a sample surface also creating a biased vertical profile (Command Reference Manual, 1999:1-27).

The etching process used to produce a silicon tip can produce a short angled ridge near the highest point on the tip (Multimode Manual, 1997:4-6). The size may vary, but it is usually approximately 0.5 μm in total length. If the tip being used has this defect,

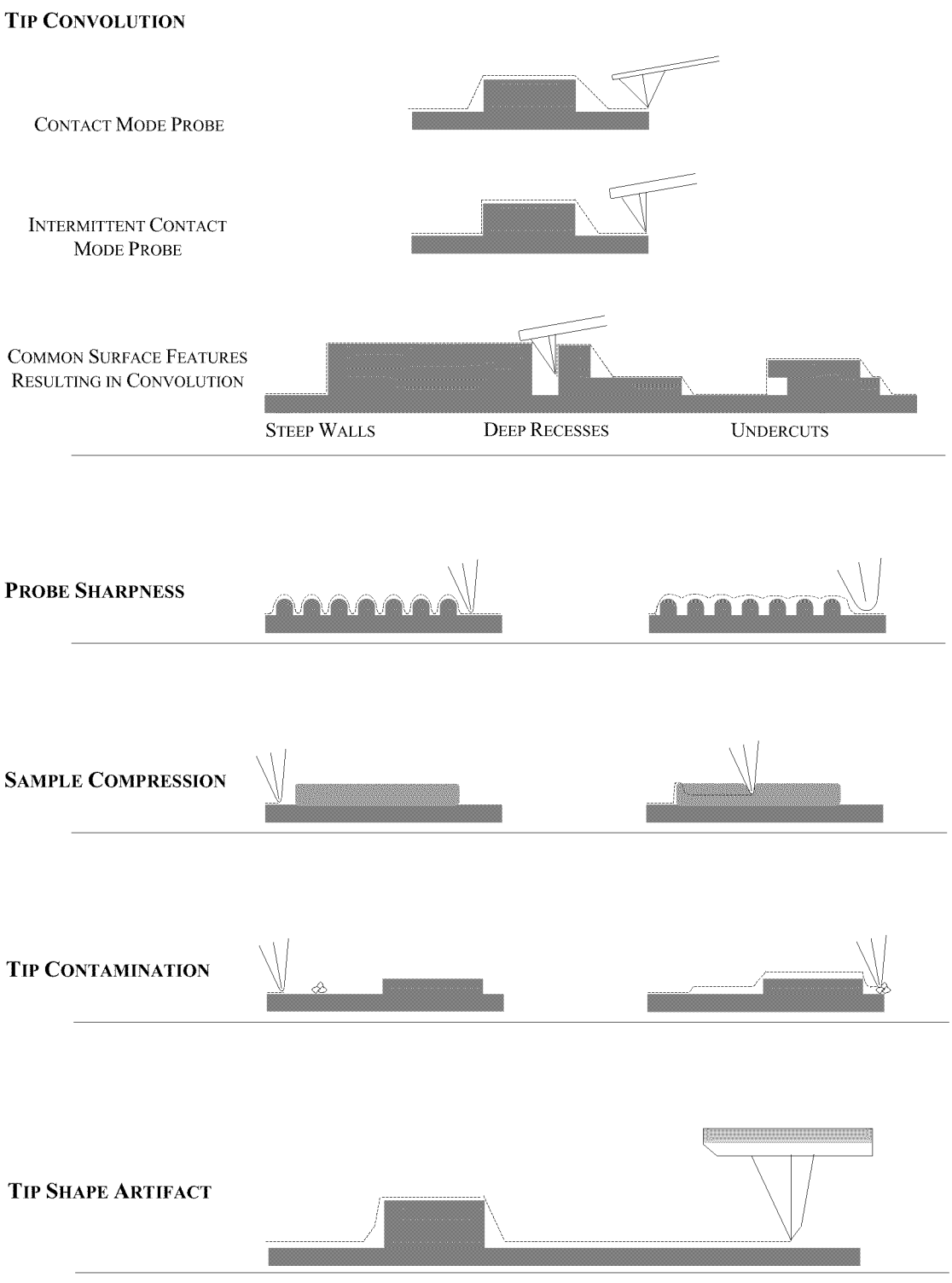

Figure 7. AFM Probe Imaging Issues

"sample features of approximately 0.5 μm in height can produce artifacts of an apparent shallow slope over scan fields of larger than 1-2 μm" (Multimode Manual, 1997:4-6).

Detection Method. The atomic force microscope used for this work uses laser beam deflection as the detection method. The ability to know the exact position of the cantilever probe is crucial to obtaining an accurate and high-resolution image of the sample's topography. The photodetector configuration is shown in Figure 8.

A diode laser (5-mW max peak output at 670nm) generates a laser beam that is "directed by a prism onto the back of the cantilever" (Bhushan, 1995:23). The laser is reflected by the cantilever onto an adjustable mirror and then to the split photodiode detector. The laser diode is built into a stage with *x*- and *y*-positioners that are used to adjust the location of the laser beam with respect to the cantilever (Bhushan, 1995:23). The photodiode is also built into an adjustable stage capable of moving the detector

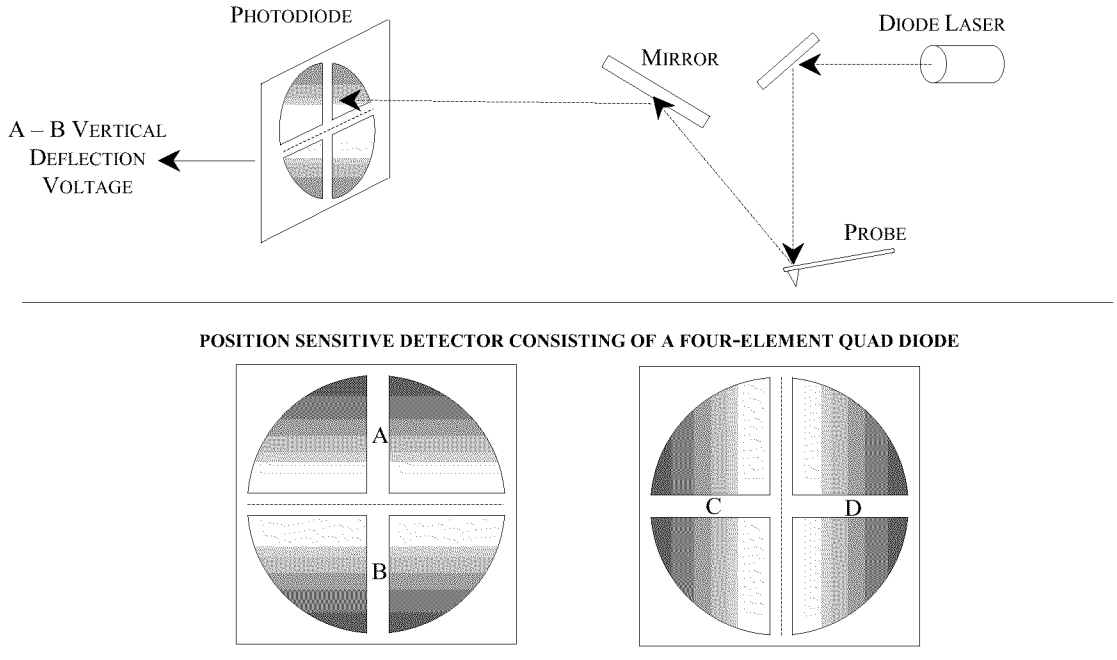

Figure 8. The AFM Detection System

vertically and horizontally. The position of the photodetector is important because it is used to adjust the total voltage generated by the photodetector and differences in voltage between various segments of the photodetector (Multimode Manual, 1997:5-23 to 5-24).

The photodiode is a position sensitive detector consisting of a four-element quad diode (Multimode Manual, 1997:2-4). As the cantilever flexes, laser light is reflected onto the split photo-diode. The bending of the cantilever is measured from the A – B difference signal. The C – D difference signal is used for measuring lateral displacements.

Laser beam deflection allows for tremendous sensitivity. Theoretically, a cantilever displacement as small as 4×10^{-4} Å could be measured with a signal to noise ratio of 1 (Morris and others, 1999:16). Random thermal excitation of the cantilever exerts a practical limitation to the sensitivity of the detector (Morris and others, 1999:16). However, measuring atomic-scale displacement can accomplished for samples with appropriate stiffness (Morris and others, 1999:16).

Control and Feedback in Contact Mode. The heart of the AFM is the feedback system used to control the tip-sample interaction. The system relies on the ability of the tip to "accurately track the surface of the sample in a controlled manner at all times" (Morris and others, 1999:24). In order to obtain high resolution in atomic force microscopy, there must be precise control of the tip-sample interaction and accurate knowledge of the tip and sample position at all times (Morris and others, 1999:4). Figure 9 shows the integrated architecture of this system.

As the AFM engages, the tip is brought into actual contact with the sample surface. Then, the piezoelectric scanner is used to drive the cantilever in the *z* direction to a predefined level of deflection known as the "setpoint". This setpoint is maintained by a *z* correction signal throughout the scan in order to preserve a constant force between the tip and the sample. Further, this ensures that the AFM is engaged in the repulsive region of is operating range and the cantilever is exerting positive pressure on the sample surface (Multimode Manual, 1997:2-31). Plotting the *z* correction signal against the $\pm x$ and *y* signals used to drive the raster scan generates the image.

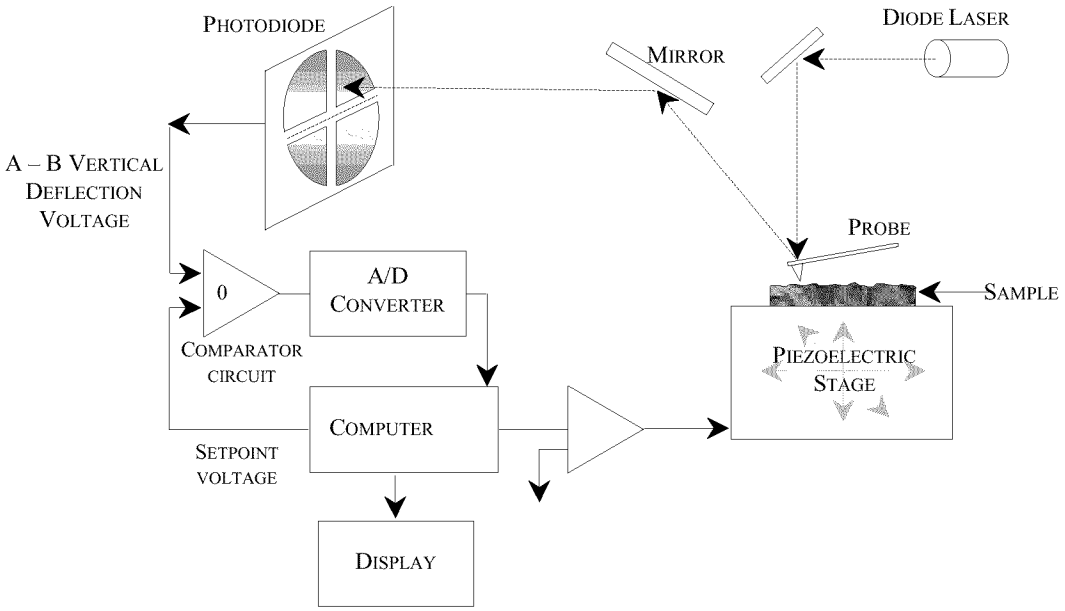

Figure 9. Contact Mode Control and Feedback

The purpose of the control system is to generate drive voltages to control the *x*-*y* scans of the piezoelectric transducer and to maintain the incoming analog signal from the detection circuitry at a constant level (Multimode Manual, 1997:2-26).

A laser generates a small spot of light that reflects off of the top of the cantilever probe. From the probe, the light is reflected onto a mirror and then to the photodetector. The photodetector generates a ± 10V difference current (A – B) based on the position of the spot of light on the quad diodes. This voltage passes through a comparator circuit and on to the analog-digital converter.

The AFM control system must be rapid and accurate. Digital Instruments uses a unique "digital signal feedback architecture" that uses two sequential gain processes. The "gains" are simply "values that magnify the difference read to the A/D converter" (Multimode Manual, 1997:2-27). First, integral control "integrates the deviation from the setpoint over a small period of time" correcting the cumulative error between the system and its target state (Morris and others, 1999:27). Second, proportional control amplifies the error between the setpoint and the measured value in order to determine the size of the finishing correction factor required.

Control and Feedback in Intermittent Contact Mode. The feedback system used in intermittent contact mode is more complicated than that used in contact mode due to the vibration of the cantilever. The tip touches the sample surface only at its lowest point of oscillation. The purpose of the feedback loop is to maintain constant cantilever oscillation amplitude. As the probe scans the sample surface, a vertical feature leaves the cantilever with less room to oscillate, decreasing the vibrational amplitude.

The signal from the photodetector is rectified and lowpass filtered into a DC voltage called RMS (root mean squared) voltage. The RMS voltage will be proportional to the amplitude of the cantilever. The tip-sample separation is adjusted in order to maintain constant amplitude and force on the sample.

As the AFM engages in intermittent contact mode, the tip is lowered until the RMS voltage equals the setpoint voltage. Initially, the computer defines the setpoint voltage as 95% of the RMS voltage. In order to ensure true engagement has occurred, the step motor halts the tip's descent, the setpoint is slightly lowered, and the feedback control monitors the movement of the *z* piezo. If there is only small *z* piezo movement, the cantilever is truly engaged with the sample surface. If there is a large *z* piezo movement, the cantilever is being damped by air trapped between the cantilever and the sample surface and the computer must readjust the setpoint voltage and repeat the engage sequence.

The Atomic Force Microscopy Image. As an image is scanned, the data is "captured" in an image data file. The data is stored in 16-bit per pixel values. Each pixel can have one of 65,536 possible values within the range ±32,768 (Command Reference Manual, 1999:B-10). The software automatically scales the data over the full resolution of the *z*-axis. Each complete AFM scan consists of 512 scan lines. Image data is sampled 512 times in each scan line. The scan is completed with a 1:1 aspect ratio for a square scan. The AFM software can capture image information on three channels simultaneously.

In contact mode, the actual image produced by the AFM scan is either the input (difference) or output (correction) applied to the *z*-axis piezo (Multimode Manual, 1997:2-26). Image information is collected in either the trace or retrace direction. There are several types of image data that can be collected. Height data consists of the output voltage to the *z* piezo, and reflects change in the piezo height needed to keep the cantilever deflection constant (Multimode Manual, 1997:6-13; Command Reference

Manual, 1999:2-31). Deflection data comes from the "differential signal off of the top and bottom photodiode segments" (Multimode Manual, 1997:2-26). Deflection data represents the force the sample exerts on the cantilever during the scan in terms of the bending of the cantilever caused by surface features (Morris, 1999:54).

In intermittent contact mode, height data "corresponds to the change in piezo height needed to keep the vibrational amplitude of the cantilever constant" (Multimode Manual, 1997:6-13). Amplitude data directly describes the surface topography by mapping changes in cantilever amplitude as the probe scans across the surface (Multimode Manual, 1997:6-13).

Phase imaging is an extension of intermittent contact mode AFM. The phase lag of the cantilever oscillation produced by a sample feature relative to the oscillation produced by the piezoelectric driver is "sensitive to material properties such as adhesion and viscoelasticity" (Babcock and Prater, 1995:1-2). The principles behind phase imaging are shown in Figure 10. The phase lag can be measured concurrently with the cantilever oscillation. Measured in degrees, the phase image provides "real-time contrast enhancement" and "clearer observation of fine features … obscured by rough topography" (Babcock and Prater, 1995:2).

Phase contrast has been correlated to energy dissipation on the sample surface resulting from changes in material properties (Bar and others, 2000:L11). Because only a small percent of the vibrational energy of the cantilever is lost to the surface, the cantilever retains it sinusoidal vibration. Only the phase of the vibration shifts according to the magnitude and character of the interaction (Bar and others, 2000:L15).

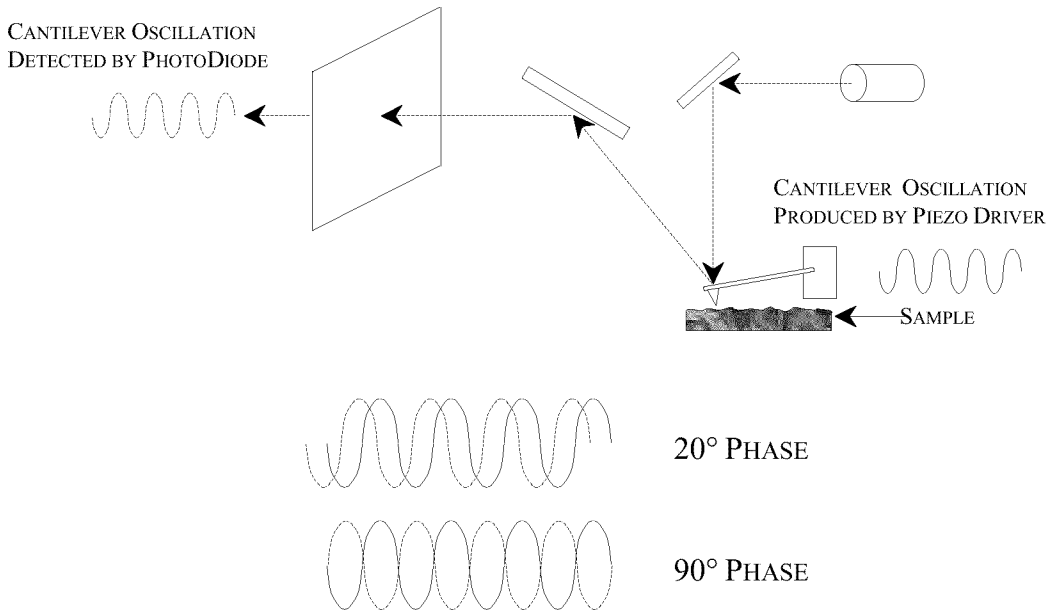

Figure 10. Phase Imaging

A third type of data can be obtained directly from the changes in amplitude of the oscillating cantilever caused by surface features. Data collection in this way is referred to "error-signal mode". This is a useful tool for detecting edges. In this work, deflection images were compared to height images for quality control purposes.

The source of the information presented in any image allows different conclusions to be drawn regarding actual features on the real sample surface. By combining several sources of information (by collecting data across multiple channels at one time), a fuller analysis can be completed. However, no matter what the source of the data, each image should be interpreted as an interaction between the probe and the real surface. This critical distinction complicates the analysis of AFM images, but is a necessary element of atomic force microscopy.

Biological Applications of Atomic Force Microscopy

Atomic force microscopy has been extensively applied in the biological sciences. AFM provides the ability to obtain high-resolution images of biological surfaces in natural or physiological conditions. Through AFM there are a multitude of ways to generate new knowledge about different systems. AFM studies have ranged from mapping the landscape of a leaf surface to visualizing the processes involved in protein assembly (Mechaber and others, 1996; Sit and Marchant, 2001:421).

Application of AFM to the biological sciences is a rapidly maturing technology. It is considered a "reliable and reproducible" tool where "the emphasis has passed from validation of the microscopes to their use to study biological problems" (Morris and others, 1999:3).

From whole cells to macromolecules, biomaterials to DNA, a complete compendium of biological applications of AFM is far beyond the scope of this review. However, a brief look at the variety of systems that have been studied is useful for placing this work in a larger context. Biological AFM work can be grouped into studies of biological molecules, interfacial interactions, biological membranes, and living systems.

Atomic force microscopy provided the first tool to image biomolecules under aqueous conditions with molecular resolution (Drake and others, 1989; Hansma and Hoh, 1994:116; Jandt, 2001:303; Radmacher and others, 1992). AFM studies have investigated the ultrastructural organization and assembly processes of collagen (Goh and others, 1997; Paige and Goh, 2001; Paige and others, 1998; Paige and others 2001; Revenko and others, 1994;Taatjes and others, 1999). The molecular and sub-molecular architecture of other fibrous proteins such as titin and amyloid fibrils, and ocular mucins

have been imaged with AFM (Chamberlain and others, 2000; Hallett and others, 1996; McMaster and others 1999). AFM has been used to accurately measure volume and study the structure of chromosomes for the purpose of classification (McMaster and others, 1996; Tamayo and Miles, 2000). Enzyme activity has been directly observed (Radmacher and others, 1994). Work on the sub molecular-level with DNA has also been done (Allison and others, 1992; Hansma and others, 1992; Murray and others, 1993; Shlyakhtenko and others, 1999; van Noort and others, 1999).

AFM has been a valuable tool for studying molecular interactions and interfaces. The interaction forces between biological molecules can be measured with AFM (Willemsen and others, 2000). AFM has allowed the adsorption of fibrinogen to be directly imaged (Cacciafesta and others, 2001; Cacciafesta and others, 2000; Gergely and others, 2000; Hemmerlé and others, 1999; Sit and Marchant, 2001). The force of other protein adhesion events has been measured as well as imaged (McMaster and others, 2000; Sagvolden, 1999). Model systems of cellular adhesions using vesicles have also been studied (Pignataro and others, 2000). Several studies have also examined the structure of cellulose and starch granules (Baker and others, 1997; Baker and others, 1998; Baker and Miles, 1997; Baker and others, 2001).

Atomic force microscopy has extended the researcher's ability to examine living systems in a way never possible before. Living eukaryotic cells have been studied in several works that have revealed significant details of the structural, mechanical, and chemical properties of the cells (A-Hassan and others, 1998; Le Grimellac and others, 1998: Nagao and Dvorak, 1999). Motile fibroblasts have been studied dynamically, revealing kinetics and mechanical properties (Rotsch and others, 1999).

Biological membranes such as black lipid membranes, reconstituted membranes, cationic lipid bilayers, purple membranes, and Langmuir-Blodgett bilayers have all been studied with AFM (Jass and others, 2000; Kolb and others, 1999; McKiernan and others, 2000; Müller and others, 1999b; Schneider and others, 2000). Atomic force microscopy has allowed researchers to measure the material properties of many of these systems as well as examine their structure and morphology (Dufrêne and others, 1997; Karrasch and others, 1994; Osada and others, 1999).

AFM studies have not been limited to structure or topography. Local electrostatic properties have been studied with relative surface charge density maps of biological membranes (Heinz and Hoh, 1999a). Investigations into the interaction forces between nanometer-scale objects can be studied with AFM to map the spatial distribution of intermolecular forces (Heinz and Hoh, 1999b).

The technology of atomic force microscopy is the basis of a biosensor technology that uses cantilevers to detect the presence of cells, proteins, toxins, or DNA (Baselt and others, 1996:789; Tamayo and others, 2001). Although only in the experimental stages, force amplified biological sensors use surface antibodies to bind a biological species to the cantilever surface and identify the particular protein, virus, or bacterium (Baselt and others, 1996:789).

Overall, the level of sophistication of biological AFM studies has significantly increased over the past decade. This review touches on only a small portion of the work that has been done.

Atomic Force Microscopy Investigations of Bacteria. Microbial investigations using atomic force microscopy have been done on a variety of organisms (yeast, bacteria, and fungi). Most of this work involves studies of the vegetative form of the organisms.

Although no atomic force microscopy studies of bacterial spores were found in the literature, one researcher has done extensive work on fungal spores. The surface ultrastructure, molecular interactions, and physicochemical properties of spores of the fungus *Phanerochaete chrysosporium* have been examined by conventional and functionalized (self-assembled monolayers of organic thiols terminated with selected chemical groups on gold-coated probes) AFM probes (Dufrêne, 2000:3287; Dufrêne and others, 1999:5350). This work was done using contact mode atomic force microscopy in fluid. Information on surface morphology was derived from deflection images.

Fungal spores are spherical particles approximately 5 μm in diameter – slightly larger than bacterial spore (Dufrêne and others, 1999:5350). The surface of the fungal spores was described as "uniformly covered with a regular pattern of rodlets" (Dufrêne and others, 1999:5351). This work also documented the morphological changes that occurred on the spore surface during germination. Dufrêne was able to map the interaction forces between the spore surface and probes functionalized with different organic thiols. This allowed a more detailed study of the biochemistry of the surfaces and a fuller explanation of biological functioning on the spore surface.

Table 4 summarizes many of the atomic force microscopy studies done on microorganisms over the last eight years. Although many focus on surface structures, others use the versatility of AFM to measure properties and map certain interactions.

Table 4. Summary of AFM Studies of Microorganisms

Microorganism	*Focus of Study*	*Mode of Operation*	*Medium*	*Reference*
Escherichia coli	Imaging surface structure	Tapping	Air	(Shibata-Seki and others, 1994)
Deinococcus radiodurans	Imaging conformational changes in the hexagonally packed intermediate layer	Contact	Fluid	(Müller and others, 1996; Müller and others, 1999a)
Lactobacillus helviticus	Imaging bacterial surface features	Contact	Fluid	(Sokolov and others, 1996)
Methanospirillum hungatei	Measuring the elastic properties of the bacterial surface	Force Measure-ments	Air	(Xu and others, 1996)
Saccharomyces cerevisiae	Adsorption of metallic cations by the cell wall	Contact	Air	(De Souza Pereira and Teschke, 1997)
Magnetospirillum gryphiswaldense	Imaging, force mapping, determining the spring constant of the bacterial cell wall	Contact	Fluid	(Arnoldi and others, 1998)
Escherichia coli	Imaging surface morphology before and after exposure to antibiotics	Contact and Tapping	Air	(Braga and Ricci, 1998)
Bacillus subtilis, *Staphylococcus epidermis*, *Pseudomonas aeruginosa*, *Salmonella typhimurium*, *Escherichia coli*, and *Haemophilus influenzae*	Differentiating gram-positive and gram-negative bacterial cells based on surface appearance	Unknown	Air	(Umeda and others, 1998)
Halobacterium salinarum and *Deinococcus radiodurans*	Imaging protein surfaces	Contact and Tapping	Fluid	Möller and others, 1999
Microbes from the subglacial ice above Antarctic Lake Vostok	Imaging bacterial structure	Tapping	Unknown	(Priscu and others, 1999)
Escherichia coli and *Pseudomonas aeruginosa*	Thickness and elasticity of murein sacculi	Contact	Air	(Yao and others, 1999)
Staphylococcus aureus	Imaging structural differences between two strains	Contact	Air	(Boyle-Vavra and others, 2000)
Pseudomonas putida biofilms	Surface morphology, roughness, adhesion forces	Contact and Tapping	Air	(Auerbach and others, 2000)
Phanerochaete chryosporium spores	Surface ultrastructure of dormant and germinating spores, physicochemical properties of spores	Contact	Fluid	(Dufrêne and others, 2000; Dufrêne and others, 1999)
Sulfate reducing bacteria	Imaging and measuring bacterial adhesion forces	Contact	Air	(Fang and others, 2000)
Escherichia coli	High resolution images of bacterial surfaces	Contact	Fluid	(Kotra and others, 2000)
Streptococcus salivarius	Imaging and measuring cell surface softness	Contact	Fluid	(van der Mei and others, 2000)
Shewanella oneidensis	Measure forces between bacteria and mineral surfaces	Force Measure-ments	Fluid	(Lower and others, 2001)

Summary

The spores of closely related *Bacillus* species represent a novel system to be studied using atomic force microscopy. The bacterial species *Bacillus cereus*, *Bacillus thuringiensis*, *Bacillus anthracis*, and *Bacillus globigii* have each been thoroughly studied in previous works. However, this thesis effort takes an original approach by seeking to differentiate these four microorganisms through their spore surface morphology.

Atomic force microscopy (AFM) is a powerful tool for discerning the surface morphology of biological specimens as well as measuring local surface forces and mechanical properties of materials (van der Mei and others, 2000:2668). Biological processes can be imaged at the cellular and molecular level. AFM also enables the investigator to visualize samples in a liquid environment (that can be designed to model physiological conditions). Although several studies have examined the cell walls of bacteria, and one study has examined fungal spores, no known work has been done with AFM on bacterial spores (Dufrêne and others, 1999:5350).

III. Methodology

Experimental Overview

This methodology was developed to exploit the advantages of atomic force microscopy in the characterization of the surface morphology of spores of *B. cereus*, *B. thuringiensis*, *B. anthracis*, and *B. globigii*. It was desired to observe the spores *in situ*, which, in the case of these organisms, was in air under ambient conditions. Following growth and sporulation, the spores were mechanically cleaned in order to remove any debris left over from the vegetative cells. The spores were deposited on graphite substrates by spin coating. Samples of each species of spore were examined by TappingMode atomic force microscopy in a reduced humidity environment. The resulting images were analyzed for distinct surface features and species-specific trends in surface texture.

Microorganisms

Organisms of the genus *Bacillus* are the focus of this work. The choice of the four *Bacillus* species was based on their taxonomic complexities, practical significance, and availability of pure cultures.

All sterilization was done in Tuttnaur Brinkmann 3870 autoclave. The standard autoclaving procedure used in this work was 121°C and 15 psi for 15 minutes. No deviations were made to this sterilization protocol during this work.

Source. All organisms used in this work were provided by Dr. Eric Holwitt of the Air Force Research Laboratories, Biomechanisms and Modeling Branch, Brooks Air Force Base, Texas. The bacteria were obtained in the form of lyophilized spores. The spores were stored in the original glass culture tubes, in a locked cabinet, at room temperature.

The *B. cereus* used in this work was identified by Dr. Jill Parker (of the Air Force Research Laboratories, Biomechanisms and Modeling Branch, Brooks Air Force Base, Texas) as strain 569. The American Type Culture Collection lists this strain as a BioSafety Level 1 organism commonly used for assaying mixtures of antibiotics (Bacteria Collection Catalog, 2001).

The *B. thuringiensis* used in this work was the variant *kurstaki* (Kiel and others, 2000). This strain was isolated by Brooks personnel from the commercially available insecticide Javelin® (Ortho® brand, no longer manufactured). The American Type Culture Collection lists this strain as a BioSafety Level 1 organism that produces parasporal entomocidal protein crystals (Bacteria Collection Catalog, 2001).

The *B. anthracis* used in this work was the Sterne strain. The source of the organism was a veterinary, nonencapsulated, live culture of the anthrax spore vaccine (Thraxol-2 Code 235-23). According to the Center for Disease Control, the Sterne strain of *B. anthracis* should be handled in accordance with Biosafety Level 2.

Finally, the *B. globigii* used here was *Bacillus globigii v. niger* isolated from anthrax simulant material originally obtained from the U. S. Army at Dugway Proving Grounds (Kiel and others, 2000). The organism is non-pathogenic (Sharp and others,

1989: 281). This bacterial strain was not listed as an ATCC certified strain, but was handled in accordance with Biosafety Level 1.

Growth. Pure cultures of bacilli were grown from the lyophilized *Bacillus* spores, in slant tubes, on nutrient agar. For consistency, each bacterial culture was grown for seven days prior to harvesting the spores.

Nutrient agar was prepared by combining Bacto® Dehydrated Nutrient Agar (manufactured by Difco Laboratories) with sterilized Millipore filtered water in a 200 mL sterilized flask. The agar was prepared in accordance with the manufacturer's instructions, at a ratio of 23g dehydrated agar for 1 L water. The agar solution was then sterilized prior to use. Approximately 5mL of the hot agar was transferred into the glass culture tubes using a sterile 25mL glass pipet. The agar in the tubes was allowed to cool and harden at an angle (allowing for greater surface area for bacterial growth). The resulting slant tube was used for culturing all microorganisms used for AFM examination.

A sterilized wire loop was used to obtain a small amount of lyophilized spores from their storage container and suspend them in room temperature, sterilized, Millipore filtered water. The suspension was vortexed to homogenize the concentration of spores. The spores were allowed to activate in the water for 1-2 hours prior to plating in the culture tubes. A sterilized cotton swab was used to spread spore suspension across the agar in the glass culture tubes.

The cultures were maintained at 37°C in an incubator for 7 days. At the end of this period, the bacteria had exhausted the nutrients supplied by the agar and were nearly completely sporulated (as indicated by Gram staining). Several tubes of agar were left

blank and incubated along with the inoculated tubes in order to determine if any contamination had occurred during the culturing process.

Each strain of *Bacillus* was grown separately and at different times. Care was taken to eliminate the possibility of cross contamination. No two strains were handled together at any one time. The work area was thoroughly cleaned with bleach and detergent before and after all work with bacterial cultures.

A separate culture of each of the four microorganisms was grown on nutrient agar (20mL) in 100×15mm sterile, polystyrene petri dishes (Fisherbrand, Ct # 08-757-12) in order to document the growth characteristics of the bacteria. The bacteria were cultured directly from the lyophilized spores in a manner identical to that used to prepare the slant tube cultures. Growth was documented after seven days in a 37 °C incubator.

Gram Staining. In order to characterize the growth of the bacteria, a Gram staining procedure was used prior to harvesting. A small amount of bacterial growth was removed from one of the slant tube cultures, mixed into 100mL of Millipore filtered water, and heat fixed onto a glass slide. The Gram staining was done using a Fisher Diagnostics Gram Stain Set (Cat. No. SG 100D).

The following Gram staining procedure was used: (1) crystal violet solution applied for one minute, slide rinsed with distilled water; (2) iodine solution applied for one minute, slide rinsed with distilled water; (3) three to five drops of alcohol/iodine solution applied, slide rinsed with distilled water; (4) safranin counterstain applied for 15-30 seconds (McClung, 1952:21). As Gram-positive bacteria, the vegetative cells should appear dark purple. The spores are resistant to the stain and did not stain well.

Spore Harvesting. Harvesting of spores began with adding approximately 4mL of 4-10°C sterile Millipore filtered water to the glass culture tube containing the growth of microorganisms. The bacterial growth on the surface of the agar was removed by shaking and vortexing the tube to dislodge all material. Five tubes of organisms were harvested at once in order to produce a larger spore yield.

The suspension of bacterial material was collectively filtered in order to remove any vegetative growth or extraneous material. The spore solution was filtered with the aid of a hand vacuum pump through sterile cellulose number one filter paper (Whatman, 42.5mm, Cat No 1001 042). The suspension was filtered three times using 2 pieces of filter paper on the first two passes and one piece only on the third pass. A Drummond Pipet-Aid (Serial No D 95085) and 25 mL Disposable Serological Pipet (Fisher Scientific cat no 13-676-10K) were used to transfer the filtrate from the bottom of the filter to the top for another pass. The used pieces of filter paper were removed using sterilized forceps. Another pair of sterile forceps was used to replace the filter paper prior to each filtration pass. The final spore suspension was placed in a 15mL polypropylene conical tube (Falcon® 2097).

In order to further remove extraneous vegetative matter, the spore suspension was taken through a series of centrifugations and sterile water washes. First the spore suspension was centrifuged at 3000 rpm in a refrigerated centrifuge (Eppendorf 5810 R centrifuge) at 4°C for 10 minutes. The refrigeration was necessary to prevent spore activation or germination. The supernatant was discarded, 10mL of cold, sterile Millipore filtered water was added, and the suspension was vortexed to dislodge the pellet and thoroughly mix the spores. The suspension was again centrifuged at 3000 rpm and 4°C

for 10 minutes. Again the supernatant was discarded, 10mL of cold, sterile Millipore filtered water was added, and the suspension was vortexed. For the third time, the suspension was centrifuged at 3000 rpm and 4°C for 10 minutes. When completed, 6 mL of cold, sterile Millipore filtered water was added. A portion of the resulting spore solution was placed in the counting chamber (see below) in order to quantify the yield. The spore suspension was maintained in a refrigerator at 4°C in order to preclude germination. Samples were prepared immediately following harvesting to minimize storage time

Spore Counting. A Petroff Hausser Counting Chamber was used to quantify the spores in the final suspension. The intent of the spore counting was to provide an order of magnitude estimation of the number of spores present in the final spore suspension. This counting chamber uses a 0.02mm cell depth and an improved Neubauer, 1/400 square mm ruling pattern. The number of spores was counted in 12 of the 25 central small squares. The average number of spores was calculated and multiplied by 25 (for the 25 central small squares). This number was multiplied by 50,000 (to convert cell volume in mm^3 to mL). The result was the approximate number of spores per mL.

Sample Preparation

One of the advantages of atomic force microscopy is its ability to produce high-resolution images of a sample surface at ambient temperatures without fixatives, preservatives, coatings or a vacuum chamber. The sample preparation method was developed in order to exploit this advantage and to directly observe the natural spore surface structure.

Mounting the spores was a classic problem of mounting a particulate sample. The deposition process must result in a sufficient number of spores put down to facilitate the microscopy. Additionally, it was desirable to observe the spores individually, rather than in clumps. Finally, the adhesion between the spore and the substrate must be sufficient to prevent the spore from dislodging under the forces imparted by the AFM probe. After exploring several options, spin coating the spores from a suspension in sterile water onto freshly cleaved graphite was selected as the best method to for examination with AFM.

Substrate. The primary substrate material used in this work was graphite. This material proved to result in the best adhesion and distribution of spores following spin coating. Substrates were also prepared using mica and glass. However, the microscopy was done using primarily the graphite substrate. Some spore images mages were obtained of spores on the other substrates in order to ensure substrate choice was not interfering with observed spore surface morphology.

The graphite used in this work was Highly Ordered Pyrolytic Graphite (HOPG) (SPI Supplies, #440HP, lot # 1060521). Graphite was the primary substrate used here because of its highly hydrophobic nature (which matches the hydrophobicity observed in the spores). The graphite used in this work was ZYH Grade (SPI-3) with a 3.5° +/- 1.5° mosaic spread (this was a measure of just how ordered the graphite was). This grade has a grain size not larger than the range of 30-40 nm. This grade was much less highly ordered than other available grades. Because of the lower level of order, the individual "strippings" exhibited some population of "steps". The quality of the final surface was sufficient for this investigation, though. The graphite was cleaved with transparent adhesive tape just prior to coating and adhered to a steel puck using a sticky-tab.

Mica is the most popular substrate used in AFM work (Morris, 1999:57). It is widely available, inexpensive, and easily cleaved to produce thin crystalline plates that are atomically flat over large areas (several microns) (Morris, 1999:57). The mica used in this work was "muscovite" mica ($K_2O \cdot Al_2O_3 \cdot SiO_2$). Disks of 0.26mm research quality (grade V-5) mica (SPI supplies, #1871, lot # 1050802) were cleaved using sticky-tab adhesives immediately prior to the spin-coating process.

Finally, the use of circular glass coverslips (15mm, Electron Microscopy Sciences, Cat # 72196-15) was explored. The glass used in this case was German glass normally used for neural cell cultures. This glass was chosen because it has been shown to be more effective with hard to attach cells.

Spore Mounting. The spores were mounted on the graphite substrate using spin coating. A Photo Resist Spinner (Headway Research Incorporated Model 1-EC101-R285 Serial Number 21330) was used. The substrate was held in place by a vacuum. One hundred micro liters of the spore suspension was placed in the middle of the substrate. The sample was allowed to sit undisturbed for five minutes to allow time for spore adhesion. The sample was then spun at 500 rpm ramped up to 2000 rpm. The sample spun at 2000 rpm for one minute.

The sample was then removed from the spin coater and placed in a 50 × 11mm polystyrene petri dish (Fisher Scientific 09-753-53A). Figure 11 shows the final samples (imaged sequentially with identical microscope settings after all atomic force microscopy was completed). Images were taken using a Zeiss Stemi S6 Dissecting Microscope (Grid divisions equal 1/10"). The image shows a faint ring of light colored material indicating the area of the spores.

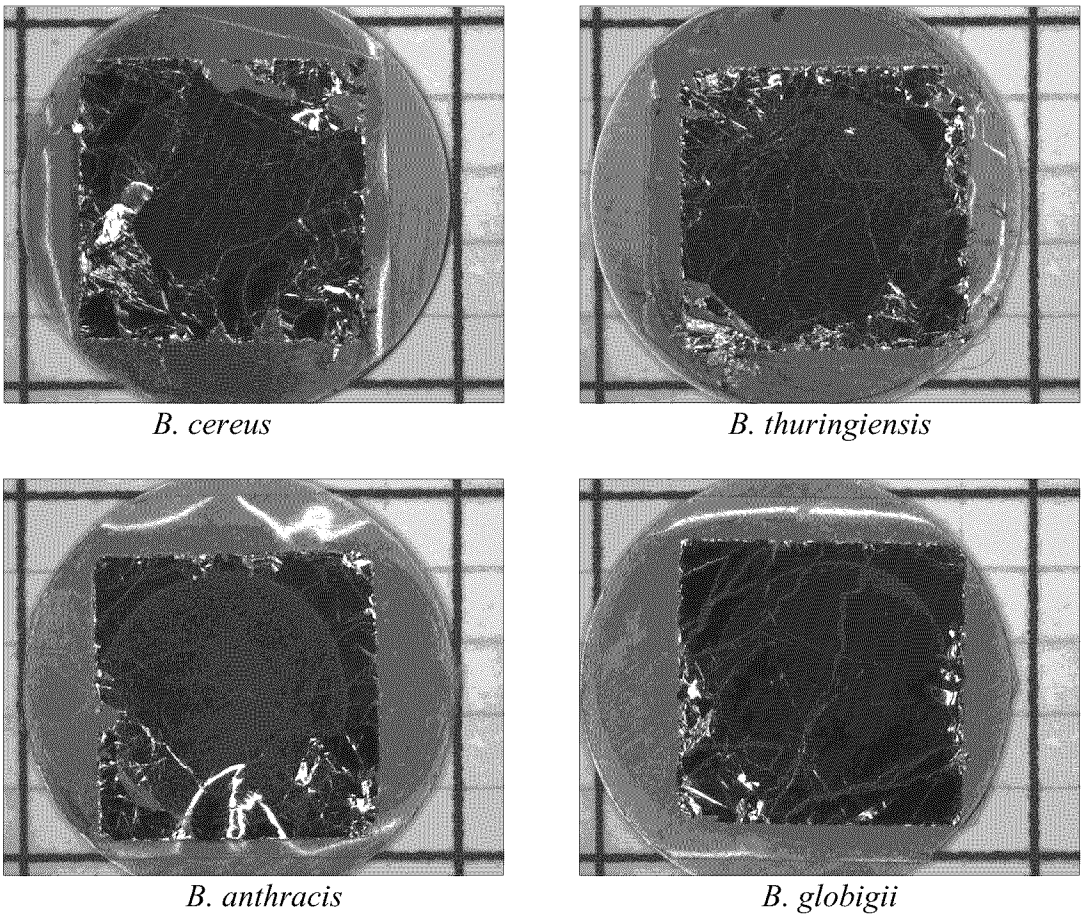

B. cereus *B. thuringiensis*

B. anthracis *B. globigii*

Figure 11. AFM Samples

Sample Handling and Storage. Samples were handled with a 15mm disk gripper (Ted Pella Incorporated) in order to prevent any physical contact with the surface. Samples were stored in 50 × 11mm polystyrene petri dishes. When not in use, all samples were stored in a glass desiccator (at room temperature) to minimize sample hydration and prevent spore germination.

Spores were examined up to eight weeks following sample preparation. There was no indication that conformational changes (including germination) had occurred. Further, it did not appear that examining the spores with the atomic force microscope resulted in any spores being dislodged from the substrate.

Atomic Force Microscopy

The atomic force microscope is a versatile tool that can be employed to characterize a surface in many of ways. Chapter 2 described the two primary employment methods: contact mode and TappingMode. Both of these techniques were tested in order to determine which produced the better images of the bacterial spore surfaces. As Figures 12 and 13 illustrate, TappingMode was the clear winner.

In Figure 12, contact mode was not able to resolve any detailed features of surface morphology. As illustrated in Figure 13, intermittent contact mode did reveal significantly more surface detail. Additionally, the use of phase imaging (only available with intermittent contact mode) allowed some measure of local surface properties not possible with contact mode imaging.

Microscope Configuration. The instrument used for this work was a NanoScope® IIIa Scanning Probe Microscope with a NanoScope® Optical Viewing System. The microscope was placed on top of a vibration isolation table. The microscope was positioned on a twenty-pound granite base, supported by four isolation pads designed to dampen vibration during scanning. An *x-y* translation stage was bolted to the top of the slab allowing for lateral positioning of the AFM. A camera optical assembly was mounted to a support pole above the AFM. The optical viewing system allowed the operator to see the sample area through a viewing aperture located on top of the AFM head. The microscope used for this work is shown in Figure 14.

Microscope Preparation. The selected sample puck was inserted onto the scanner tube using a disk gripper. The sample was held in place by an internal magnetic

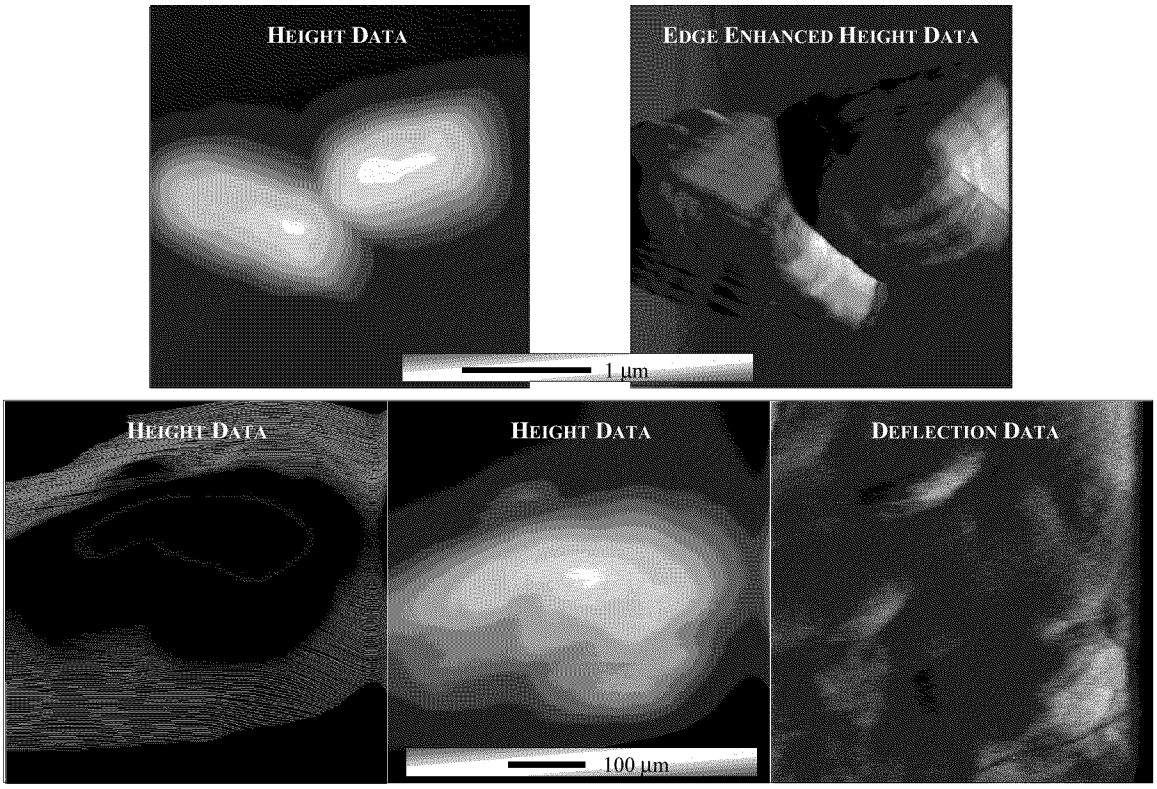

Figure 12. Contact Mode Atomic Force Microscopy Images of *B. cereus* Spore

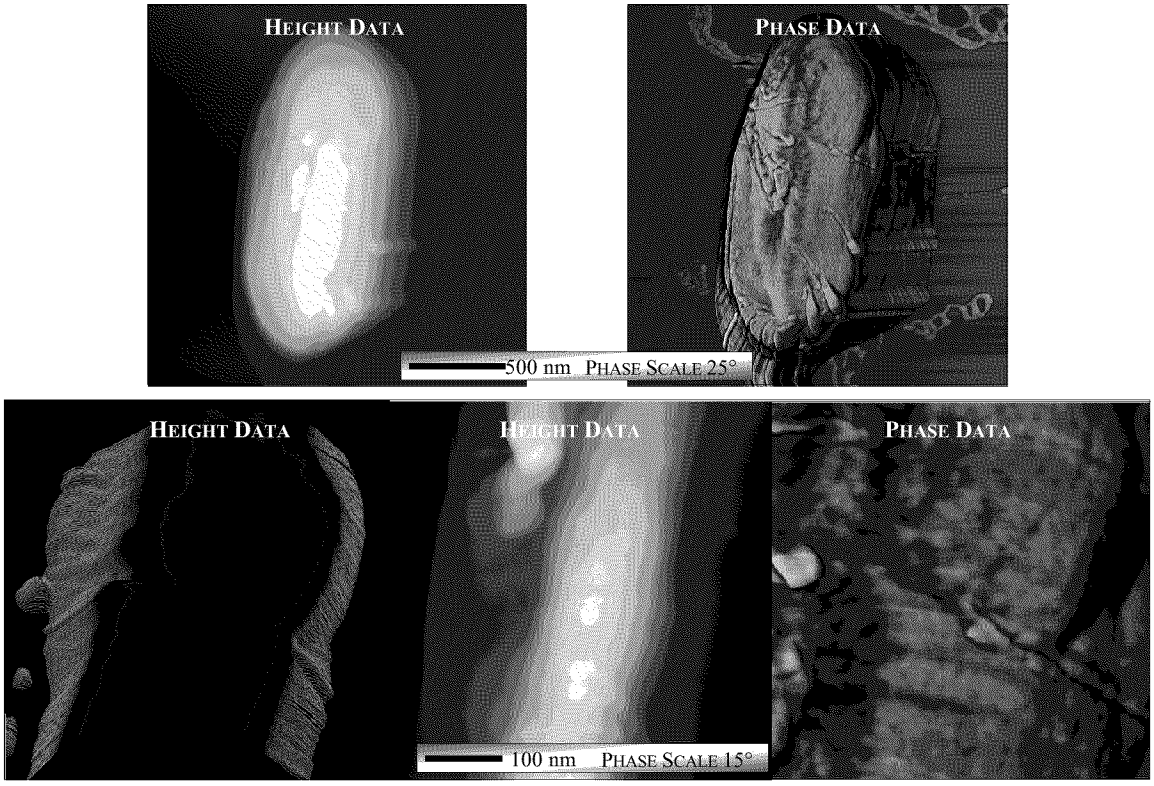

Figure 13. TappingMode Atomic Force Microscopy Images of *B. cereus* Spore

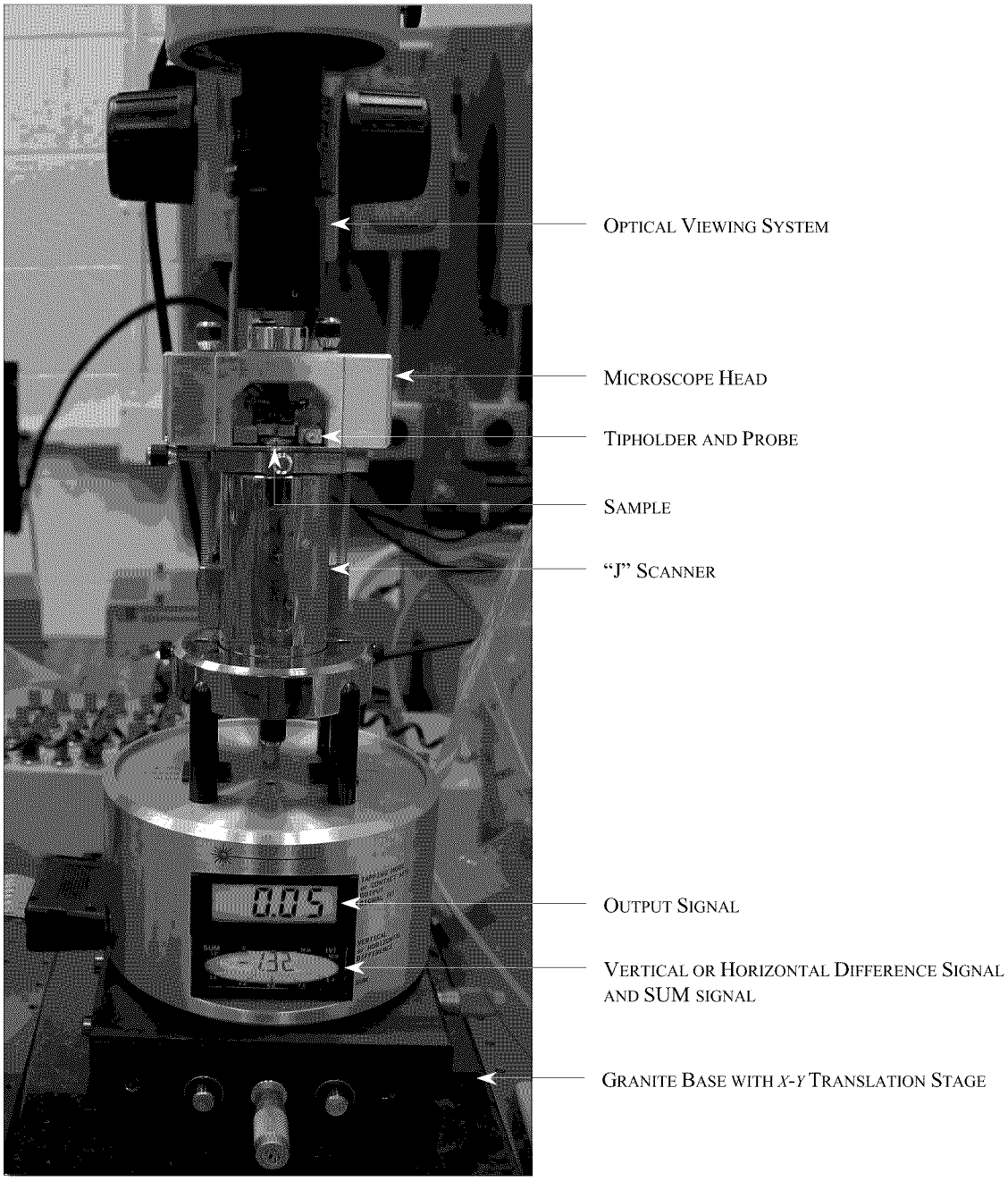

Figure 14. AFM Configured for TappingMode Operation

stage and aligned so as not to interfere with the position of the tipholder. The probe height was adjusted so that the tip rested just above the sample surface. Care was taken to ensure the tip did not impact the surface.

The selected probe was loaded into the tipholder with tweezers. Care was taken to prevent damage to both the substrate and the tip. The process was monitored using a 10×30 monocular (Specwell) and a Fiber Optic Illuminator (Model 190, Dolan-Jenner Industries, Inc.). The tipholder was inserted into the AFM head and the tipholder clamping screw was engaged. The probe was changed for each species in order to prevent cross-contamination.

The laser was aligned using the Optical Viewing System. The focus was adjusted to the sample surface. The cantilever height was adjusted so it rested just above the surface and slightly out of focus. Using the positioning screws, the laser beam was centered on the tip of the cantilever.

Next, the photodiode was positioned relative to the reflected laser beam. The mirror lever on the back of the AFM head was adjusted to maximize the SUM signal displayed on a elliptical bar graph on the bottom of the AFM. For contact mode operation, the SUM signal was adjusted to 5-9 volts. For TappingMode, the SUM signal was adjusted to 1-3 volts. The photodiode adjustment knobs are used to zero the top/bottom differential signal.

The photodetector was further adjusted with a detector offset signal that provided a "dynamic feedback signal for surface height tracking" (Multimode Manual, 1997:6-3). Corrections to this parameter were made prior to engaging the microscope and were not changed through the duration of the scan. For contact mode imaging the vertical

deflection signal was adjusted to –2.0 to –3.0 volts. For TappingMode, the vertical deflection signal was adjusted to ±1.0 volt.

The control settings are adjusted per the instruction manual and the specific sample being examined. In each case, settings were optimized to yield the clearest image possible. All settings were recorded.

Reduction of Humidity. In order to minimize the effects of any water vapor present on the sample surface, a crude humidity control chamber was employed while performing all spore scans. After a spore was isolated within the range of the AFM controls, a plastic bag was inserted over the microscope and secured around the microscope's base. Nitrogen gas (from a tank of liquid nitrogen) was introduced at < 5 psi. After purging the chamber for a few minutes, the flow of nitrogen was reduced and a low positive pressure of nitrogen gas was maintained throughout the remainder of the scan.

Characterizing Spore Surface Morphology. The surface morphology of the spores was characterized using TappingMode AFM. Images were obtained using scan rates of 0.5 Hz. The cantilever was tuned to resonant frequency by the Digital Instruments control software *Auto Tune* function. The values for the Setpoint and Drive Amplitude were selected by the computer and the controller during this routine were usually not altered throughout the scan. It was, however, sometimes necessary to optimize these parameters to improve image quality

The spores were visible on the Optical Viewing System monitor as small black spots. The cantilever was centered above one of these spots. It was first necessary "find" the spore. The scan size was decreased sequentially from 20μm^2 down to 1–2 μm^2 in

order to zoom in on the spore. Good images could not be obtained in TappingMode using scan sizes greater than approximately 5 μm. The spores were easily distinguishable from extraneous debris, vegetative cells, or other artifacts by their characteristic size and shape (ellipsoidal, 1-2 μm in length, 0.5-0.75 μm in diameter).

Throughout the scan, certain parameters were adjusted in order to obtain optimal image quality. The drive frequency was adjusted lower than the resonant peak of the cantilever so that it coincided with an approximate ten percent decrease in the vibration amplitude.

Several images were obtained from each spore at varying scales. At a minimum, the total spore was imaged at a scan size of 1.75–2 μm^2. Images of the spore surface were also obtained at scan sizes of 750 nm^2 and 500 nm^2.

Image Modification and Analysis

Once the atomic force microscope scanned a surface, the image data was captured in a digital file. These images contain a tremendous amount of information that must be interpreted and analyzed. The Digital Instruments Control Software offers several image modification and analysis options that were used to facilitate this interpretation. Further, the software allows several quantitative measures of surface characteristics to be determined. This allows a more rigorous analysis of the similarities and differences observed in the surface morphology of the different spore species.

Image Modification. It was often necessary to modify the images produced by atomic force microscopy scanning in order to enhance features, eliminate noise or scan lines, correct for bow and tilt, or isolate specific features. The following sections are an

explanation of the modification commands used by the instrument software, how the image data was manipulated, and what information was displayed in each image.

Edge Enhancement. The *edge enhance* command was used to "accentuate boundaries (edges) between dissimilar areas of an image" (Command Reference Manual, 1999:13-12). The *edge enhance* software routine "detects an image by applying Sobel kernels to 3×3 pixel cells" (Command Reference Manual, 1999:13-12). The form of these kernels was shown in Figure 15. The kernels (small matrices of numbers) are mathematically combined with the digital image data resulting in a maximal response along the vertical and horizontal grid of the images larger pixel array. The Sobel operator emphasizes regions of high spatial frequency that correspond to edges by performing a two dimensional gradient measurement on the image (Castleman, 1996:464-465). The Sobel operator was effective in enhancing edges, however, some loss of height resolution occurs (Command Reference Manual, 1999:13-12).

GRADIENT COMPONENT *X*-DIRECTION

-1	-2	-1
0	0	0
1	2	1

GRADIENT COMPONENT *Y*-DIRECTION

-1	0	1
-2	0	2
-1	0	1

Figure 15. Sobel Kernels used in *Edge Enhancement* Image Modification

The effect of edge enhancement on a height image is shown in Figure 16. Note the significant over-enhancement of the spore edges. Virtually all useful information is lost in these areas following edge enhancement. Also, edge enhancement results in a

different vertical scale than present in the original height image. Edge enhancement does accentuate the smaller features observed on the spore surface. The top view of the height data obscures these features to the point that they are not recognized.

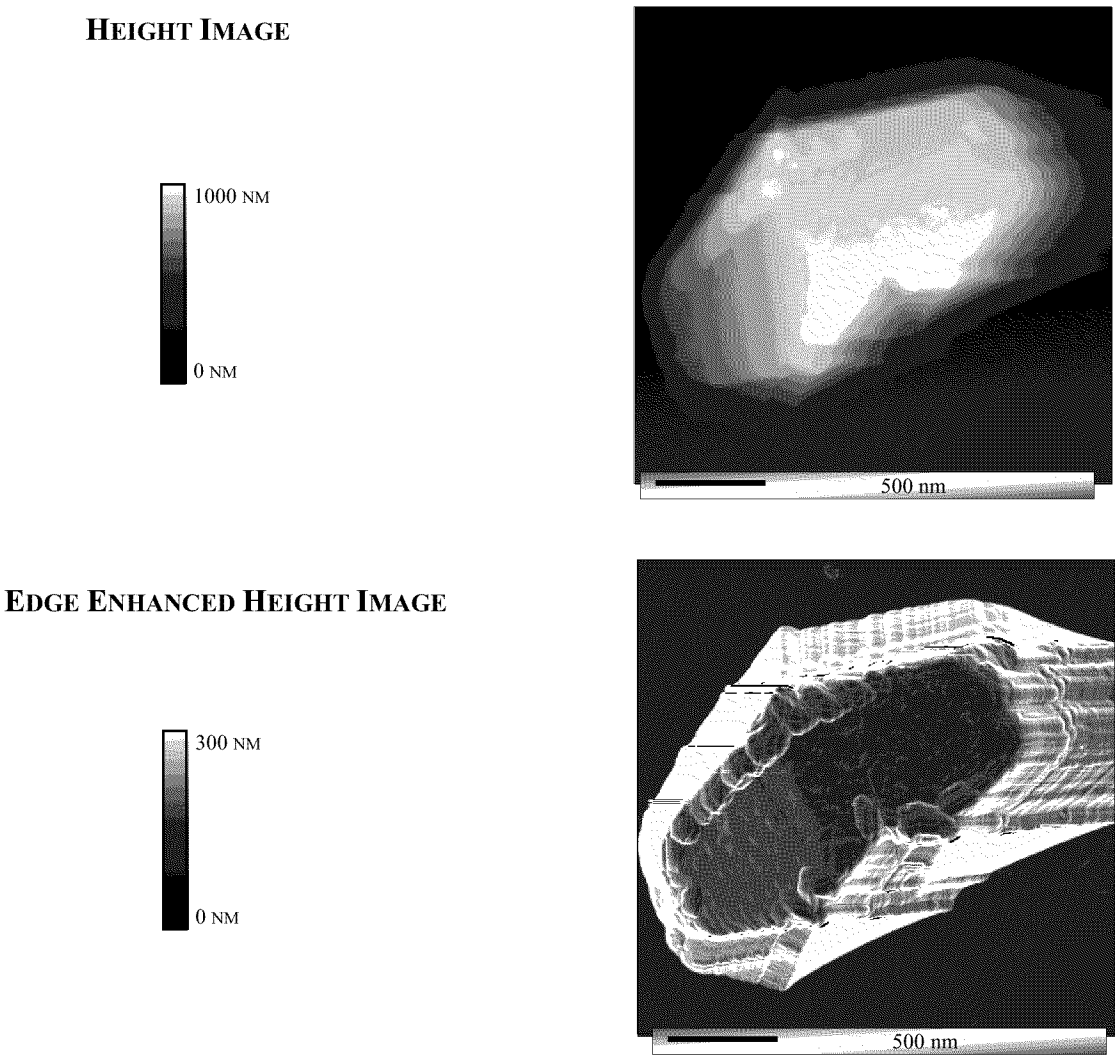

Figure 16. Effect of Edge Enhancement on Height Data
(*Bacillus thuringiensis* Spore 7)

Erasing Scan Lines. Occasionally during a scan, noisy scan lines appear in an otherwise acceptable image. The *erase scan lines* command was a software operation that replaces the line(s) by interpolation with neighboring data.

Flattening. The presence of a bacterial spore on a flat substrate surface produced a sporadic, tall feature in a predominantly flat area. The *flatten* command was used to eliminate unwanted features from a scan area. After masking the area of the image represented by the spore, the remaining portions of the scan lines are used to "calculate individual least-squares fit polynomials" (Command Reference Manual, 1999:13-18). These polynomials are subtracted from each scan line. Flattening an image alters the height characteristics of the original data (Command Reference Manual, 1999:13-19). The effect of flattening (first order) can be seen in Figure 17.

Plane Fitting. The *plane fit* command was used to correct for image distortions caused by tilt or bow. The software routine for this command calculates a single polynomial of selectable order for a given image. This polynomial was subtracted from each line in the image. The fit operation was applied along both the x- and y-axis. The effect of plane fitting (first order x-y) can be seen in Figure 17.

Image Analysis. The AFM software provides several methods by which the surface properties of a sample can be quantified. Two operations will be used in this work: surface texture analysis and section analysis.

Surface Texture Analysis. A surface is the actual boundary of an object and its environment (Dagnall, 1980:15). The texture of the surface describes its natural form and is defined as the composite of large and small irregularities (ASME B46.1, 1995:2). The small, finer irregularities are described by the surface's roughness.

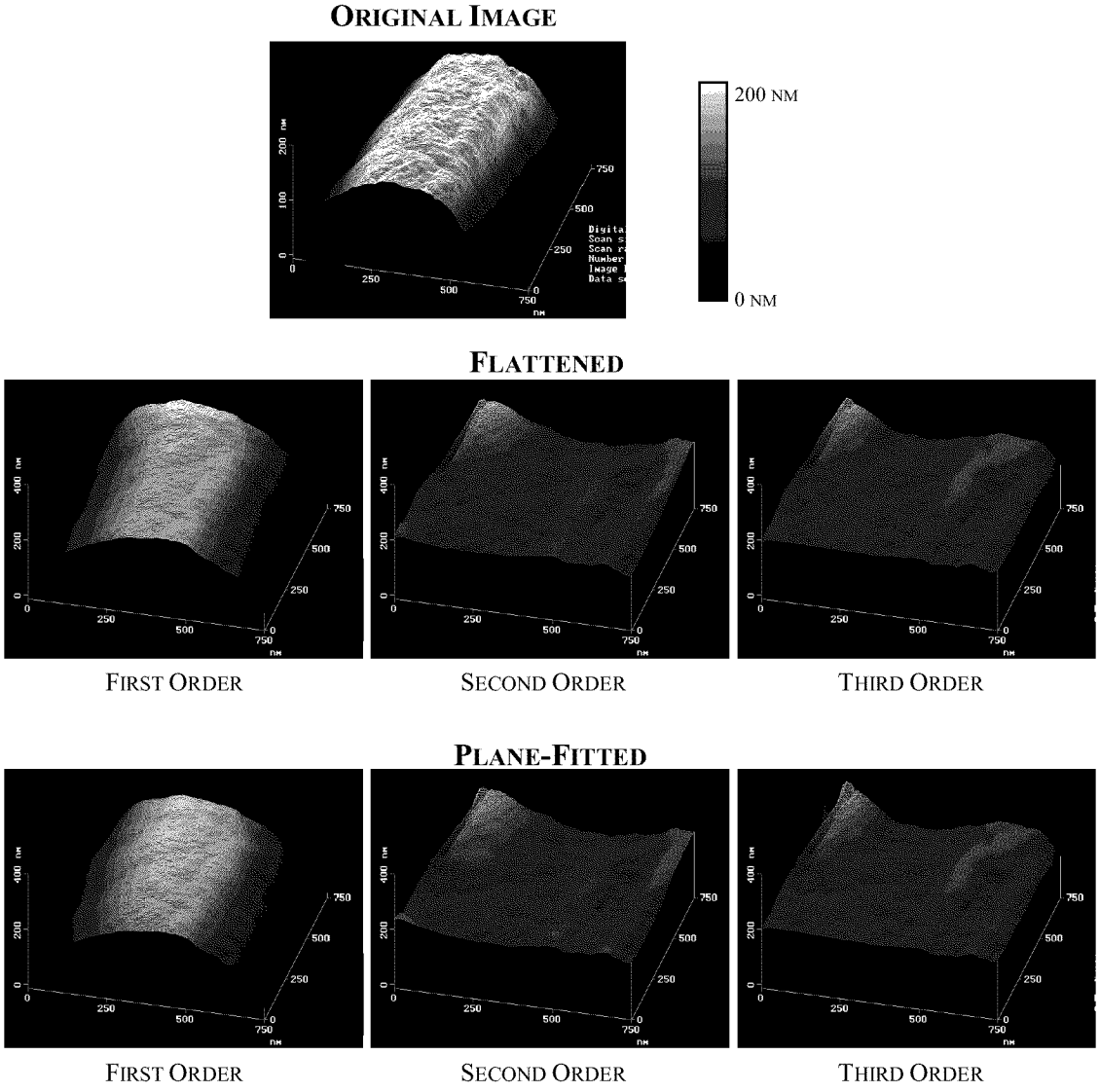

Figure 17. Effects of Plane-Fitting and Flattening Digital Images
(*B. globigii* Spore 5)

This analysis focuses on quantitatively and qualitatively describing surface texture using roughness, power spectral density, and bearing. Roughness analysis looks at a surface in terms of height deviations measured from a line of reference. Bearing analysis uses a histogram to represent the probability density of surface heights (ASME B46.1, 1995:11). The power spectral density is the Fourier decomposition of the measured surface profile into its component spatial frequencies (ASME B46.1, 1995:14).

Roughness Analysis. A roughness analysis was conducted on the five initial spore scans for each of the four bacterial species using the Digital Instruments AFM off-line analysis software. For consistency, the 750nm^2 scans were used. Each image was plane fitted (first order, *x-y*) prior to analysis. The image statistics were obtained by sampling with a 250 ± 2nm^2 box in five areas on the image. All sampling was done in the central region of the image in order to avoid distortions on the peripheral edge of the image. There was no sign of second or third order distortion indicating a need for a higher order plane fit or flattening.

Figure 18 shows the software interface used to complete the roughness analysis. The five white boxes indicate the five areas that were sampled on the spore surface.

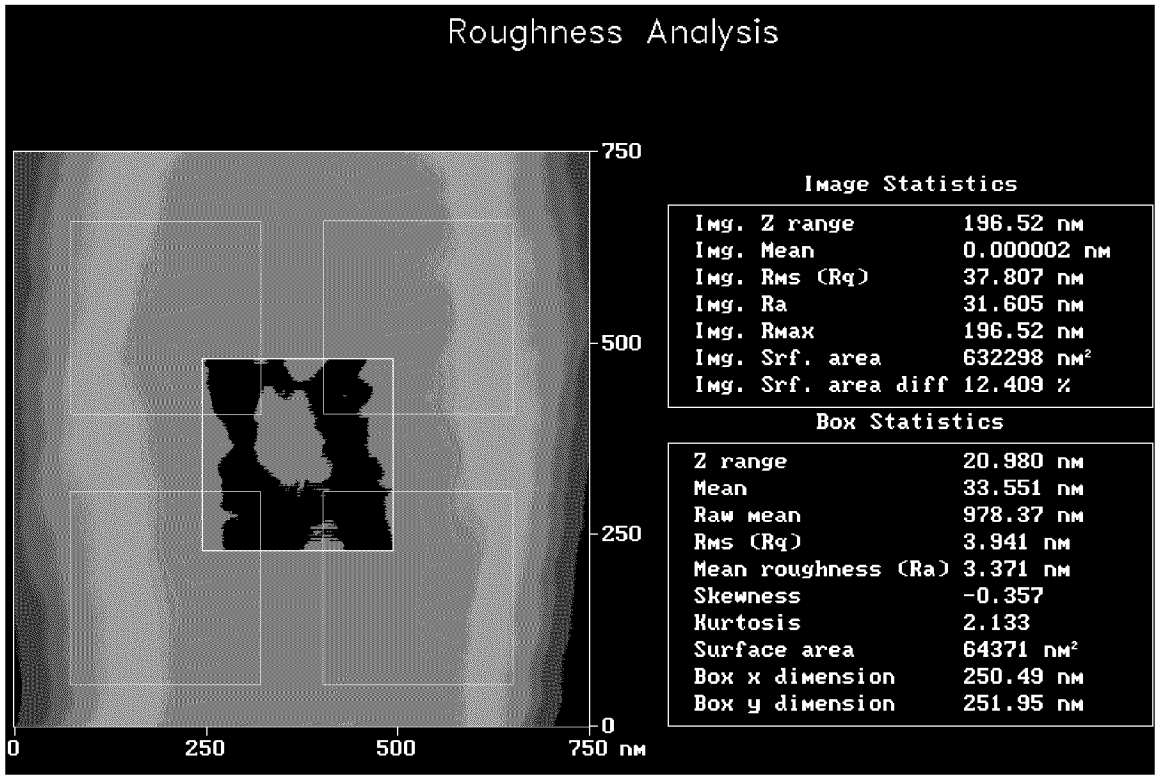

Figure 18. Roughness Analysis
(*B. anthracis* Spore 10)

The software has the capability to calculate 45 different parameters as part of the roughness analysis. Eight were chosen as a basis of comparison between the spores of the four different species: Z-range, surface area, mean, raw mean, mean roughness, RMS roughness, kurtosis, and skewness.

The *Z Range* was the peak-to-valley difference in height values within the analyzed region. This parameter provides an indication of the range of surface features in the area of analysis.

The three-dimensional area enclosed by the area of analysis was calculated by the *surface area* parameter. This value was the sum of the area of all of the triangles formed by three adjacent data points.

The *mean* and *raw mean* are measures of the average height across the surface. The average of all of the *Z* values within the analyzed area was the *mean*. The *mean* can be positive or negative because the *Z* values are measured relative to the z value when the microscope was engaged. This value was altered due to the plane fitting applied by the software in order to correct for the tilt in the plane of the data. The *raw mean* was the average of all of the *Z* values within the analyzed area without application of plane fitting.

The arithmetic average of the absolute values of the surface height deviations measured from the mean plane in the area of analysis was the *mean roughness* (R_a).

$$R_a = \frac{1}{L_x L_y} \int_0^{L_y} \int_0^{L_x} \left| f(x,y) \right| dxdy$$

Where: $f(x,y)$ = Surface relative to the center plane

L_x, L_y = Dimensions of the surface

The standard deviation of all of the *Z* values within the analysis area was calculated as the *RMS* (R_q). This value was also not corrected for tilt in the plane and will be affected by plane-fitting.

$$R_q = \sqrt{\frac{\sum \left(Z_i - Z_{avg}\right)^2}{N}}$$

Where: Z_{avg} = Average of the Z values within the given area

Z_i = Current Z value

N = Number of points within the given area

The *kurtosis* was a non-dimensional quantity that was used to evaluate the shape of the data about a central mean. It was a measure of whether the data are arranged flatly or sharply about the mean.

$$Kurtosis = \left\{ \frac{1}{N} \sum_{j=1}^{N} \left[\frac{x_j - \bar{x}}{\sigma} \right]^4 \right\} - 3$$

Where: σ = Standard deviation

Skewness was a measure of the symmetry of surface data about a mean data profile. This parameter can be positive or negative. When *skewness* was zero, an even distribution of data around the mean was suggested. When *skewness* was strongly non-zero, an asymmetric, one-tailed distribution was suggested (such as a plane with a sharp spiked or deep pit feature.

$$Skewness = \frac{1}{R_q^{\,3}} \frac{1}{N} \sum_{j=1}^{N} R_j^{\,3}$$

Where: R_q = RMS roughness

The eight parameters used to measure surface roughness offer quantitative insight into one aspect of surface texture. The power spectral density and bearing analysis were used to augment this analysis for a fuller picture of the character of the spore surfaces.

Power Spectral Density. The Power Spectral Density (PSD) is a function used for analyzing surfaces with periodic features. Power is roughness amplitude squared (in units of length squared). The power spectrum is a plot of power as a function of spatial wavelength or frequency. The Digital Instruments software was used to calculate a two-dimensional isotropic power spectral density for five samples of each species of spore at the $500nm^2$ image size. Only the first five spores of each species were examined because that was the maximum number of spores that could be compared at one time through the software.

A power spectral density (PSD) transforms a surface's real spatial elements (in three dimensions) into an array of spatial frequency constructs (sine waves of different spatial frequencies) using Fourier transforms.

The frequency distribution is approximated by the software by:

$$PSD(f) = \frac{2d_0}{N}\left|\sum_{n=1}^{n=N} e^{\frac{i2\pi}{N}(n-1)(m-1)} z(n)\right|^2 \qquad \text{for:} \quad f = \frac{m-1}{Nd_0}$$

Where: L = Length of the digitized profile

N = Number of points sampled

d_0 = Sampling interval

i = $\sqrt{-1}$

f = Frequency range from $\frac{1}{L}$ to $\frac{N/2}{L}$

The goal of this analysis was a plot of two-dimensional isotropic PSD versus wavelength for each spore sample surface. "Isotropic" refers to an average taken over all directions of the data. The two dimensions are the lateral *x-y* directions. The software calculates several other measures of power spectral density. The two-dimensional isotropic PSD was chosen because of its application over both lateral dimensions. The 2D isotropic PSD is obtained from:

$$2D\ isotropic\ PSD \quad = \quad \frac{P}{2\pi f(\Delta f)}$$

Where: P = Power, derived from squaring the FFT of the image

Figure 19 shows the software interface used to analyze the power spectral density of the spore surfaces.

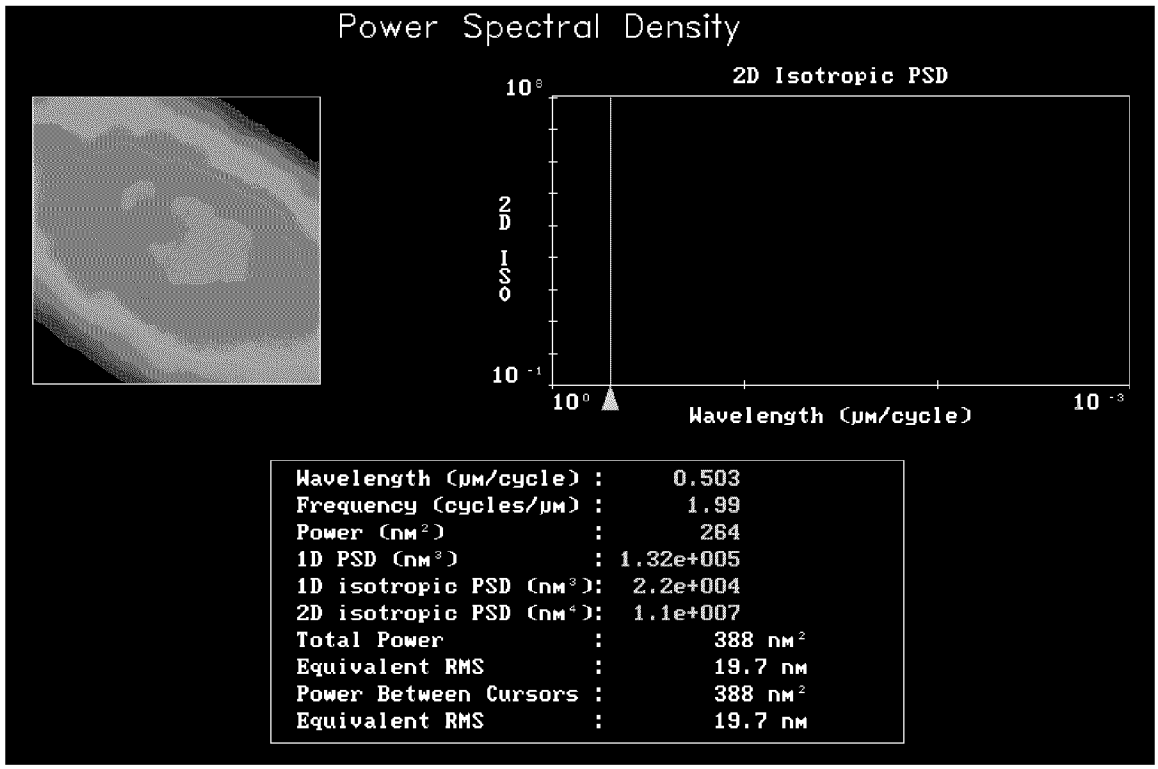

Figure 19. Power Spectral Density Analysis
(*B. anthracis* Spore 4)

Bearing Analysis. Bearing analysis provides a means to study the distribution of surface height over a sample. Bearing reveals the amount of a surface that lies above or below a given height. The Digital Instruments AFM software off-line analysis software was used to generate histograms based on the number of pixels that occur at various *Z* heights.

For consistency, the 500nm^2 scans were used. Each image was plane fitted (first order, *x-y*) prior to analysis. The image statistics were obtained across the entire image area without sampling.

Figure 20 shows the DI software interface for the bearing analysis.

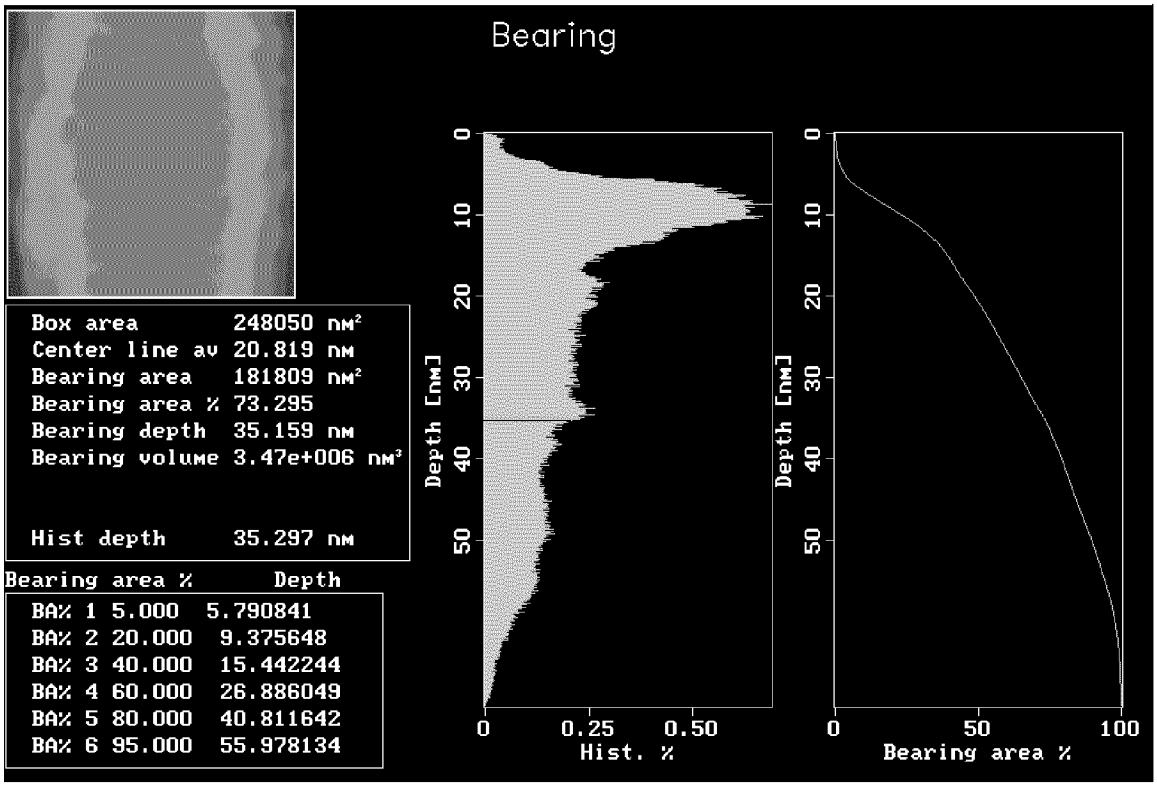

Figure 20. Bearing Analysis
(*B. anthracis* Spore 2)

Section Analysis. A section analysis was used as a tool for obtaining information regarding the topology of a spore surface. This analysis does not reveal features below the surface. The section analysis of spores clearly shows the convolution of probe tip and spore at the edges of the spore.

Figure 21 shows the Digital Instruments software interface for the bearing analysis.

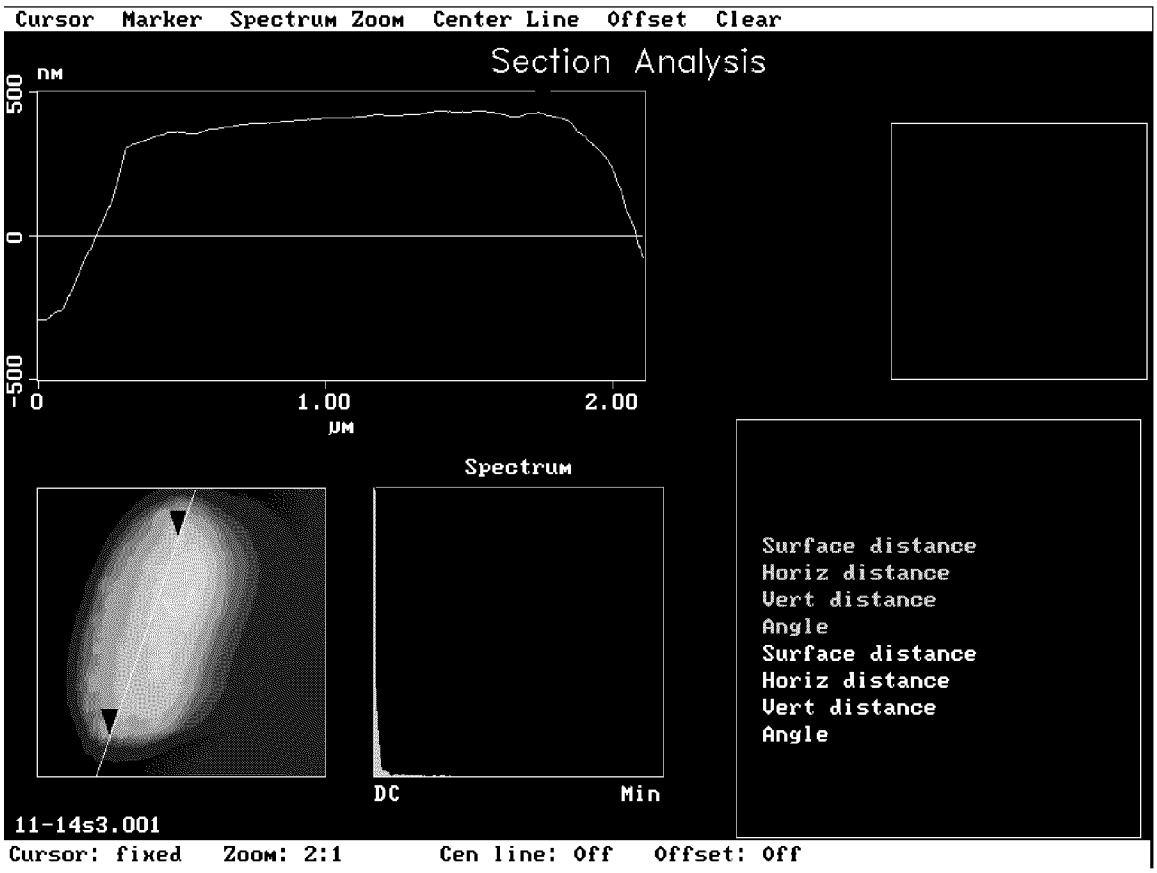

Figure 21. Section Analysis
(*B. thuringiensis* Spore 3)

IV. Results and Analysis

Overview

Results primarily consist of images of spores acquired from atomic force microscopy. These are digital images compiled from different types of information obtained during each AFM scan. As such, the images can be examined both qualitatively and quantitatively. Both types of results are presented here as well as an interpretation and analysis in the context of the stated research objectives. The surface morphology of a total of thirty-seven total spores of *B. cereus*, *B. thuringiensis*, *B. anthracis*, and *B. globigii* are presented.

Observations on Growth, Harvesting, and Sample Preparation

The growth, harvesting and sample preparation proceeded as outlined in the previous chapter. None of the blank agar tubes used for quality control purposes showed any sign of growth and no signs of cross-contamination were ever noted.

Growth on plates of nutrient agar showed characteristic colonies for each bacterial strain. Cultures were incubated for seven days at 37°C to produce the colonies shown in Figure 22. The larger colonies observed in the case of *B. cereus* and *B. thuringiensis* are likely due to motility of the vegetative cells not present in *B. anthracis* or *B. globigii*. The darker color of the *B. globigii* is indicative of the black-pigmented *B. globigii* var. *niger* (Nakamura, 1989).

BACILLUS CEREUS

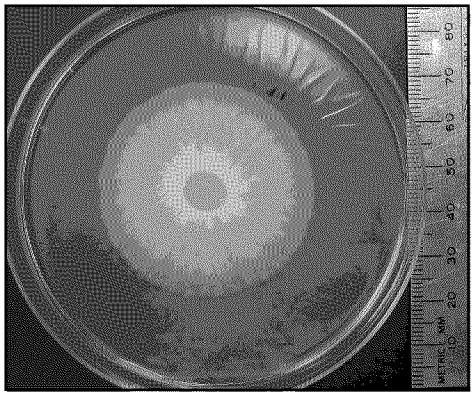

BACILLUS THURINGIENSIS

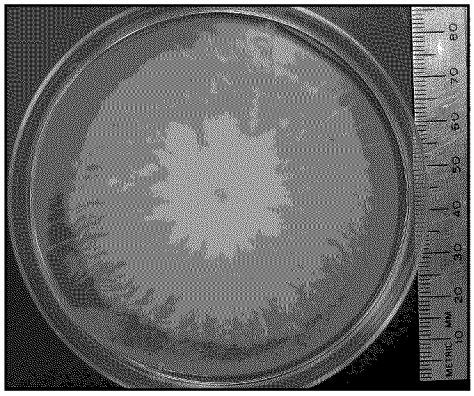

BACILLUS ANTHRACIS

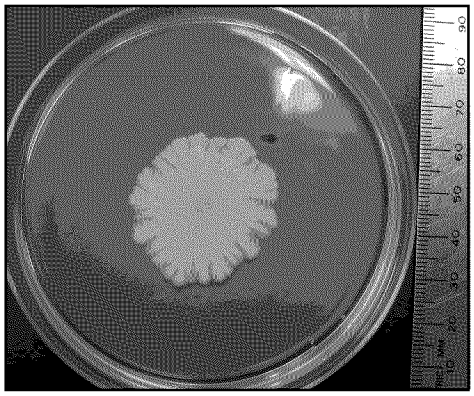

BACILLUS GLOBIGII

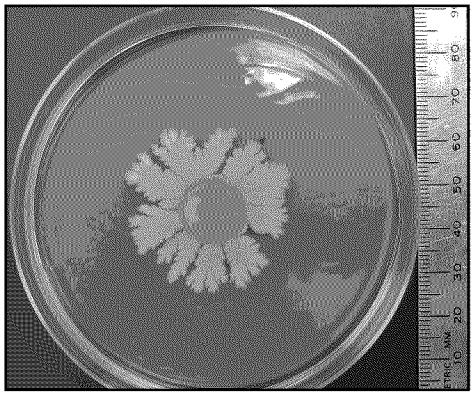

Figure 22. Comparison of Colony Morphology

After seven days of incubation, Gram stains of each culture showed significant sporulation, although some vegetative cells were also observed. The final concentration of spores post-harvesting was on the order of 10^8 spores/ml (consistent for each of the four bacterial species).

Each sample was examined using the NanoScope® Optical Viewing System. The bacterial spores, as well as other unidentified material, were clearlyvisible as small, dark spots that easily contrasted with the light appearance of the graphite substrate. In each case, the overall characteristics of the sample surface proved suitable for imaging individual spores of each species. The graphite substrate was not perfectly flat. Ripples, clefts, and other imperfections were observed optically. However, none of these flaws proved problematic on the scale of a single spore.

The *B. cereus* sample produced the largest population of individual spores with no extraneous material observed on the substrate surface. The individual spores were clearly visible as small black circular objects. Several clumps of spores were visible as larger black dots.

The *B. anthracis* sample appeared to be covered by a slightly lower population of individual spores. However, long, string-like features, as well as clump-like features, were observed on the *B. anthracis* sample.

The *B. globigii* sample had a moderate population of spores. The *Bacillus globigii* sample did not show any clumps of spores or other non-spore features.

B. thuringiensis had the lowest concentration of spores. Clumps of spores were clearly visible, as well as features that appeared to be filaments of vegetative growth.

Imaging Issues

Several imaging issues presented themselves while characterizing the spores. Each issue derived directly from the fact that the atomic force microscope images the interaction between probe and surface. The image reflects the real properties of the sample surface as well as the real properties of the sharp, silicon probe, the piezoelectric scanner, the photodiode detector, the integrated control and feedback system, the atmospheric conditions in the immediate vicinity of the sample surface and the probe, as well as the microscope settings imparted by the operator. All of these factors contribute to the resulting image.

First, the height of the spores was significant when compared to the length of the tip. This resulted in a convolution. This term is used to describe the image that results from the interaction of the geometry of the probe and the geometry of the feature being scanned. In this case, there is a convolution of the tip and sample along the edges of the spore. The angle of the tip relative to the spore is not symmetrical, resulting in elongated edges on the right side of the spore and a clear edge on the left side of the spore. This effect is illustrated in Figure 23. In Figure 23A, the probe is shown as it scans across the spore (not to scale). Although slightly exaggerated for clarity, the results of the convolution are seen in the images of *B. globigii* spore 4. The convolution causes only the top portion of the spore to be reliably imaged. Significant distortion is observed at the edges of the spore images. The geometry of the probe results in different distortions on different sides of the spore. This distortion is demonstrated by a three-dimensional line plot (Figure 23B), a top view of the phase image (Figure 23C), and a cross section of the height image (cross section in Figure 23D, top view of height image in Figure 23E).

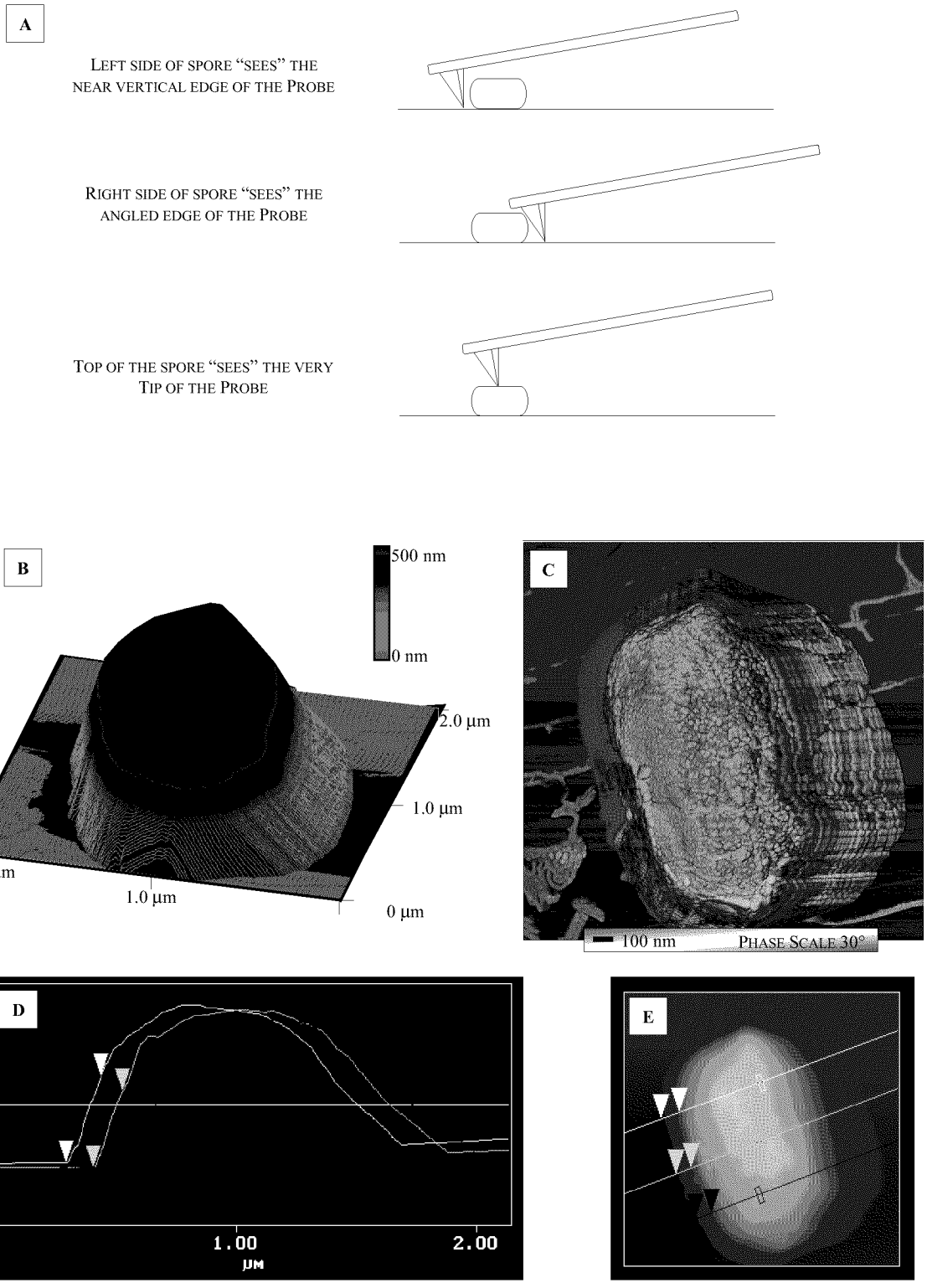

Figure 23. Tip Convolution with Bacterial Spore
(*B. globigii Spore 4*)

The second imaging artifact common to this work is a "blind area" observed on several of the phase images. This is illustrated on both sides of the spore in Figure 24. These areas show a distinct lack of phase contrast. These blind areas of a scan that corresponded to edges or around features that were vertically distinct from the usual surface structure. Further, these areas were influenced by different microscope settings such as the direction of the data (trace or retrace) and drive frequency. When encountered, every attempt was made to minimize the size of the blind areas by optimizing microscope settings. However, in some cases complete elimination of the areas was not possible.

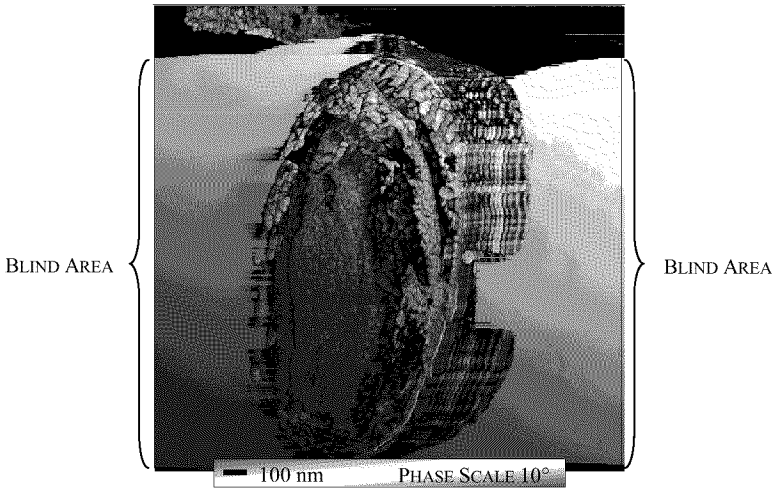

Figure 24. "Blind Area" on Phase Image
(*B. thuringiensisi Spore 4*)

The third image anomaly encountered was a distortion when sequentially smaller scan sizes were employed. Each fully characterized spore was imaged using scan areas of 1.75-2.0μm^2, 750nm^2, and 500nm^2. Smaller scan areas produced slightly distorted images with features that did not exactly correspond to features observed in images

produced by larger scan areas. Although subtle, this warping can be observed in the images presented in Figure 25. The $250nm^2$ image does not correspond to an equal area on the $500nm^2$ image directly above. It appears that the area represented as square in the $250nm^2$ image is rectangular in the $500nm^2$. Figure 26 shows the same areas on the same spore examined with the Digital Instruments software *zoom* command that interpolates image data to magnify a portion of an image to a larger size.

This distortion could be attributed to non-linearity in the piezoelectric scanner at small scan sizes. The calibration grid used in this work ($10\mu m \times 10\mu m$) was too large for an accurate calibration on the scale of the spores observed in this work. Further, the AS-130 "J" scanner is a larger scale scan size scanner at $125\mu m \times 125\mu m$.

It is also possible that the surface itself is distorting due to scanning. The pliable nature of a biological surface could be warping under the forces of the probe localized over a small surface area combined with the theoretical "looseness" of the exosporium.

Although the precise cause of the distortion is not known, the value of information below $500nm^2$ scan sizes appears limited. Some images were still captured at $250nm^2$. These should be interpreted with care.

Overall, the quantitative measurement of the size of features cannot be assumed to be completely accurate. This problem is compounded when trying to compare features from two different spores, scanned on different days, with different controller settings, and different probes. Further, the magnitude of the predicament is unknown.

Overall, some high quality images resulted from this work. Each image should be interpreted with due care, for what is seen may not be what is actually present on the real surface. Controlling for these problems and quantifying their size is not a trivial problem.

500NM^2 SCAN SIZE
PHASE IMAGE

RECTANGLE INDICATES
APPROXIMATE AREA OF
250 NM^2 PHASE IMAGE

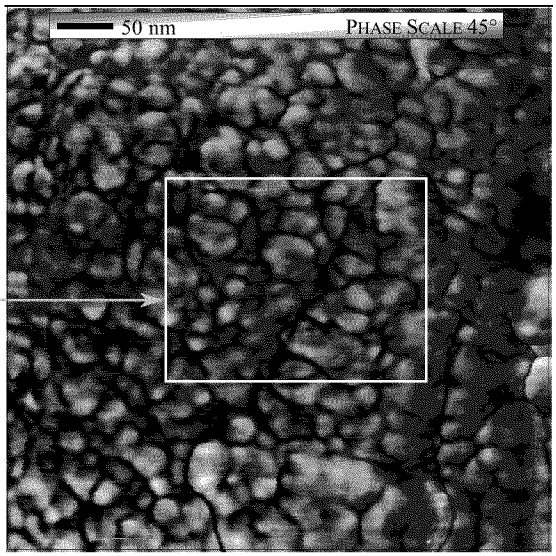

250NM^2 SCAN SIZE
PHASE IMAGE

RECTANGLE INDICATES
APPROXIMATE AREA OF
150 NM^2 PHASE IMAGE

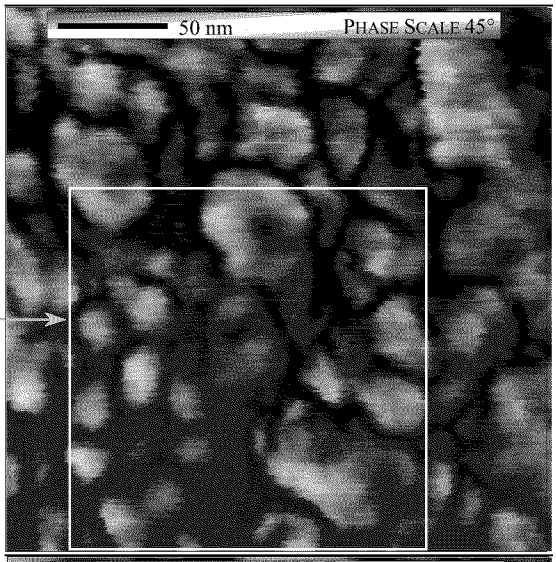

150NM^2 SCAN SIZE
PHASE IMAGE

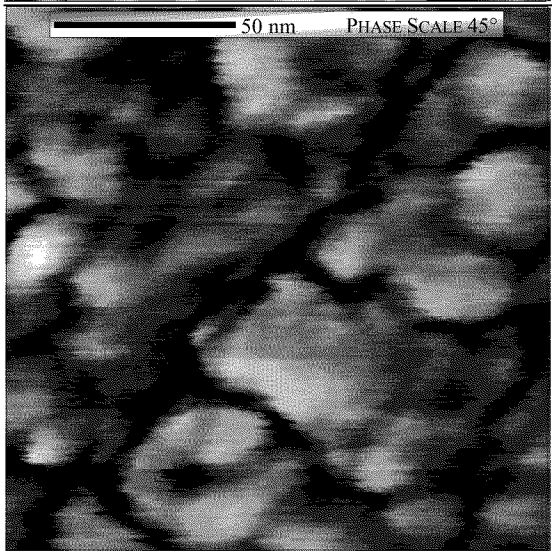

Figure 25. Image Distortion Using Sequentially Smaller Scan Sizes
(*B. globigii Spore 3*)

499.5 NM^2 IMAGE SIZE
ZOOMED FROM
750NM^2 SCAN SIZE
PHASE IMAGE

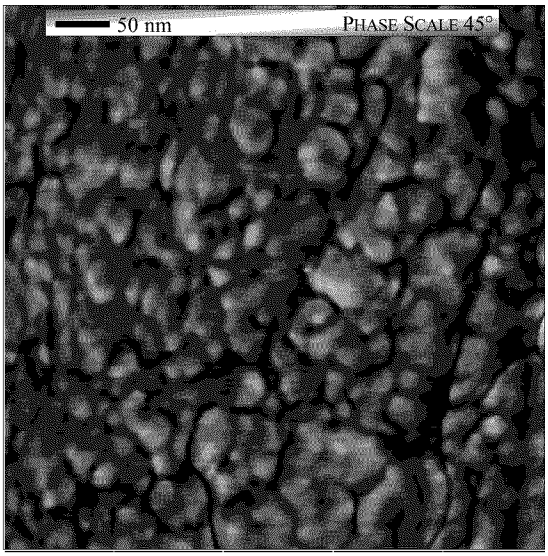

251.0NM^2 IMAGE SIZE
ZOOMED FROM
500NM^2 SCAN SIZE
PHASE IMAGE

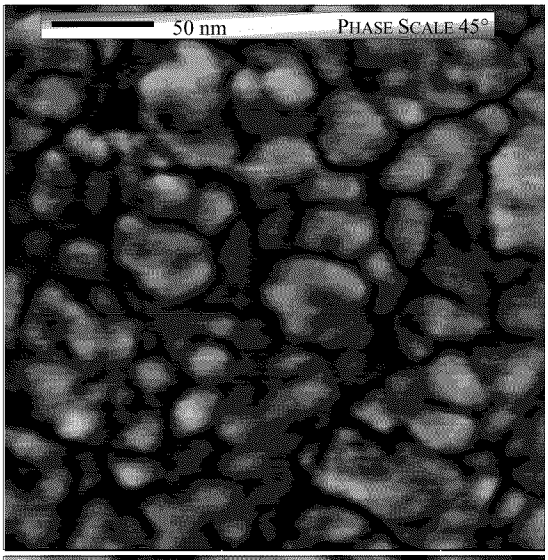

166.5 NM^2 IMAGE SIZE
ZOOMED FROM
500NM^2 SCAN SIZE
PHASE IMAGE

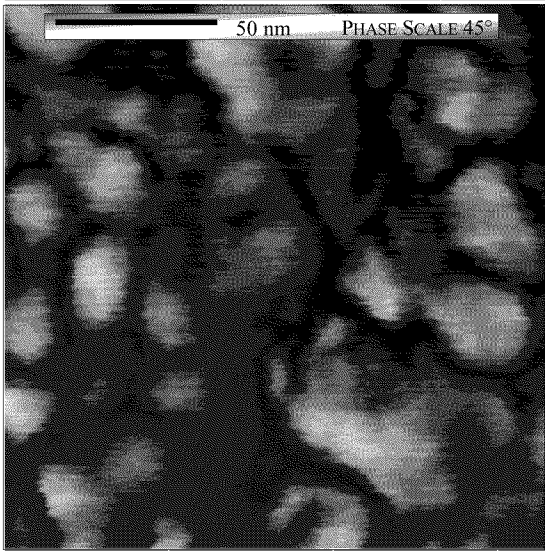

Figure 26. Software Image Magnification
(*B. globigii Spore 3*)

Image Reliability and Quality

In order to ensure the images obtained represented the actual structure of the spore, several tests were performed. Overall, the repeatability of surface features and the clarity of the images engendered a high degree of confidence in the ability of atomic force microscopy to produce reliable images of the surface morphology of the bacterial spore.

First, there was never an indication that the tip damaged the surface of the spore in spite of repeated scans over long periods of time (up to four-five hours). The images obtained remained relatively stable over the range of scan sizes from 500nm to greater than 2μm. As discussed earlier, this was not the case for scans less than 500nm.

Machine parameters can have significant impacts on any AFM image. For all images obtained, microscope settings were optimized to obtain the clearest image possible. Often, parameters would be changed while scanning the same spore to optimize the image at any given scale. Also, the resonant frequency of the cantilever would change during a scan (observed by comparing the resonant frequency before and after scans). This change was most likely due to the humidity reduction.

Spores were identified based on their characteristic shape and size. Occasionally, a scan would result in a feature that did not resemble a spore. Several of these unidentified features are shown in Figure 27. It is believed that these features are extracellular debris produced during the sporulation process (in the case of A and B) or bacterial cells that either did not sporulate or have germinated (in the case of C and D). In the case of the two putative vegetative cells, the lack of tip-sample convolution on the edges of the feature indicates the feature is significantly smaller in the vertical plane than an average spore.

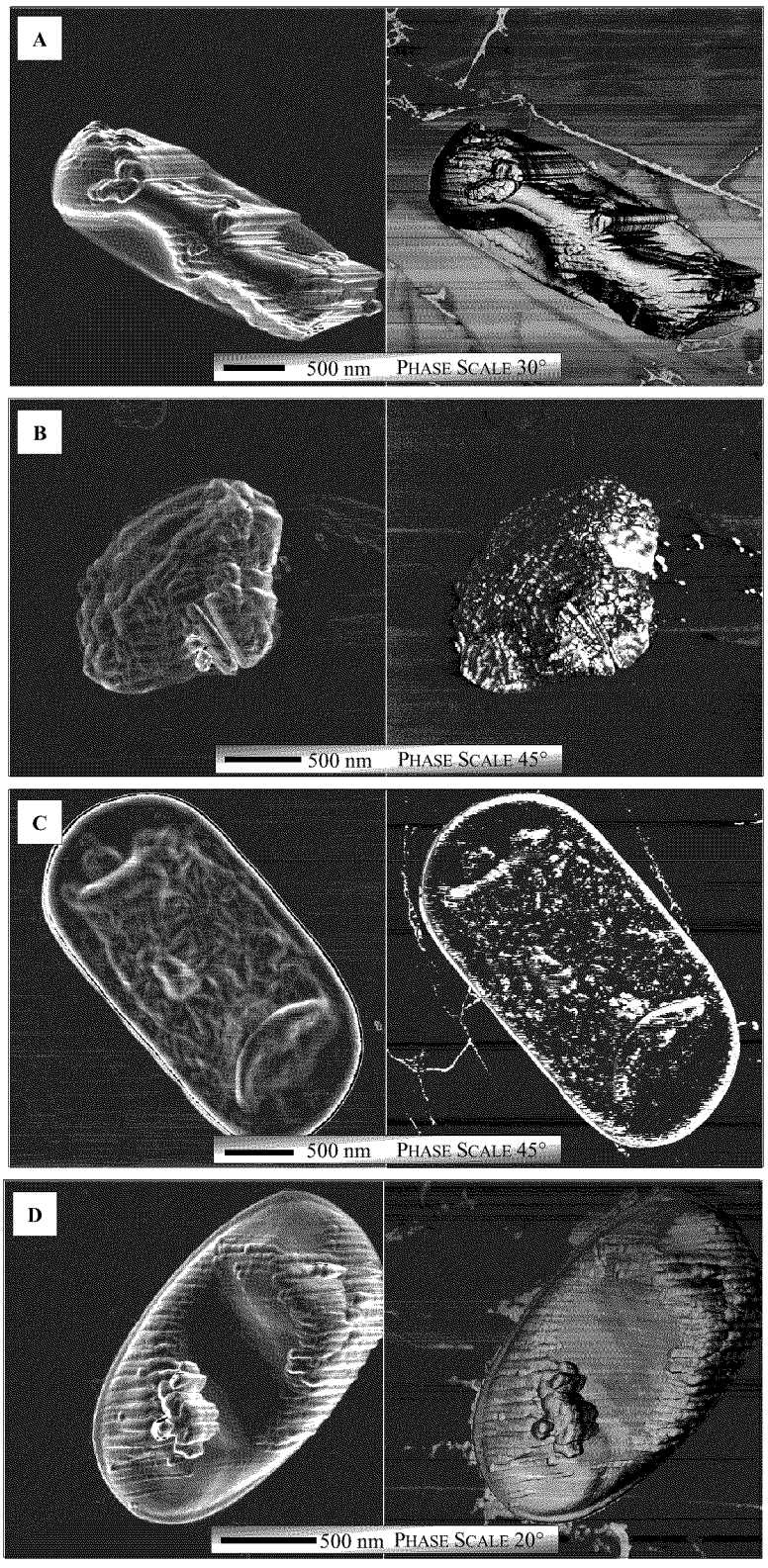

UNIDENTIFIED FEATURE OBSERVED ON *B. ANTHRACIS* SAMPLE (MICA SUBSTRATE)

UNIDENTIFIED FEATURE OBSERVED ON *B. ANTHRACIS* SAMPLE (MICA SUBSTRATE)

APPARENT VEGETATIVE CELL OBSERVED ON *B. GLOBIGII* SAMPLE (GRAPHITE SUBSTRATE)

APPARENT VEGETATIVE CELL OBSERVED ON *B. GLOBIGII* SAMPLE (GRAPHITE SUBSTRATE)

Figure 27. Non-Spore Features
(Height Images Edge Enhanced)

Characteristic Surface Morphology

Atomic force microscopy images of spores are presented on three scales: complete spore, 750nm^2 scan size, and 500nm^2 scan size. The full spore images are shown as edge enhanced images of height data and as corresponding images of phase data. The other scan sizes are shown as surface graphs of height data (*y* axis is pitched at 60°) with corresponding images of phase data. Results are presented as raw data (no plane fitting, flattening or other image modifications other than edge enhancement).

Each spore was assigned a number designator (one through seven for *B. cereus* and one through ten for *B. thuringiensis*, *B. anthracis*, and *B. globigii*). These do not represent all of the spores that were examined. The numbered spores were chosen based on the quality and completeness of the images obtained.

The vertical scale in each of the thirty-seven spores is presented according to the color gradients in Figure 28. The vertical scale in the edge enhanced height images follows that of the phase images. The maximum value in the scale for each phase image is listed immediately below the image.

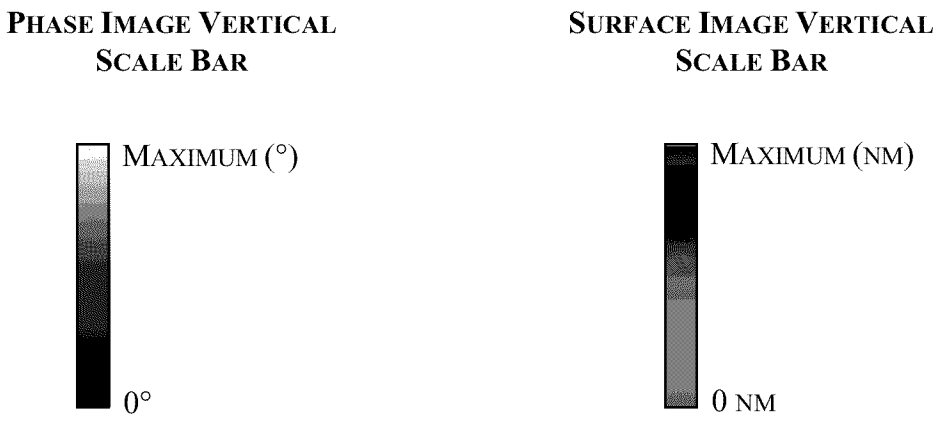

Figure 28. Vertical Scale Color Gradients for Spore Images

Bacillus cereus. The *B. cereus* spores are shown in Figures 29, 30 and 31. Only seven spores were imaged due to equipment difficulties.

Spores appeared consistently ellipsoidal. The surface of the spore was smooth with a marked sculpturing appearing along the long axis of the spores. The sculpturing consisted of shallow grooves (~5nm deep) and steps. No extraneous contamination was observed.

Phase images indicate a rather homogeneous surface lacking the grain-like structure seen with greater clarity in other spore species. Several different cantilever probes were used to obtain these mages. Thus it is expected that the lack of phase contrast is a real phenomena and not related entirely to the probe.

There are some areas on the spore surfaces which exhibit distinct phase contrast in the smaller scan size images. In spores 5, 6, and 7 there are features that appear to have sharper phase contrast and to rise above the local spore surface. This could be attributed to different material on the spore surface or the presence of something below the outer surface layer that is altering surface properties.

No exterior hair-like nap or any appendages extending from the spore were observed. Some unidentified material was present in the vicinity of the spores on the substrate surface.

In spore 1, the wavy appearance around the middle of the spore is likely not a real feature, but a scanning artifact. The shifting if the image appears equally on each side of the spore. This could be caused by drift in the scanner or a slight shifting of the spore position on the substrate as the probe scans across the middle of the spore.

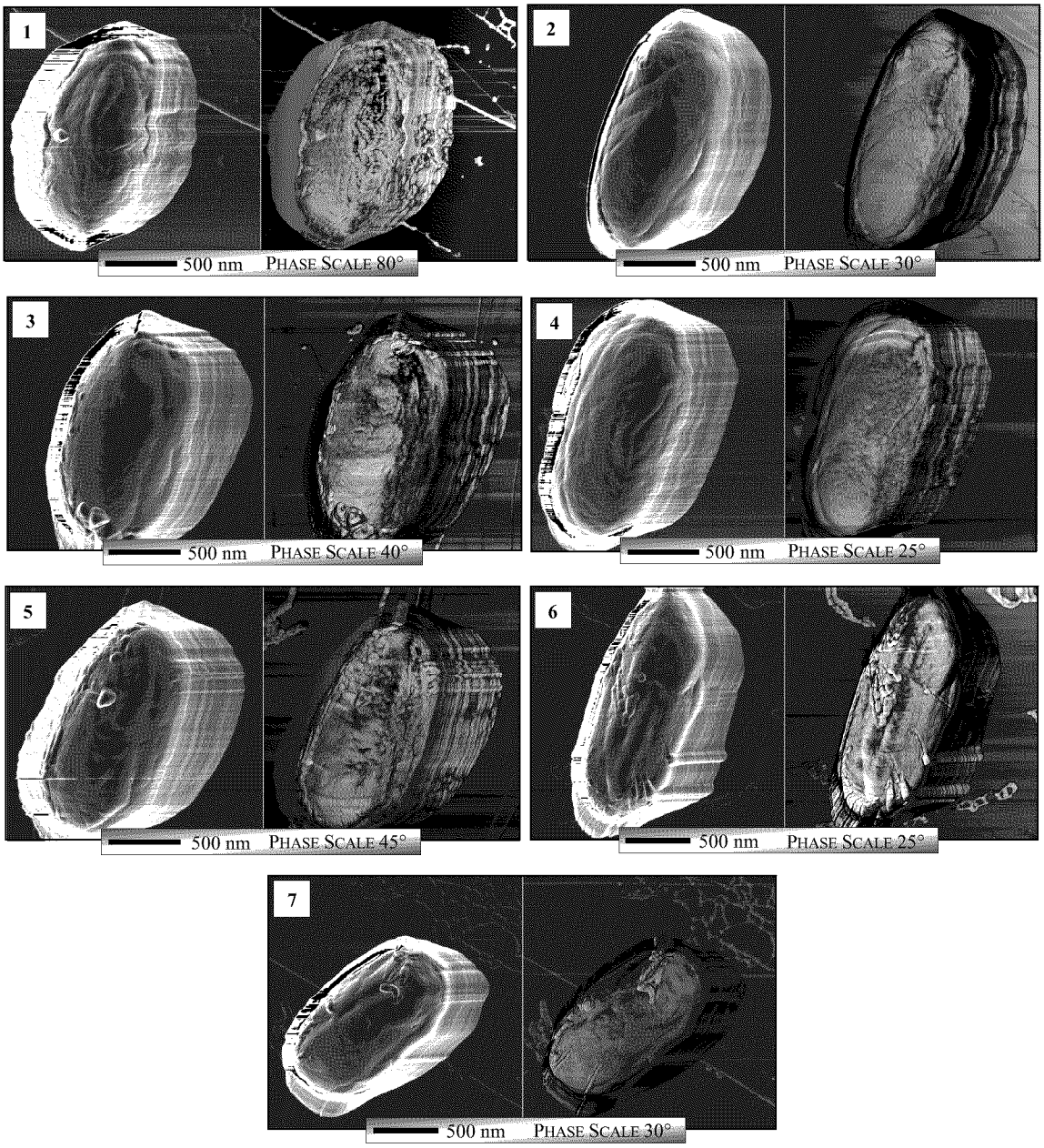

Figure 29. *B. cereus* General Spore Structure
(Left Image from Edge Enhanced Height Data, Right Image from Phase Data)

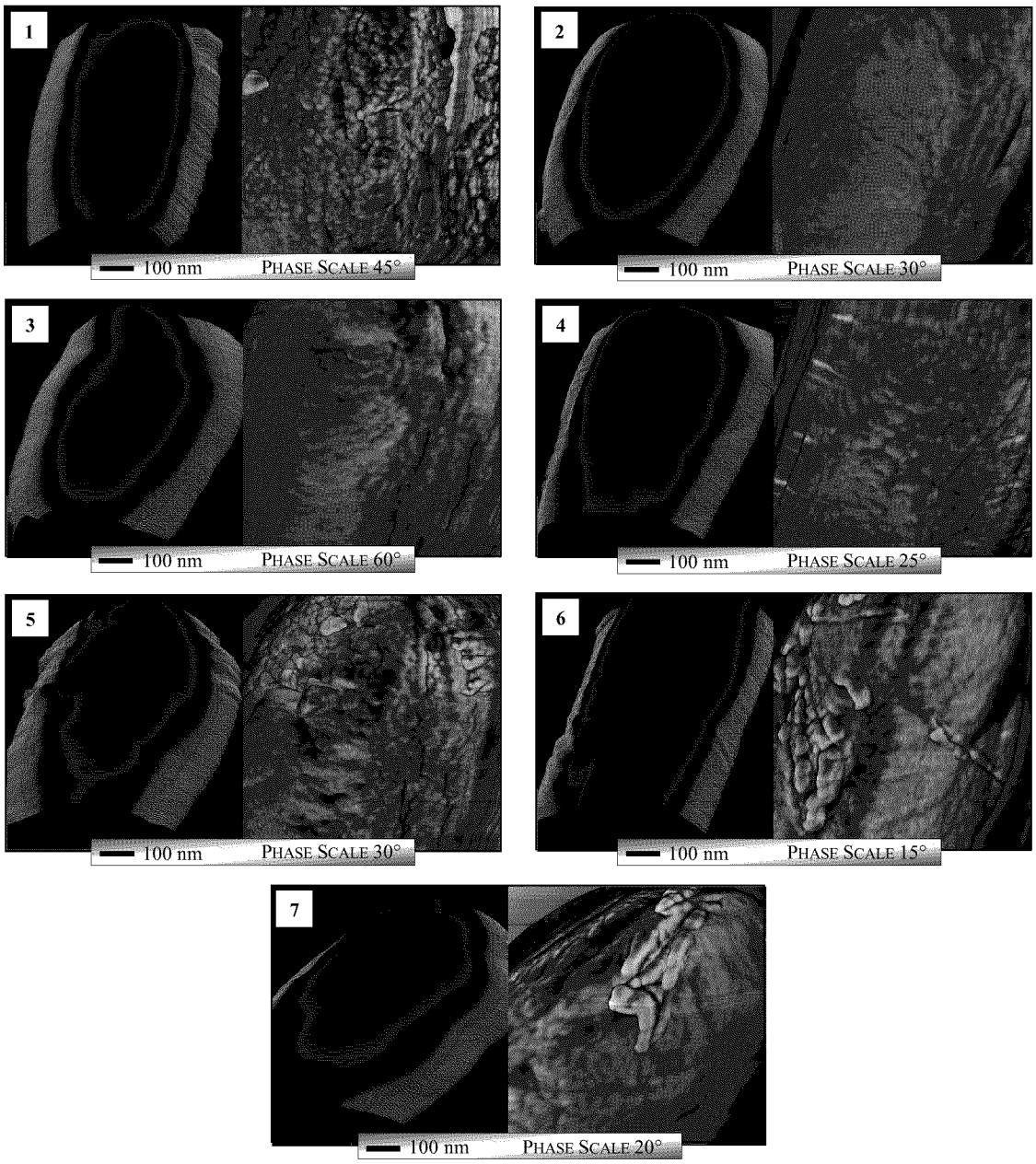

Figure 30. *B. cereus* Surface Morphology (750nm^2 Scan)
(Left Image is Surface View from Height Data, Vertical Scale = 100nm; Right Image is Top View from Phase Data)

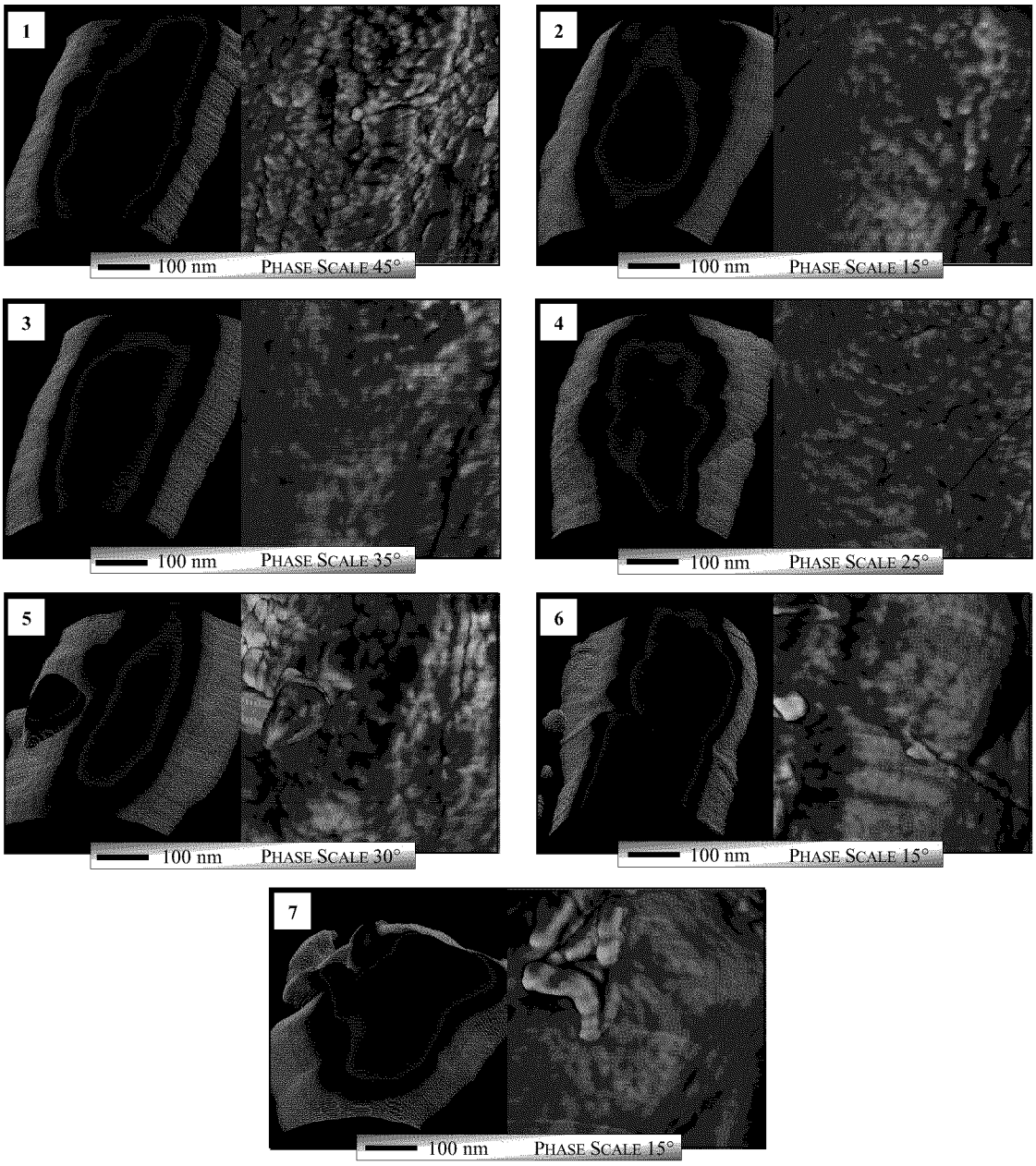

Figure 31. *B. cereus* Surface Morphology (500nm^2 Scan)
(Left Image is Surface View from Height Data, Vertical Scale = 50nm; Right Image is Top View from Phase Data)

Bacillus thuringiensis. The spores of *B. thuringiensis* are shown in Figures 32, 33 and 34.

B. thuringiensis spores fell into two categories: those with parasporal crystals and those without. The presence of parasporal crystals and the loose exosporium at the base of spores 2, 3, and 5 will be discussed in more detail later in this chapter.

Spores without parasporal crystals resembled *B. cereus* spores in their size and shape. There was also similar sculpturing on the surface consisting of grooves and steps generally oriented along the long axis of the spore. The surface of the spores was generally regular with some sculpturing observed along the long axis of the spores.

The presence of parasporal crystals is indicated in spores 7, 8 and 10. The regular, square or angular shapes of the spores suggest crystals near the surface, beneath the exosporium. These features were not observed in the spores of *B. cereus*, *B. anthracis*, or *B. globigii*. The spores with the parasporal crystals had significantly more surface features that appeared "bumpy". The bump-like features were irregularly shaped and varied in diameter from 20-30nm. These bumps corresponded to areas of light and dark contrast in the corresponding phases images. The overall shape of these spores was also significantly different. Approximately half of the spores' top surface was virtually flat; the remainder sloped down to the edge at a consistent angle (148° for spore 7, 149° for spore 8, and 148° for spore 10).

Spores 1, 2, and 7 show features that could be surface contamination. No exterior hair-like nap or any appendages extending from the spore were observed.

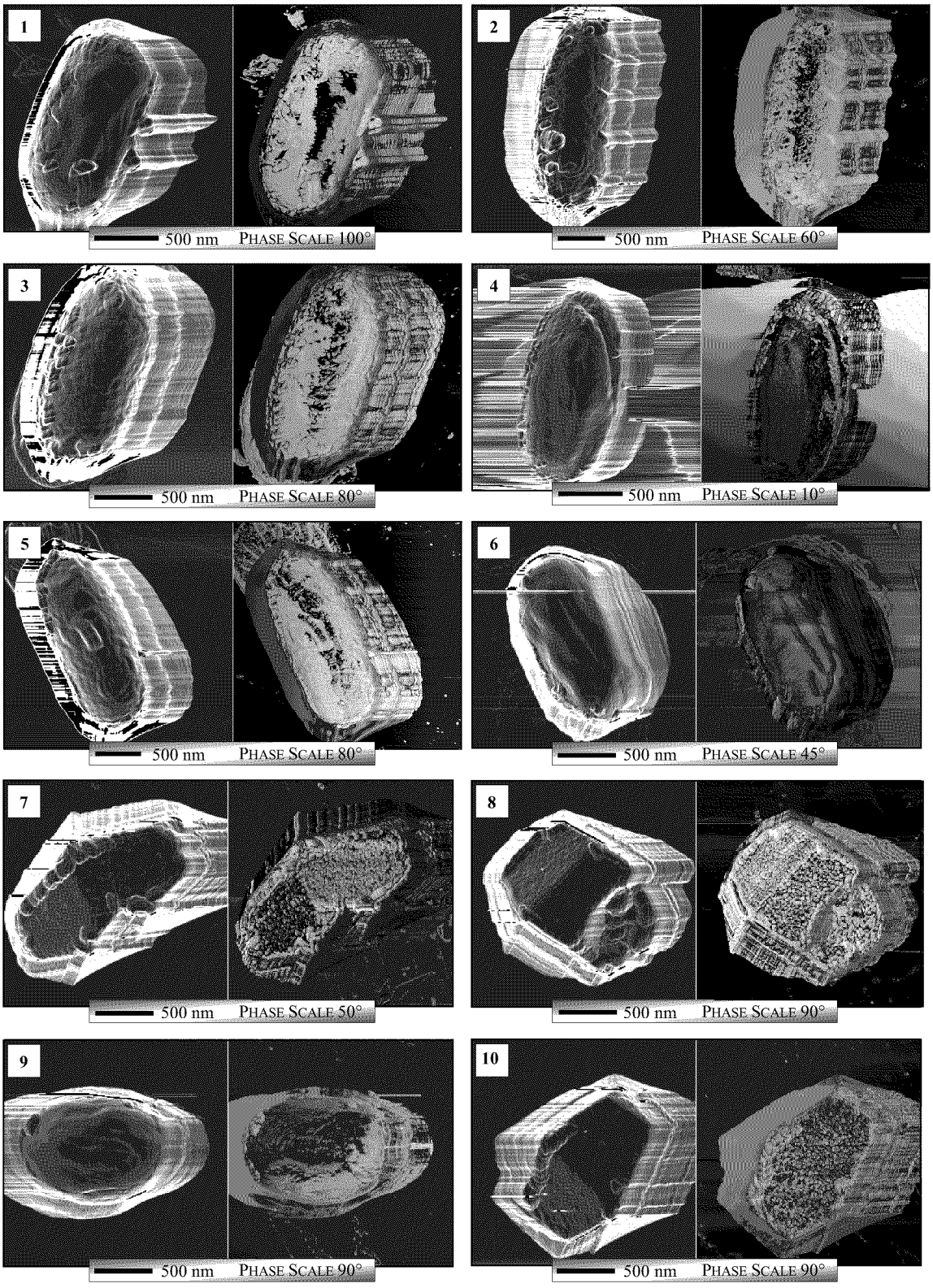

Figure 32. *B. thuringiensis* General Spore Structure
(Left Image from Edge Enhanced Height Data, Right Image from Phase Data)

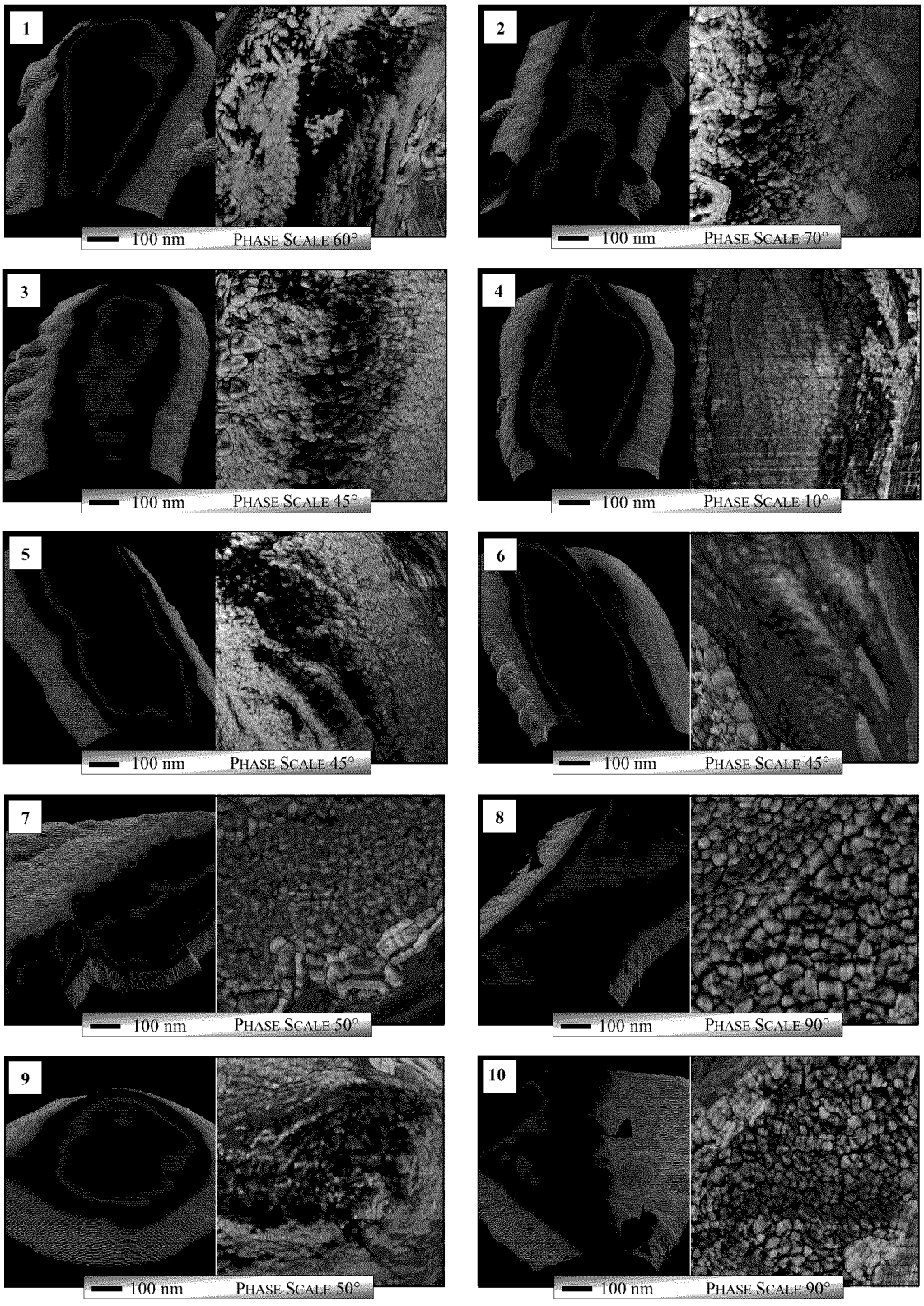

Figure 33. *B. thuringiensis* Surface Morphology (750nm^2 Scan)
(Left Image is Surface View from Height Data, Vertical Scale = 100nm; Right Image is Top View from Phase Data)

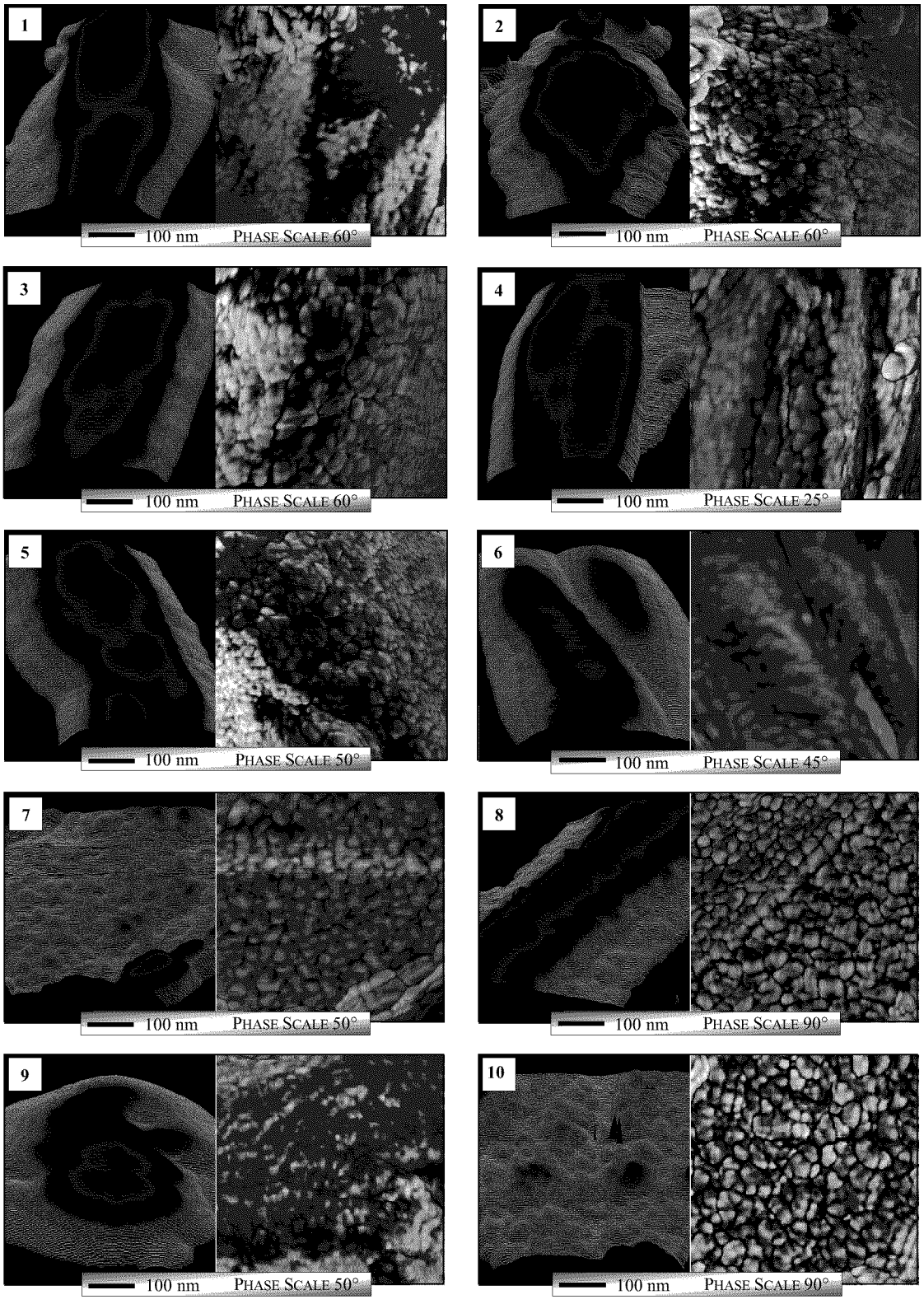

Figure 34. *B. thuringiensis* Surface Morphology (500nm^2 Scan)
(Left Image is Surface View from Height Data, Vertical Scale = 50nm; Right Image is Top View from Phase Data)

Bacillus anthracis. The spores of *B. anthracis* are shown in Figures 35, 36 and 37.

The top, exterior surface of the spores appeared uneven. The surfaces were not as smooth as seen in *B. cereus* spores or as rough as seen in *B. thuringiensis* spores that had parasporal crystals. There did not appear to be an order or periodicity to the smaller surface features.

There were long, vein-like structures arranged irregularly (but generally along the long axis of the spore). It is not clear if these structures are due to features on the exterior spore surface or are caused by features underlying the exosporium. The vein-like structures range from 50-120nm wide but less than 15nm in height above the regular surface. The larger "veins" appeared consistently in the phase images – indicating either a correspondence in height and phase data or different material properties present in and around the "veins".

Phase data at all scales suggest the exterior surface is not homogenous. Six of the ten spores (4, 5, 6, 8, 9, and 10) showed a marked line of significantly less phase shift in the middle of the spore extending along the spore's long axis. Images obtained at the $500nm^2$ scale show a detailed grain-like structure with no apparent regularity. Phase images allowed clear resolution of features as small as 10-20 nanometers. The spores did not demonstrate phase contrast at a uniform scale. This could be a result of properties of the spore, or the particular settings of the atomic force microscope.

The spores generally did not appear to have contamination on their surface. Spores 4, 8, and 9 did show small irregularly shaped features on some portions of the edges of the spore. No exterior hair-like nap or any appendages extending from the spore were observed.

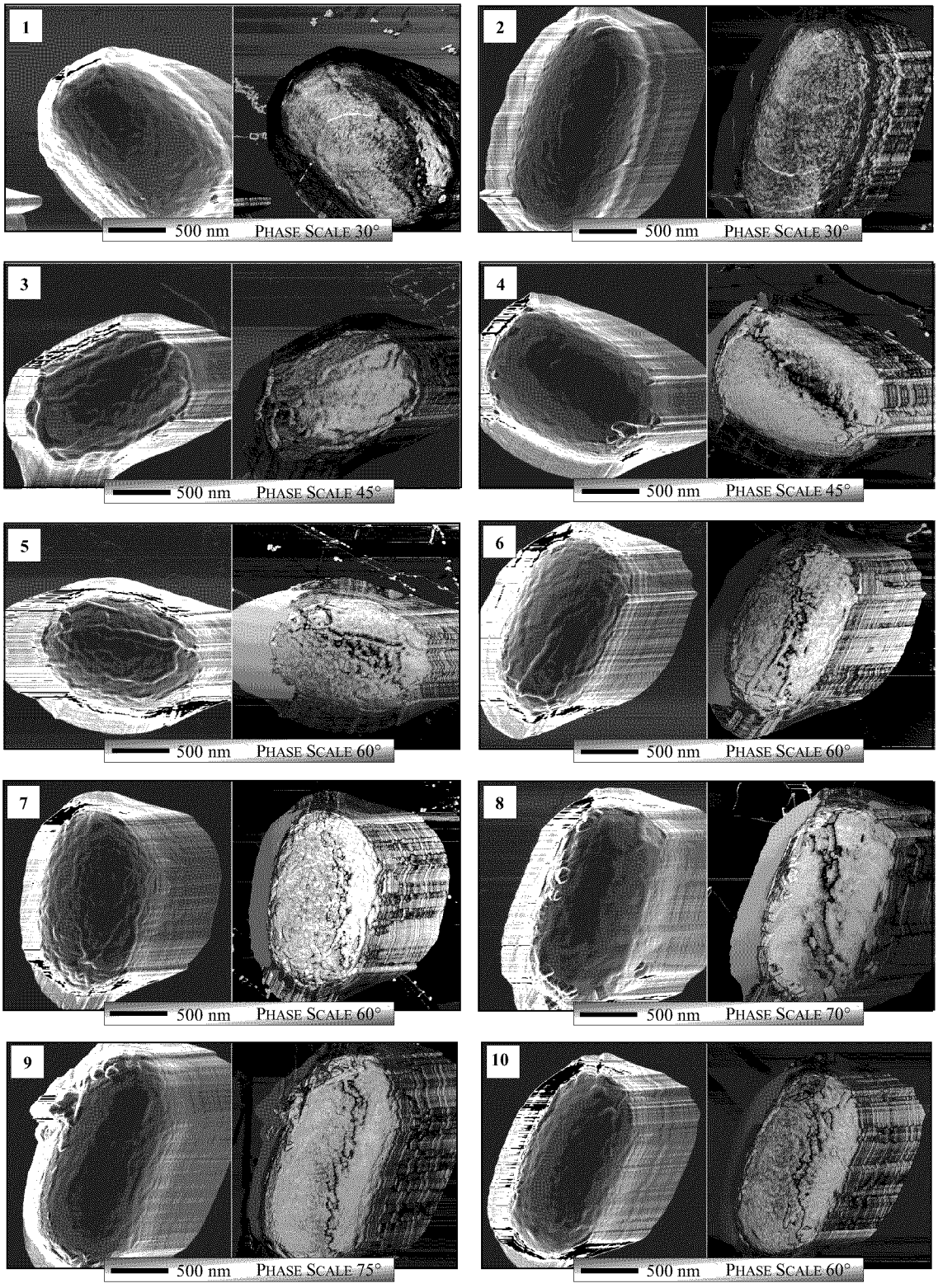

Figure 35. *B. anthracis* General Spore Structure
(Left Image from Edge Enhanced Height Data, Right Image from Phase Data)

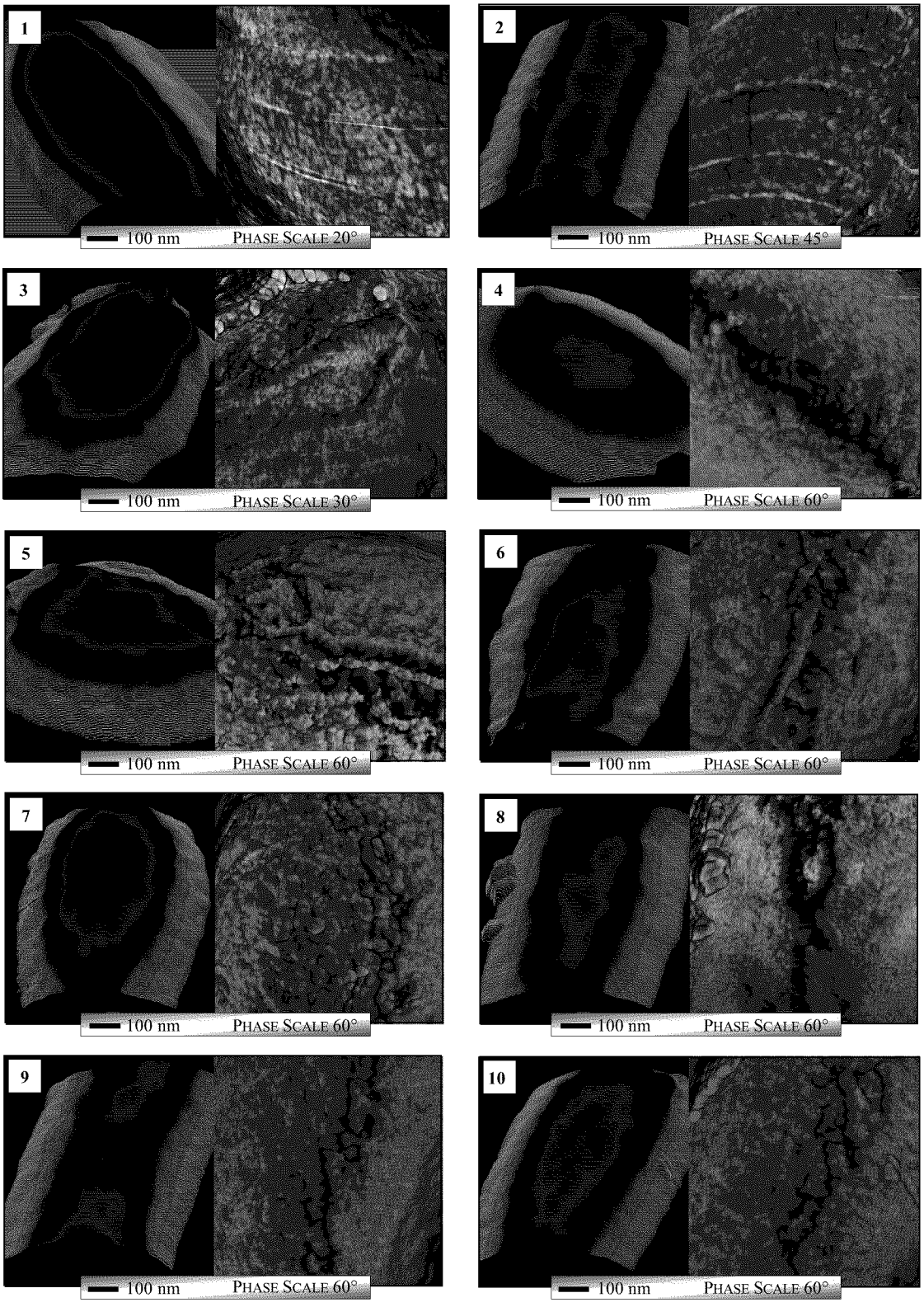

Figure 36. *B. anthracis* Surface Morphology (750nm^2 Scan)
(Left Image is Surface View from Height Data, Vertical Scale = 100nm; Right Image is Top View from Phase Data)

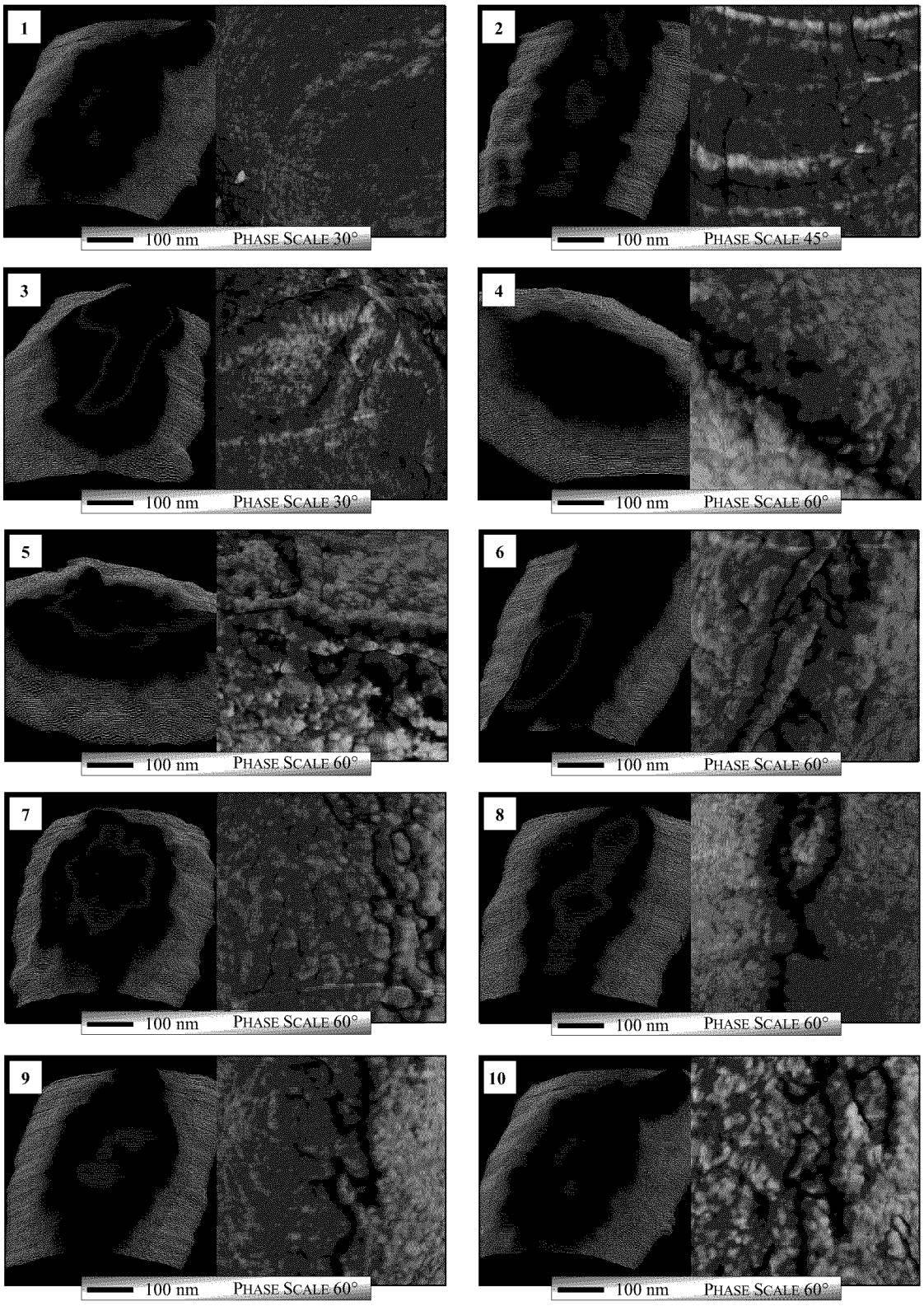

Figure 37. *B. anthracis* Surface Morphology (500nm^2 Scan)
(Left Image is Surface View from Height Data, Vertical Scale = 50nm, except for spore 3 = 80nm; Right Image is Top View from Phase Data)

Bacillus globigii. The spores of *B. globigii* are shown in Figures 38, 39 and 40. The top, exterior surface of the spores was more textured than the other species. Features varied in height and did not appear to be arranged in any regular pattern. It is not clear if these structures are due to features on the exterior spore surface or are caused by features underlying the exosporium. Although generally ellipsoidal in shape, several spores appeared irregular and distorted.

The features on the surfaces of the *B. globigii* spores appeared highly irregular and lacked any readily distinguishable pattern or periodicity. Steps and grooves appear along the long axis of several of the spores reminiscent of similar features observed in *B. cereus* spores.

Phase data at all scales suggest the exterior surface is not homogenous. These spores did not show the significantly less phase shift in the middle of the spore extending along the spore's long axis that was observed in other species. Images obtained at the $500nm^2$ scale show a detailed grain-like structure with no apparent regularity. The grains appeared on the same scale for all of the images (10-30nm in diameter). This structure extended uniformly across the spore's upper exterior surface. The spores did not demonstrate phase contrast at a uniform scale. This could be a result of properties of the spore, or the particular settings of the atomic force microscope. However, the contrast in the phase images did correspond to the surface features observed in the height images

The phase images of spores 7 and 8 show a unique pattern of parallel lines. These features will be discussed further in a later section.

The spores generally did not appear to have contamination on their surface. No exterior hair-like nap or any appendages extending from the spore were observed.

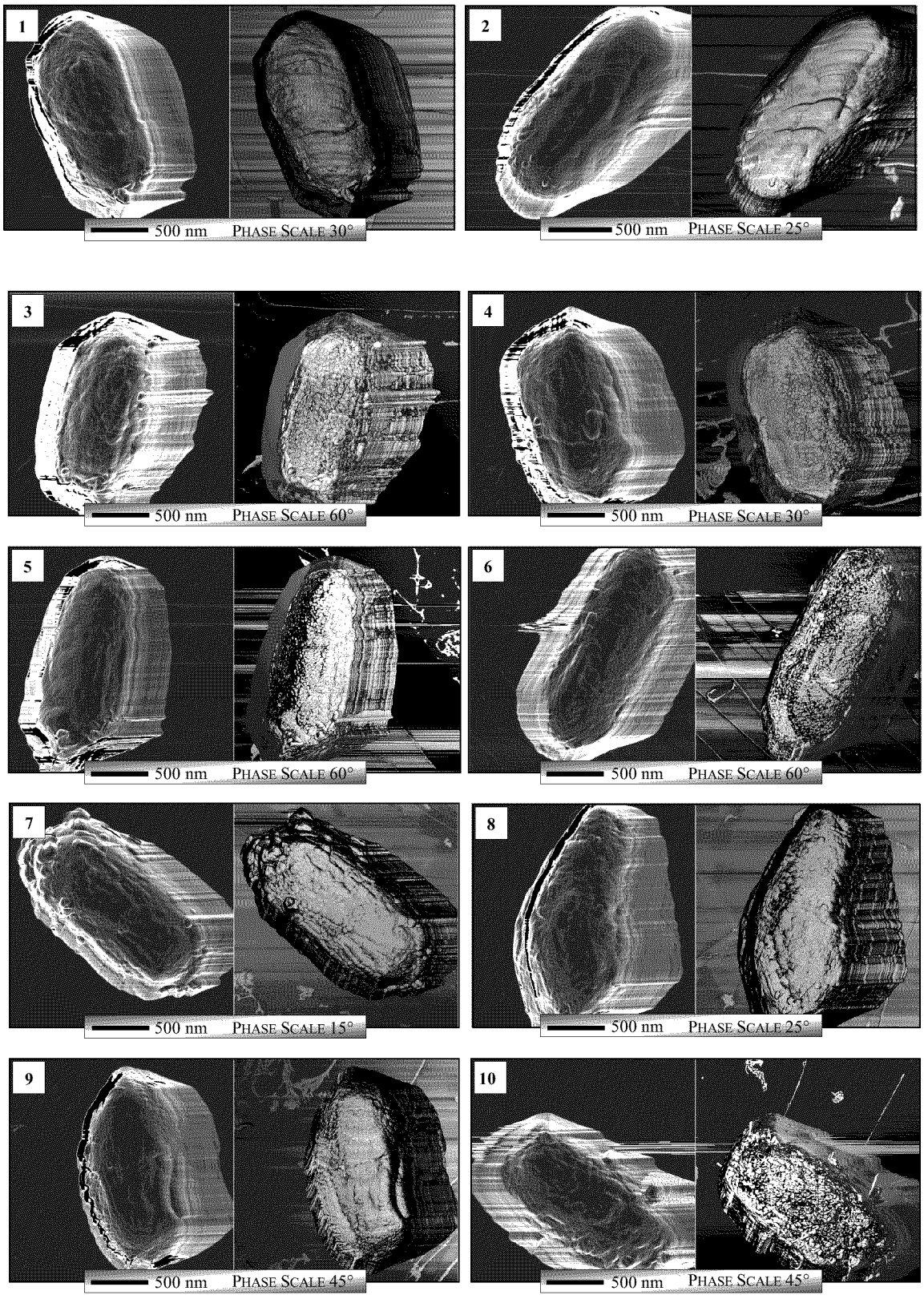

Figure 38. *B. globigii* General Spore Structure
(Left Image from Edge Enhanced Height Data, Right Image from Phase Data)

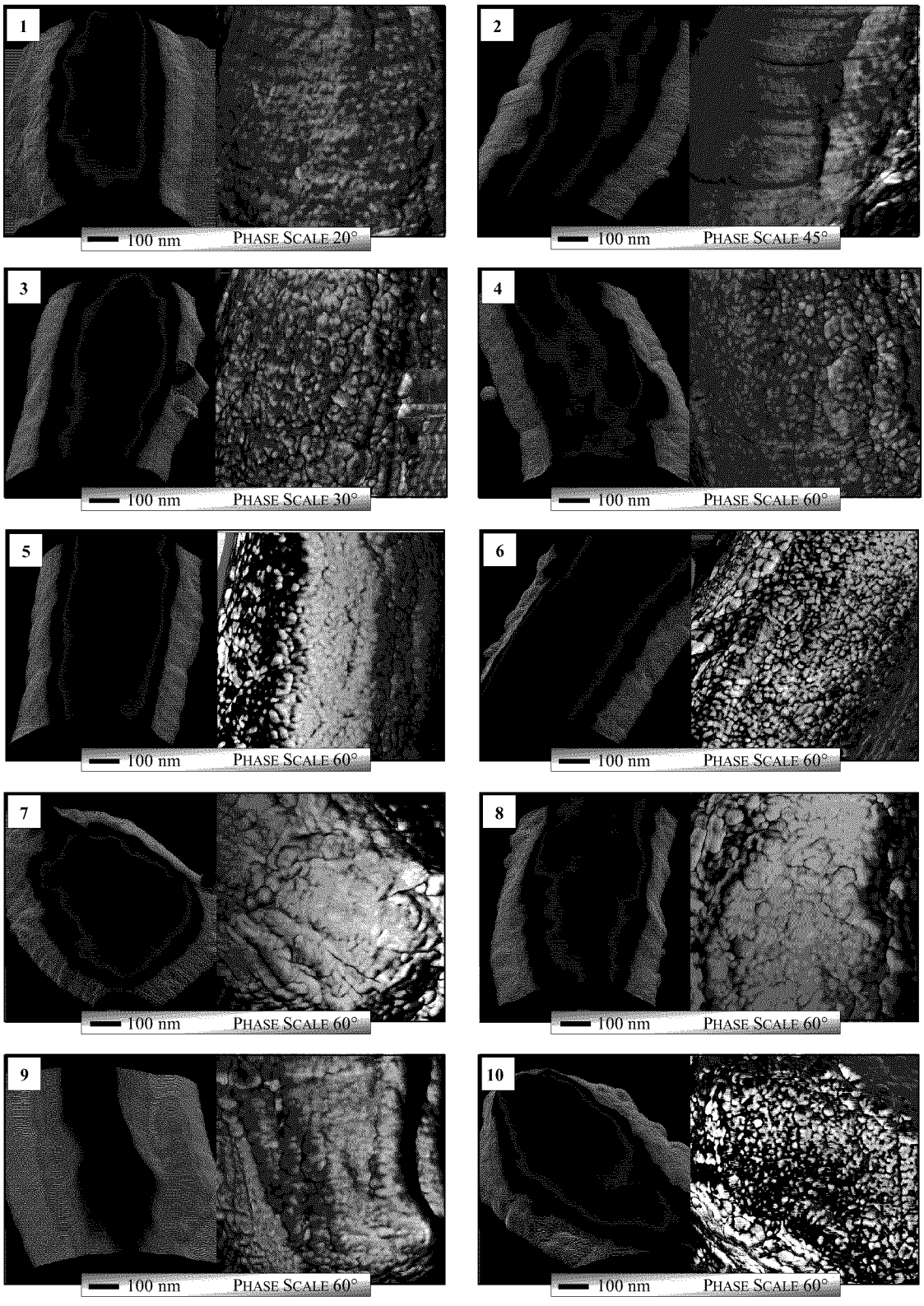

Figure 39. *B. globigii* Surface Morphology a (750nm^2 Scan)
(Left Image is Surface View from Height Data, Vertical Scale = 100nm; Right Image is Top View from Phase Data)

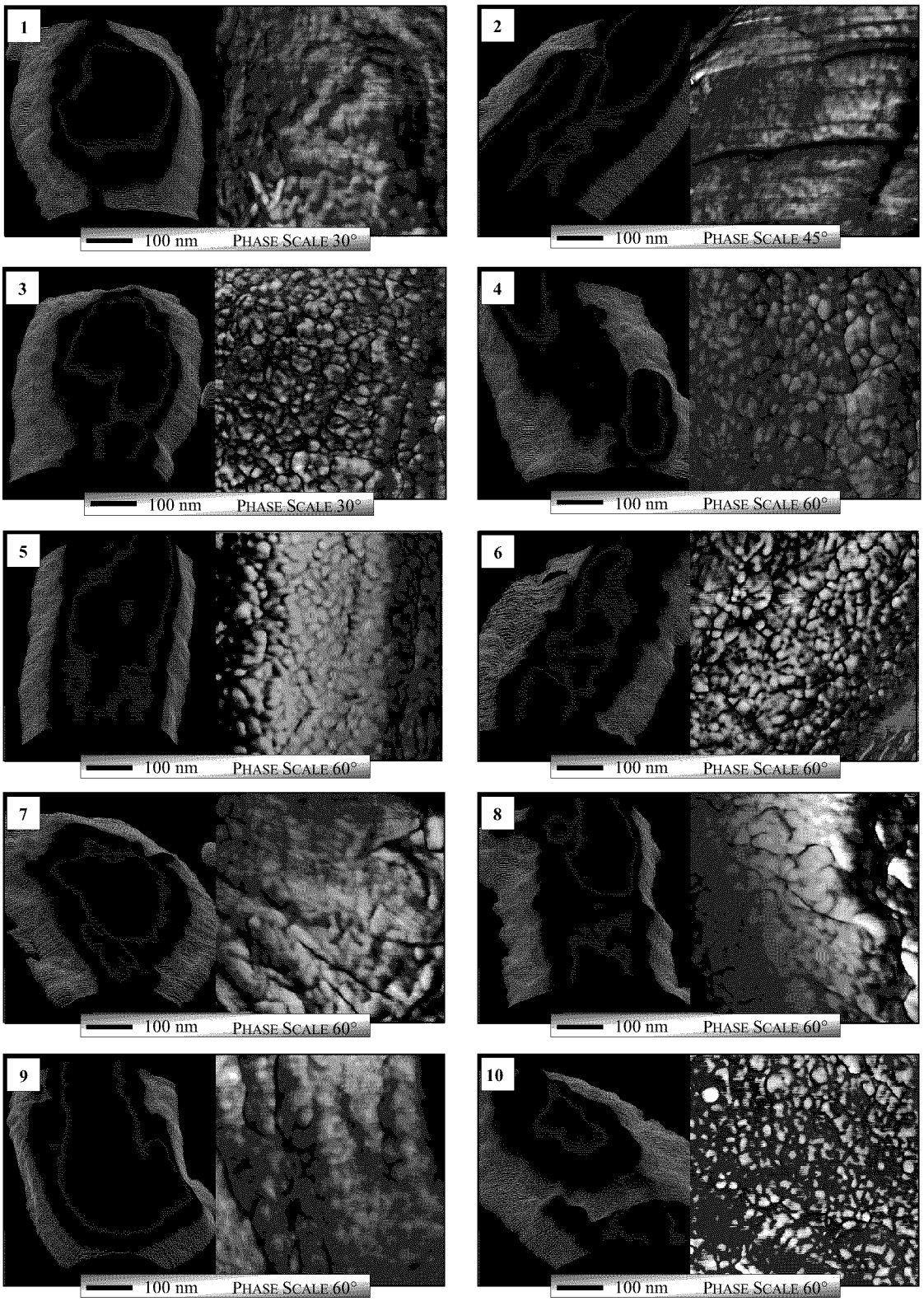

Figure 40. *B. globigii* Surface Morphology (500nm^2 Scan)

(Left Image is Surface View from Height Data, Vertical Scale = 50nm, except for spore 1 = 60nm, spore 8 = 60nm, and spore 9 = 100nm; Right Image is Top View from Phase Data)

Novel Spore Features

Several unique features were observed on the surfaces of spores that require a more detailed examination. First, the parasporal crystals in *B. thuringiensis* are described. This is followed by observations of a loose exosporium extending beyond the immediate surface of several spores (also in *B. thuringiensis*). Next, the phase images of *B. globigii* spores 7 and 8 are presented to highlight several linear, parallel features.

Parasporal Crystals. Although not observed on every spore of *B. thuringiensis*, the presence of parasporal crystals was observed in several instances. The crystal appeared either adjacent to the spore, or integral to the spore structure.

The two examples of crystals adjacent to the spores are shown in Figures 41 and 42. In both cases these are non-numbered spores not presented previously. Also, in both cases the crystals appear to be flat and square. The dimensions of the crystal in the first example were 780nm × 840nm (length and width) and 260-280nm in height. The second crystal was 730nm × 730nm (length and width) and approximately 700nm in height.

A section of *B. thuringiensis* spores 7, 8, and 10 is shown in Figure 43. The section analysis yields a clearer indication of the surface structure imparted by what is hypothesized to be a parasporal crystal beneath the exosporium. The features vary in size. Where the crystal in spore 7 covers nearly the entire top surface of the spore, the crystal in spore 8 appears to only cover one third of the top surface. It also appears that the upper surface of spore 8 is distorted due to the presence of the crystal. The flatness of the crystals suggests a similar geometry to those observed in Figures 41 and 42. Because the spores appear to be beneath the exosporium, only the top surface is visible.

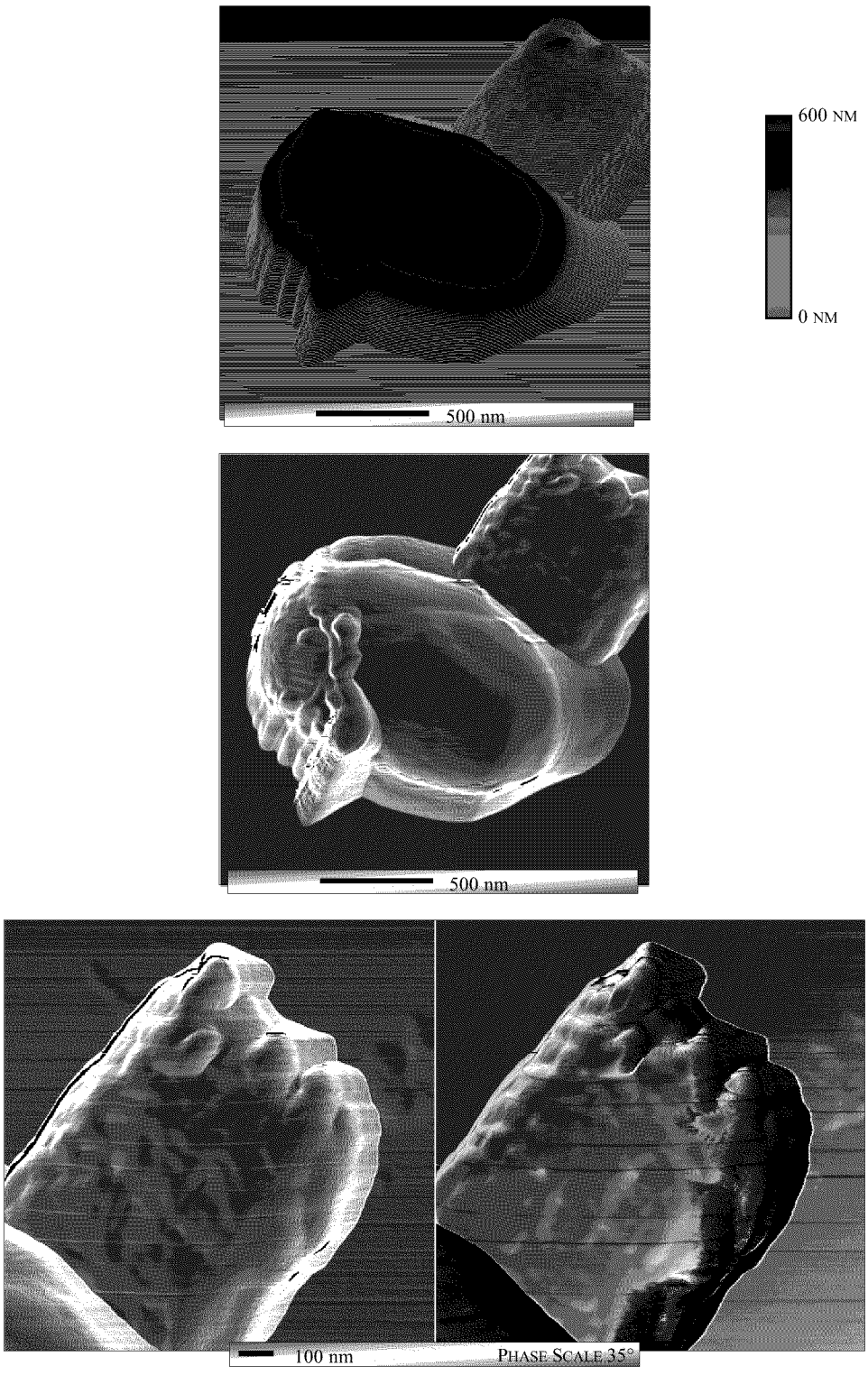

Figure 41. First Example of Parasporal Crystal
(*B. thuringiensis*)

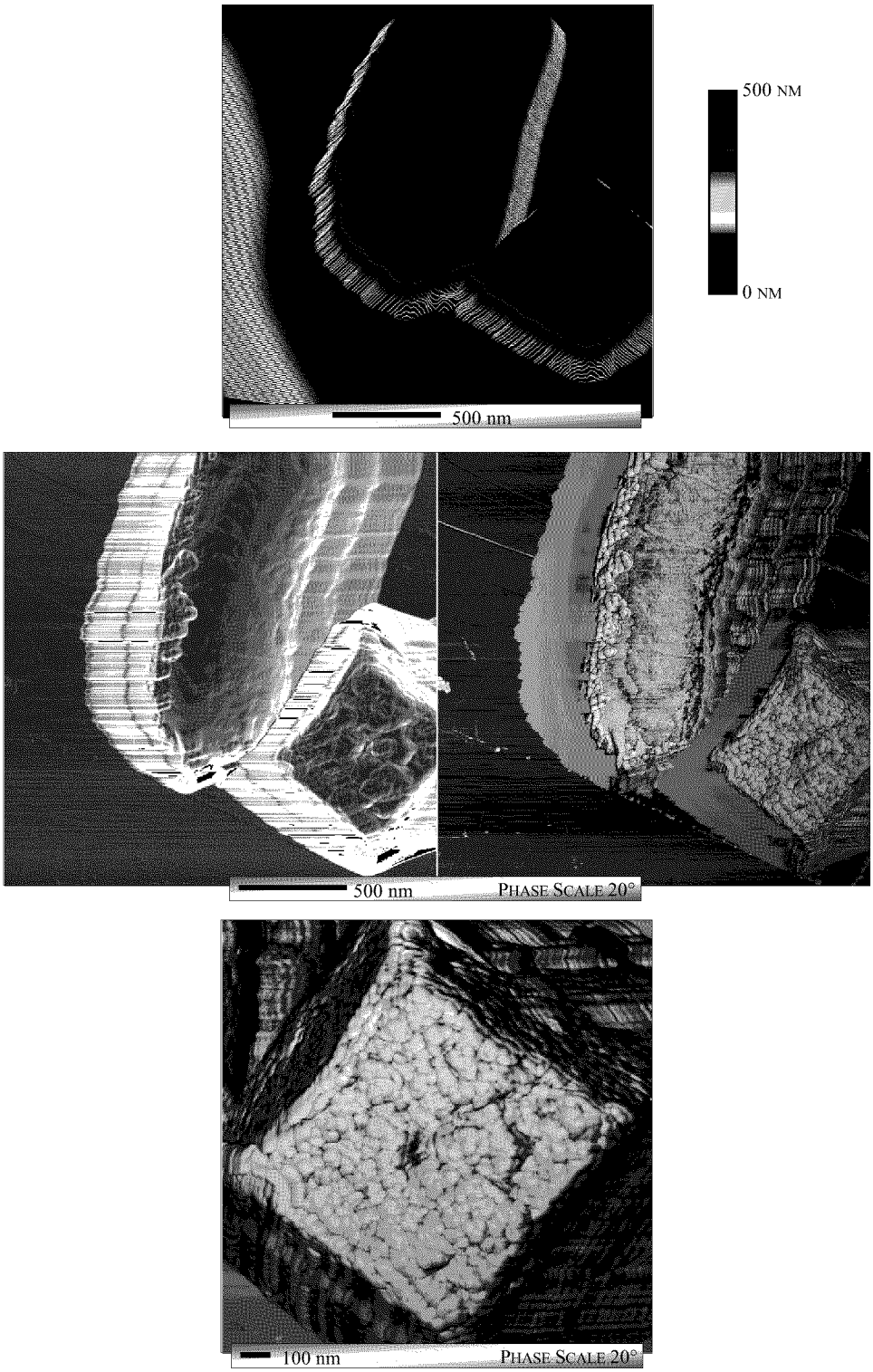

Figure 42. Second Example of Parasporal Crystal
(*B. thuringiensis*)

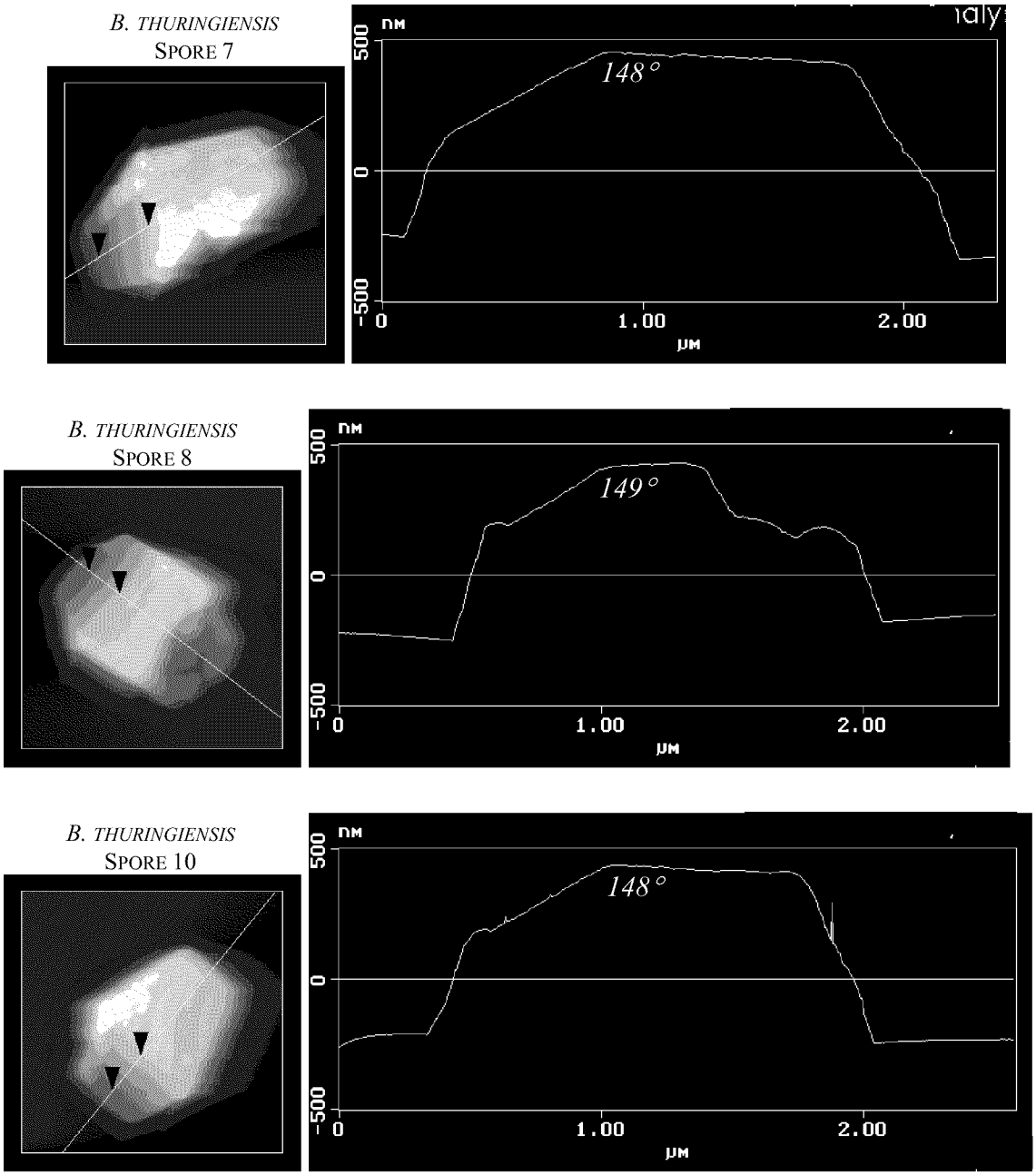

Figure 43. Section Analysis of *B. thuringiensis* Spores 7, 8 and 10

The corrugations on the surface of the crystal in Figure 42 (at approximately 30nm) are reminiscent of the section of a rhombohedral crystal imaged by electron microscopy in 1976 (the corrugations there were periodic at 24nm) (Gerhardt and others 1976:440).

The parasporal crystals in Figures 41 and 42 appear to have a cubic structure. The parasporal crystals that appear in Figure 43 should also have a cubic structure. At first, this does not appear to be the case. The angled appearance of the later crystals suggests a rhomboidal structure. This however, does not correspond to the type of insecticidal toxin that should be found in this strain of *B. thuringiensis*.

The strain of *B. thuringiensis* used here should produce bipyramidal inclusions of Cry1 toxins (Aronson, 1993:955). However, no bipyramidal structures were observed in the AFM images collected as part of this work. The cubic crystal structure corresponds to the insecticidal toxin Cry2 (Schnepf and others, 1998:779). Thus, it is hypothesized that the parasporal inclusions observed here are Cry2 toxin crystals.

The seemingly disparate geometries observed in Figures 41, 42, and 43 can all be associated with the cubic structure. This is readily done for Figures 41 and 42.

In Figure 43, the inclusions observed in *B. thuringiensis* spores 7, 8, and 10 appear to be cubic crystals with the (111) plane cleaved. The theoretical depression angle for this case would be 144.7°. A complete derivation of this angle is presented in the Appendix. The actual angles were measured as 148° for spore 7, 149° for spore 8, and 148° for spore 10. This is a relatively good agreement.

Although not every *B. thuringiensis* spore could be associated with a parasporal crystal, the crystals that were imaged appear to have a consistent cubic structure. When the crystal appeared adjacent to the spore this structure was more pronounced. When the crystal appeared on the upper surface of the spore, the cubic structure seemed to be cleaved along the (111) plane. In this case, the crystal might have formed incompletely or in a manner slightly different due to its position on the spore.

Loose Exosporium. As previously discussed in Chapter 2, the exosporium has been described as a loose sac surrounding the spore. This was not evident from the majority of spores examined. However, in three instances, loose exosporium was observed around the edges of *B. thuringiensis* spores that corresponded to electron microscopy images of "loose exosporium" (Hachisuka and Kozuka, 1981). These examples are presented in Figures 44, 45, and 46.

The structure of the anomalous areas at the base of the spores is similar in structure to the spore surface (based on the phase images). The features are 5-18nm high (spore 2), less than 5nm high (spore 3), and 4-10nm high (spore 5).

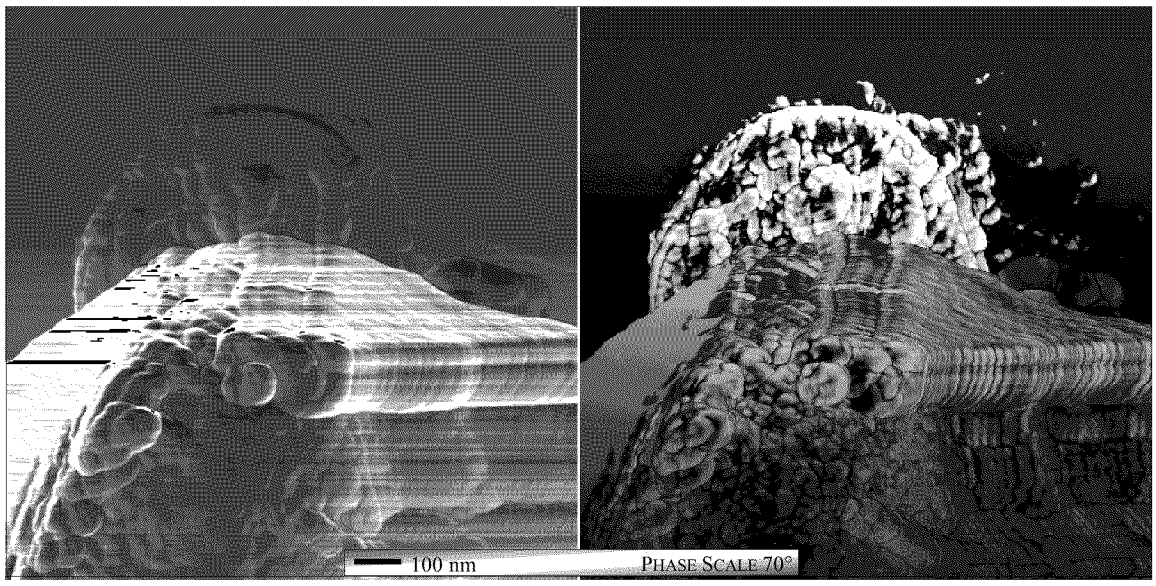

Figure 44. Apparent Exosporium From *B. thuringiensis* Spore 2

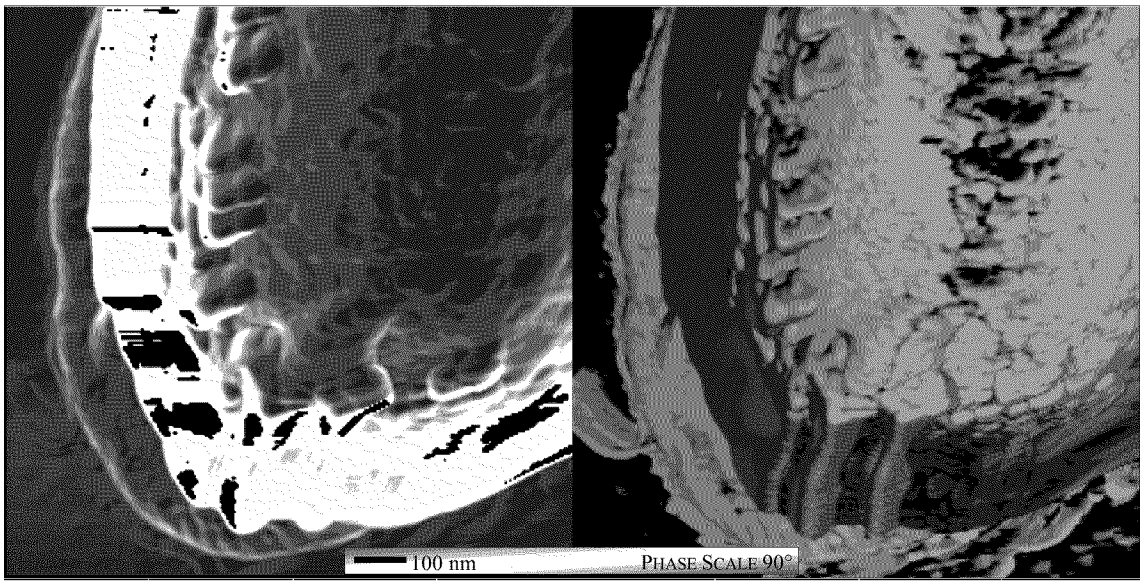

Figure 45. Apparent Exosporium From *B. thuringiensis* Spore 3

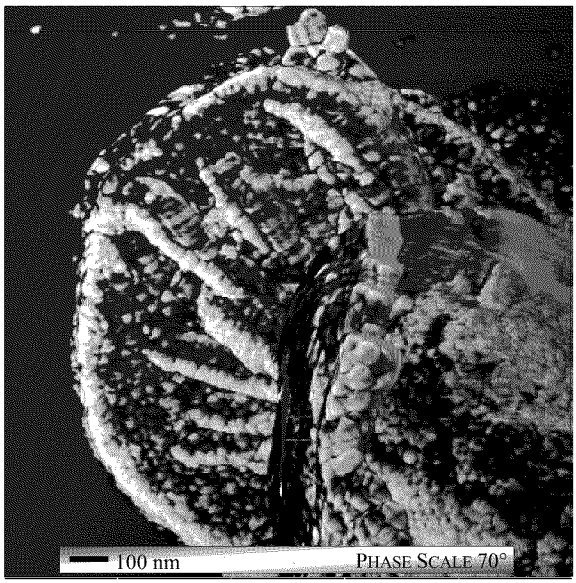

Figure 46. Apparent Exosporium From *B. thuringiensis* Spore 5

Striations on *B. globigii* Phase Images. Figures 47 and 48 show phase images of two *B. globigii* spores (8 and 7). These phase images reveal striated features (short parallel lines of contrasting phases) that do not correspond to any features observed in the corresponding height images. These features are reminiscent of Yves Dufrêne's images of fungal spores (Dufrêne, 2000; Dufrêne and others, 1999).

In each spore, the striations are 4-10nm wide. Their orientation across the spore surface is generally uniform. The striations do not appear across the entire surface. However, it is not clear if this is because they were not present, or because they were not imaged. The overall pattern expressed by these phase images is consistent with phase images from the other eight *B. globigii* spores.

500NM^2 SCAN SIZE
PHASE IMAGE

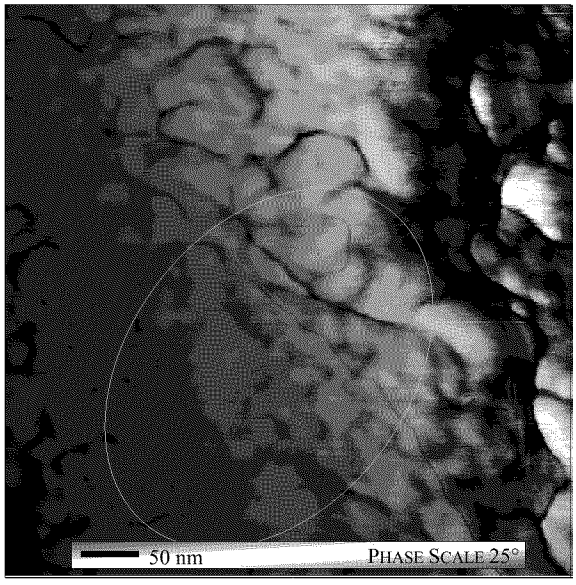

Figure 47. Phase Image Striations
(*B. globigii* Spore 8)

750NM^2 SCAN SIZE
PHASE IMAGE

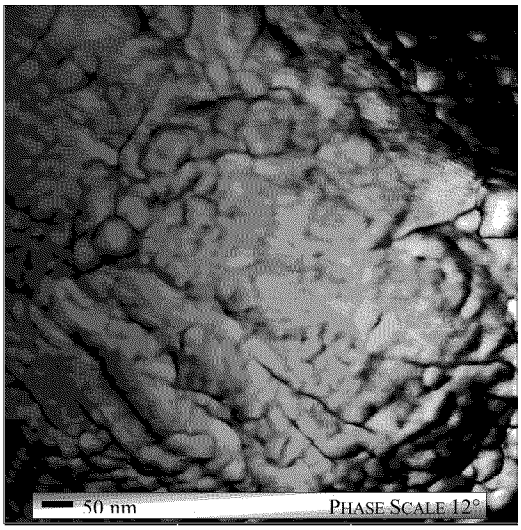

500NM^2 SCAN SIZE
PHASE IMAGE

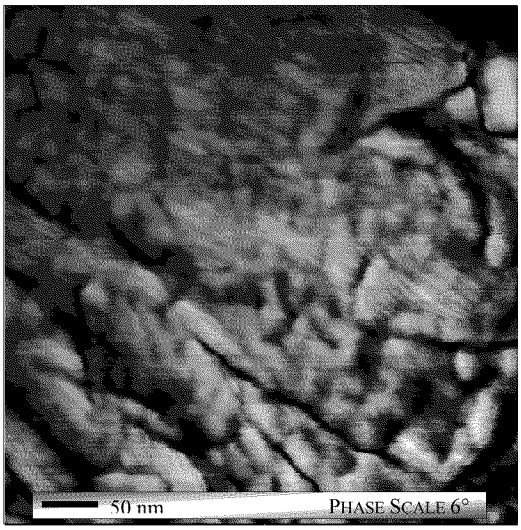

250NM^2 SCAN SIZE
PHASE IMAGE

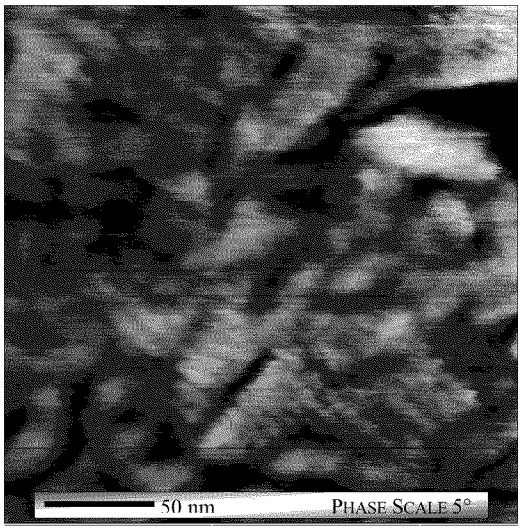

Figure 48. Phase Image Striations
(*B. globigii* Spore 7)

Correlation of Height and Phase Information

Images obtained from height and phase data represent different features on a sample surface. One way to compare and correlate the two types of data is by subtracting one image from the other. Figure 49 illustrates images before and after subtraction and shows how phase and height information can be combined in order to see a fuller picture of a surface. The circles indicate the same features on each of the three images.

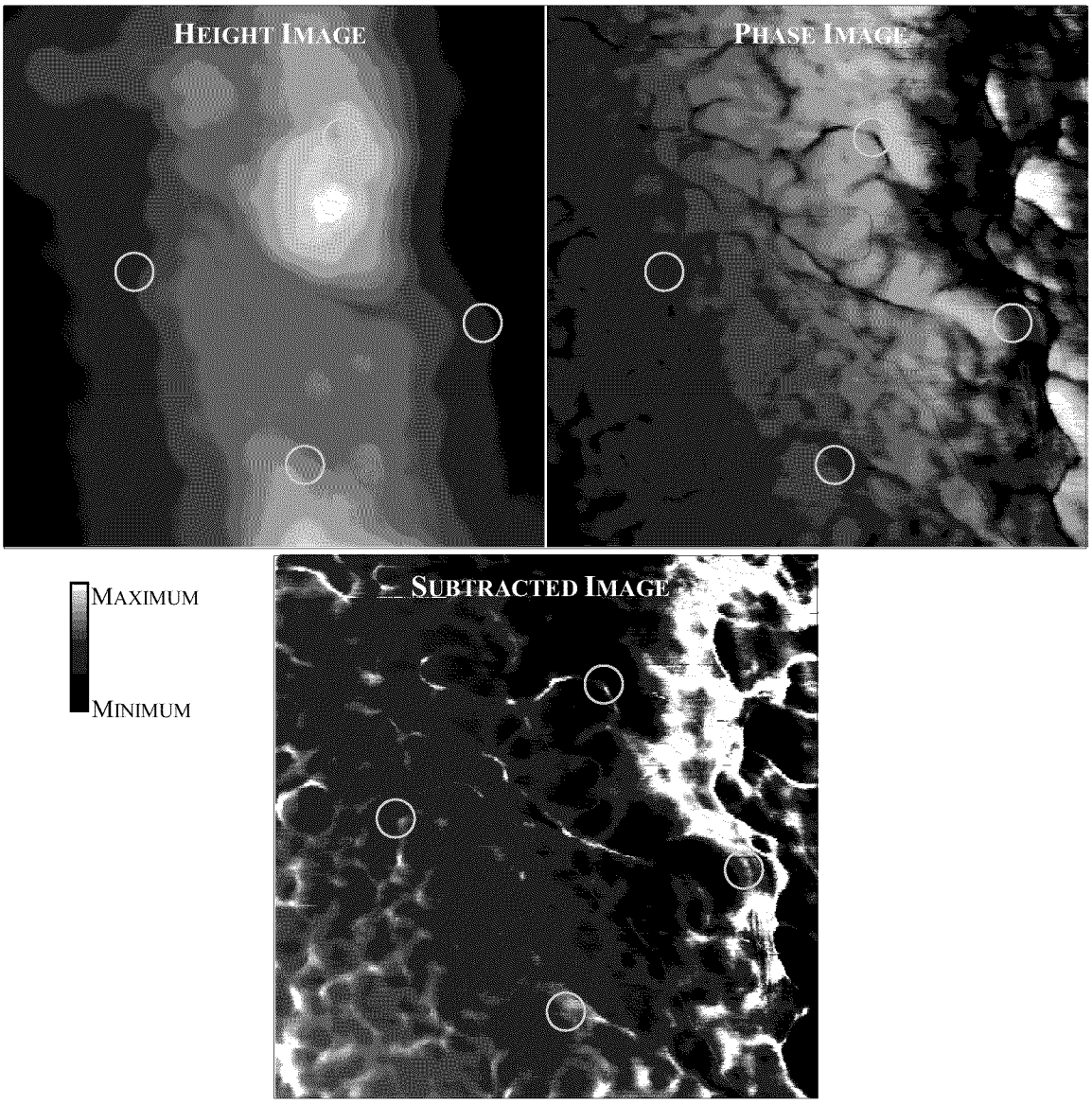

Figure 49. Correlating Height and Phase Images By Subtraction
(*B. globigii* Spore 8)

Another example of image subtraction is shown in Figure 50. Again, this illustrates that there is some correspondence between vertical features and phase contrast, but this association is not universal or complete.

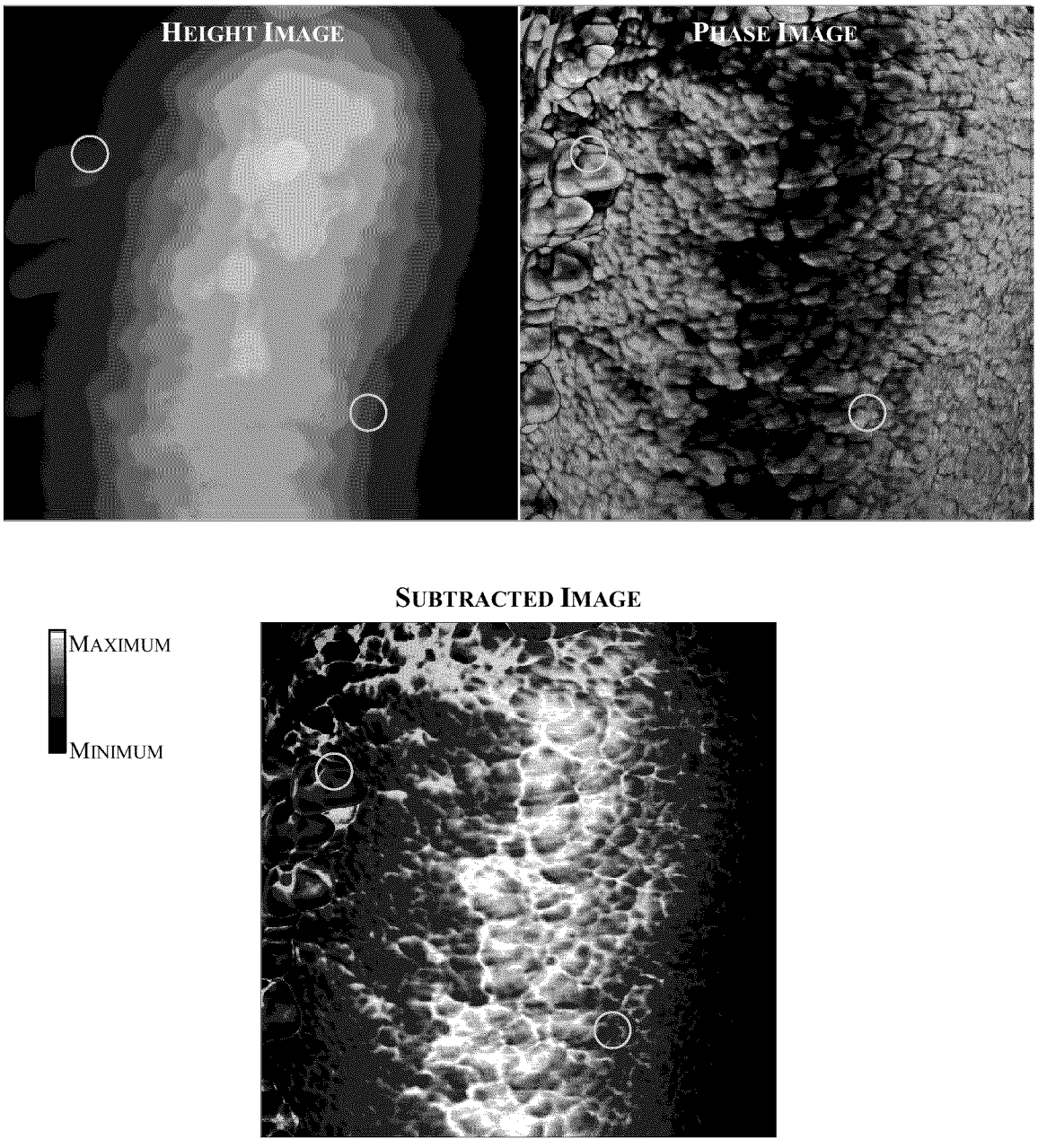

Figure 50. Correlating Height and Phase Images By Subtraction
(*B. thuringiensis* Spore 3)

Roughness Analysis Results

A roughness analysis was performed on each spore in order to determine if quantitative differences in surface roughness exist between bacterial species. Eight quantitative measures of surface roughness were calculated by the Digital Instruments AFM software (by sampling 750nm^2 scans of the spores' surface in 250nm^2 boxes five times).

Figures 51 through 58 summarize this data. Each point is the mean of the five sampled measurements. The error bars represent one standard deviation above and below the mean.

The Z-Range results (Figures 51) indicate the range of vertical variation on the surface of the spores. The variation was similar for each species. Certain spores showed greater variation than others. This is due to the presence of a vertical surface feature.

The surface area results (Figures 52) again show significant similarity between the four bacterial species. *B. cereus* spores exhibited the most variability in surface area for each individual spores and *B. anthracis* showed the least.

The mean and raw mean data is perhaps the most difficult to interpret. The mean of the surface is the average of all of the *Z* values in a defined area *with respect to the Z value when the microscope was engaged*. This caveat makes comparisons from different scans of the microscope of limited value. This mean is also affected by plane-fitting the data. The raw mean is simply the mean without the application of plane-fitting.

The mean data shows the same trends observed in the other roughness measurements (except for the raw mean). The raw mean indicates significant variability in *B. anthracis* and *B. globigii* (Figures 53 and 54).

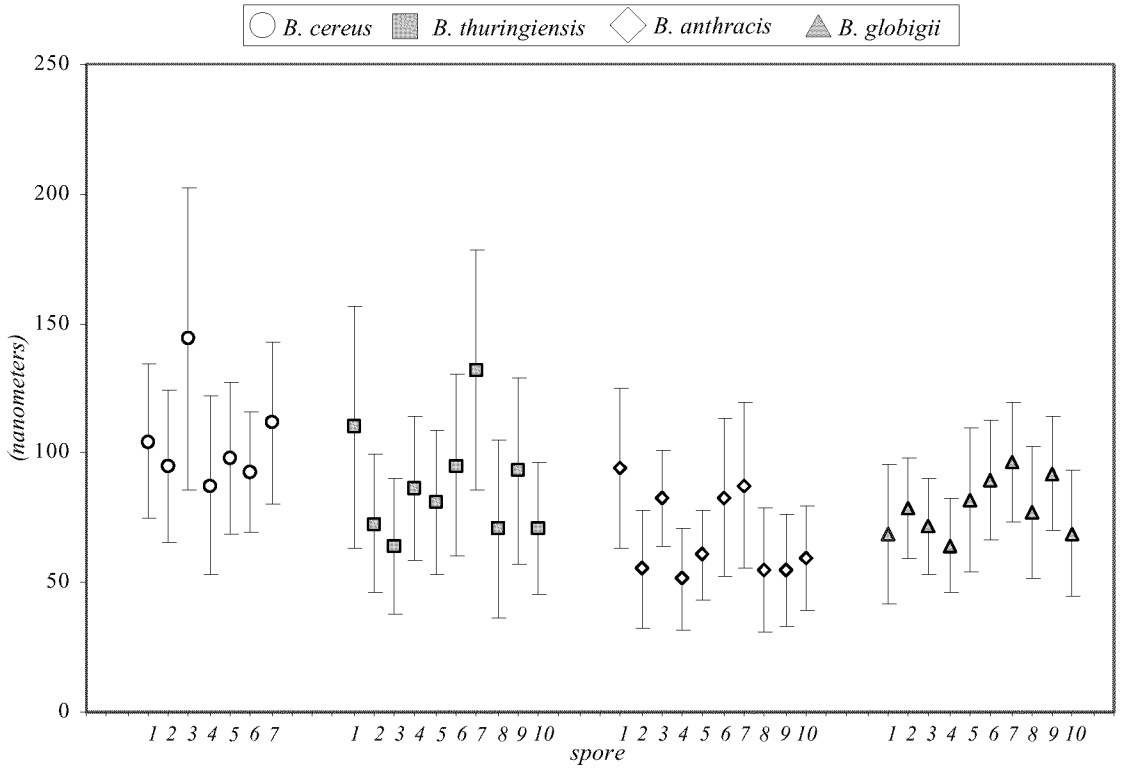

Figure 51. Roughness Analysis: Comparison of Z-Range

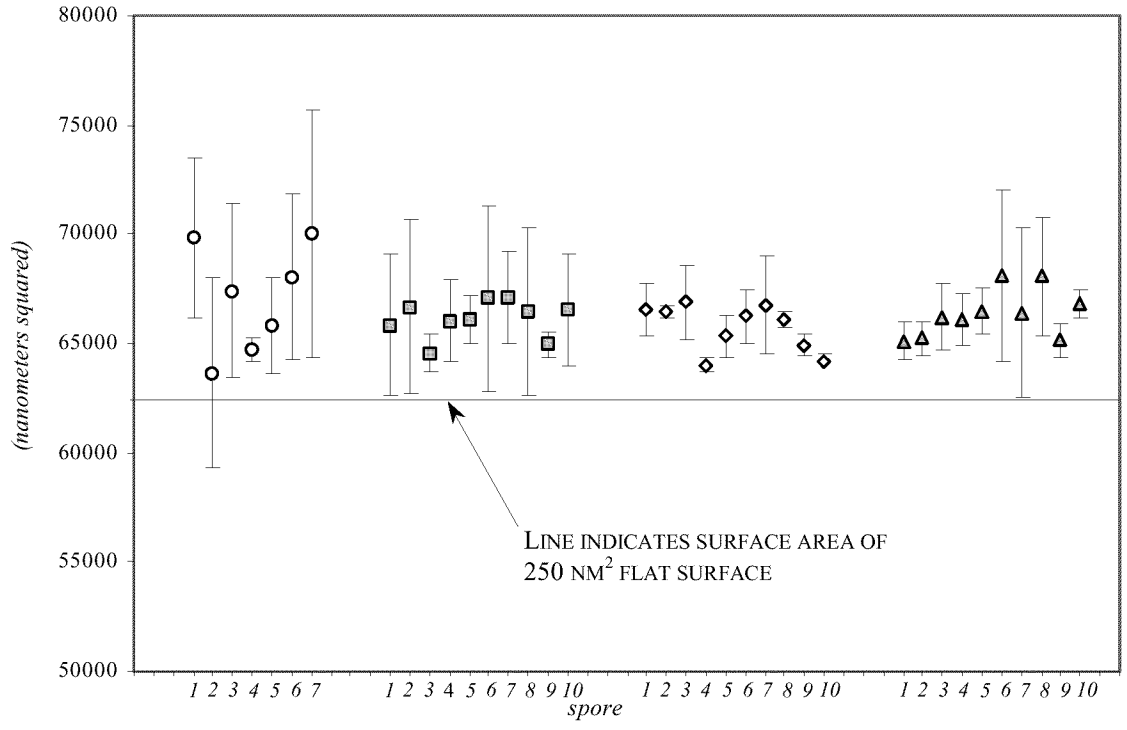

Figure 52. Roughness Analysis: Comparison of Surface Area

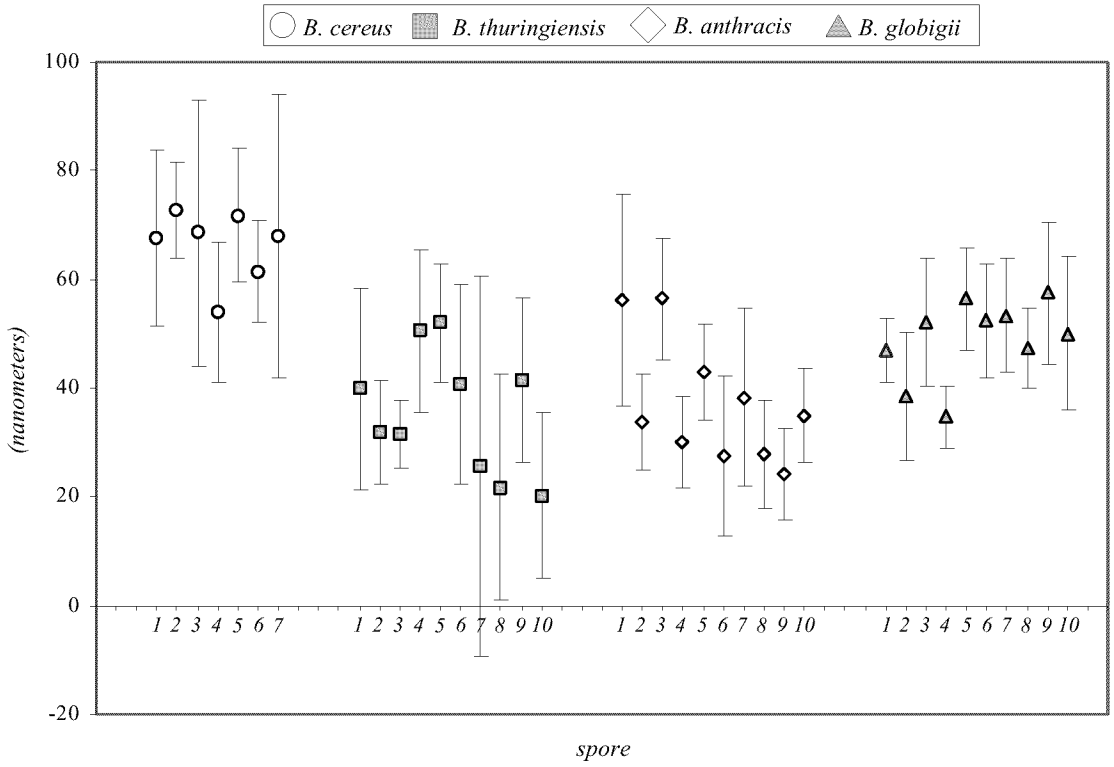

Figure 53. Roughness Analysis: Comparison of Mean

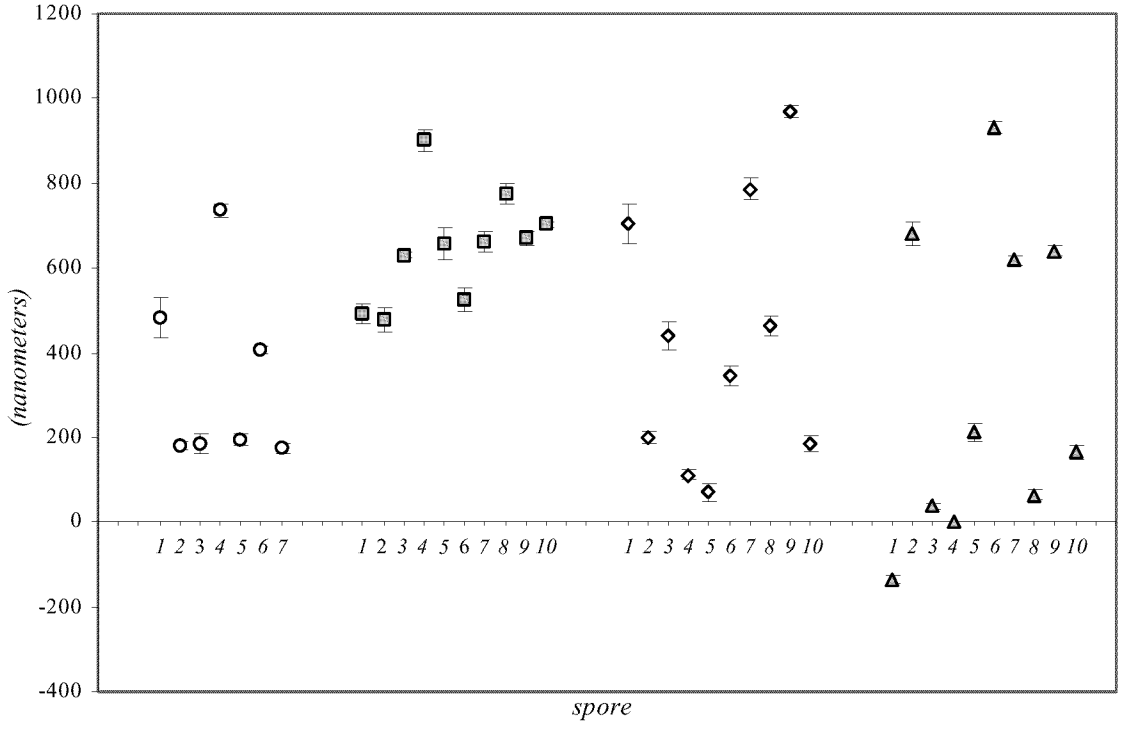

Figure 54. Roughness Analysis: Comparison of Raw Mean

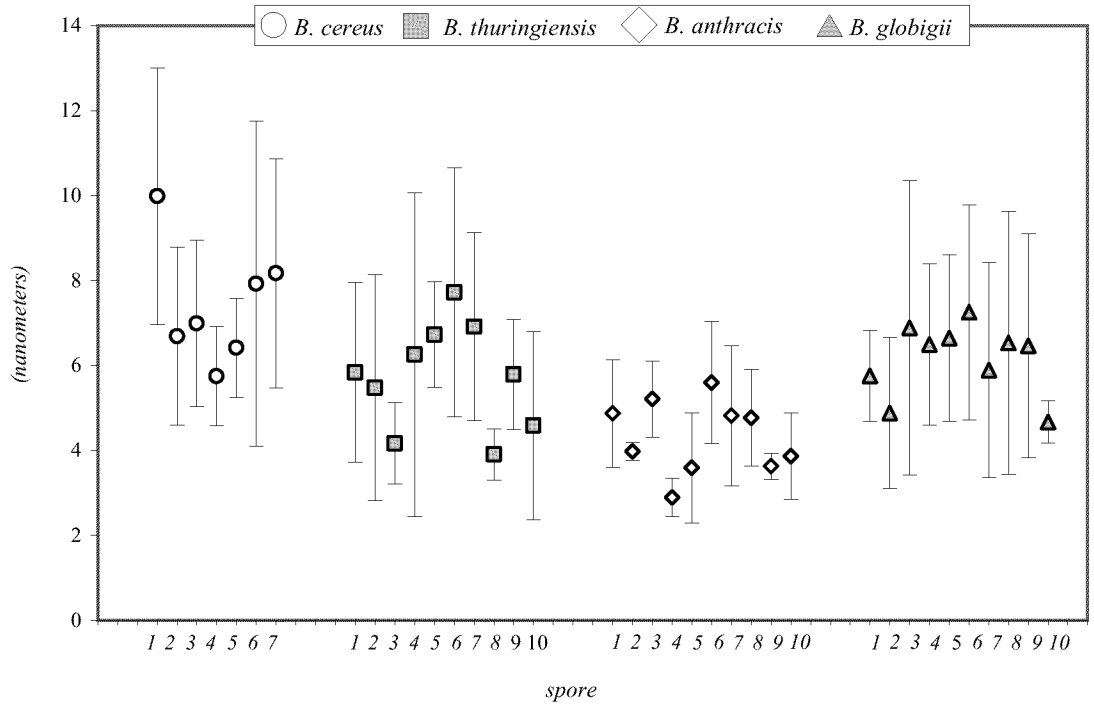

Figure 55. Roughness Analysis: Comparison of Roughness, R_a

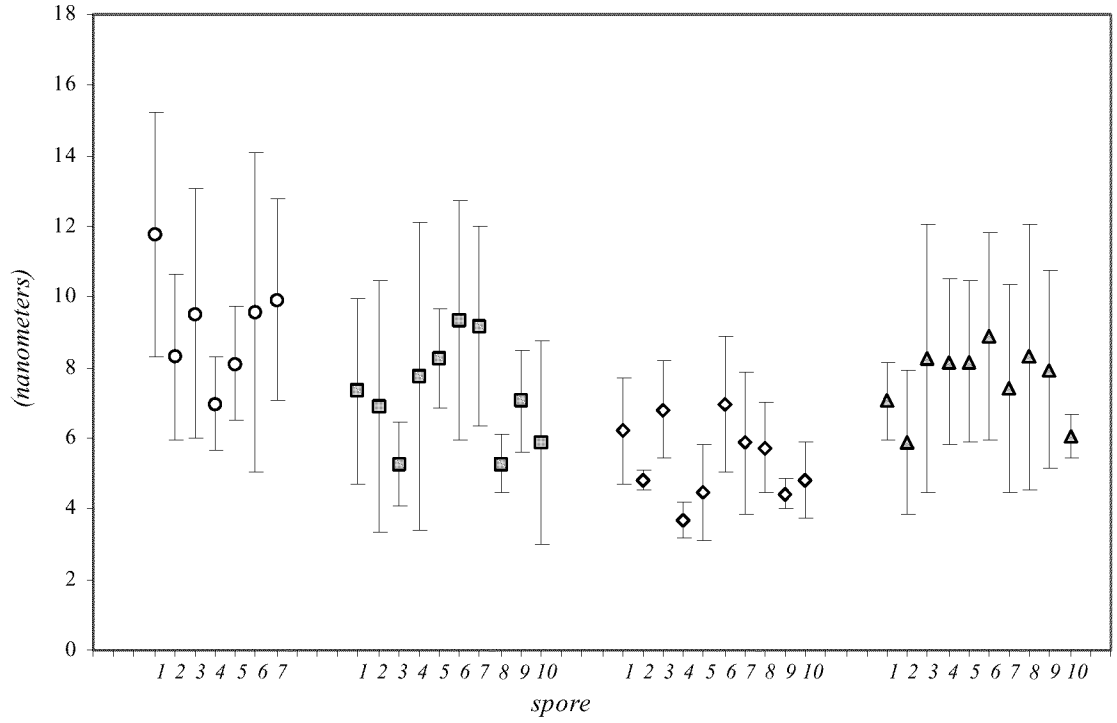

Figure 56. Roughness Analysis: Comparison of RMS Roughness, R_q

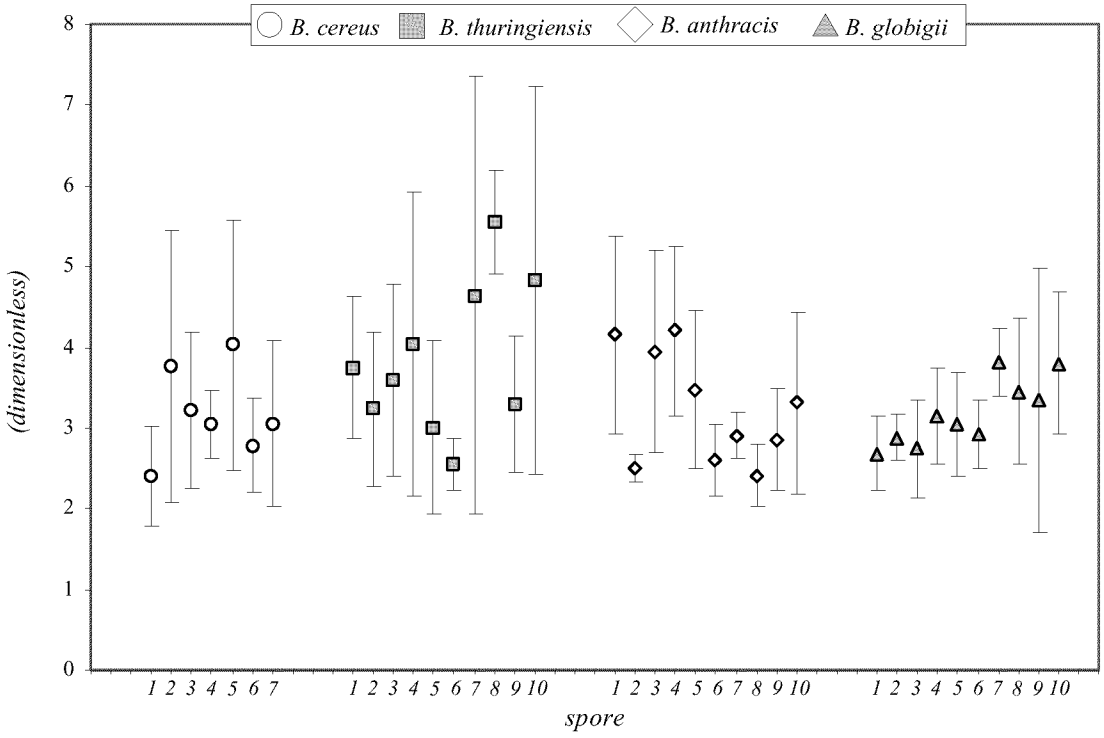

Figure 57. Roughness Analysis: Comparison of Kurtosis

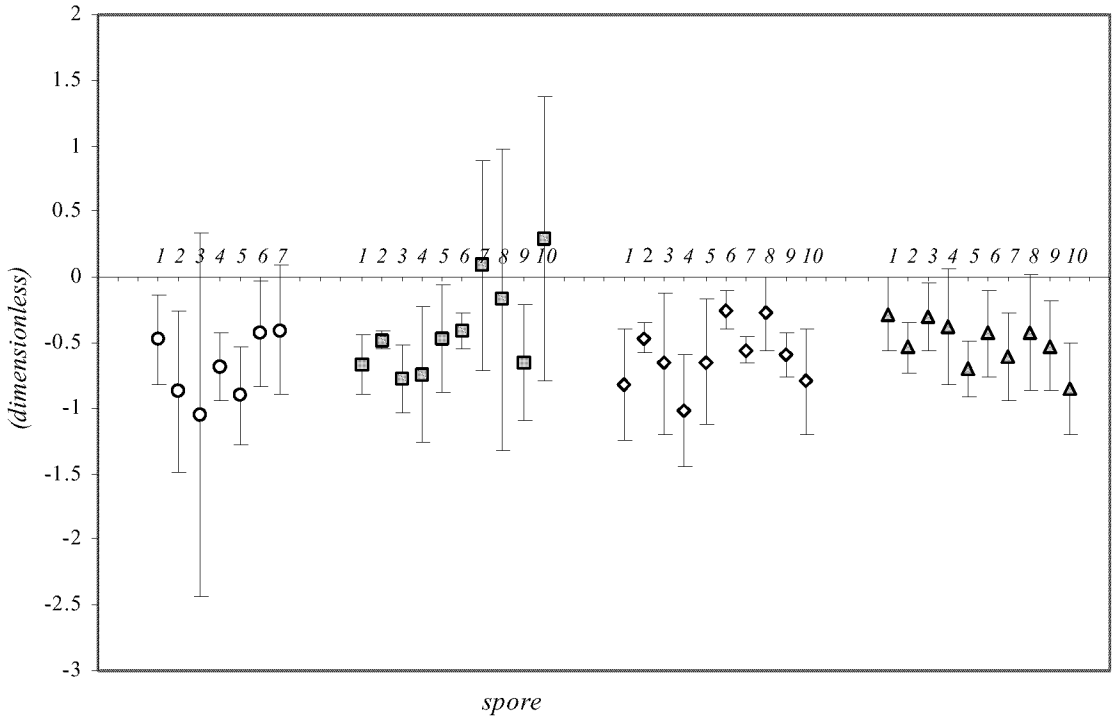

Figure 58. Roughness Analysis: Comparison of Skewness

Comparison of the roughness R_a and RMS roughness R_q (Figures 55 and 56) indicates similarity between species as well as significant variations on the surfaces of each spore. Overall, the roughness is very small (< 15nm) for all species. The spores of *B. anthracis* did exhibit slightly lower roughness (R_a and R_q) as well as less variation on the surface of the individual spores.

The kurtosis and skewness data (Figures 57 and 58) provide information on the shape of the height distribution around the mean. The kurtosis results show that the height data is arranged closely around the mean. The skewness results indicate a slight negative skew in the distribution around the mean. There does not appear to be any significant differences between bacterial species. However, some spores exhibit significantly more variation than others indicating a more heterogeneous and uneven surface for some spores.

The roughness analysis provides some indication of the distribution of vertical features on the surfaces of the bacterial spores. The results show that in terms of the spatial frequency of vertical features, the four species examined here are not readily distinguishable. This does not mean that the spores cannot be differentiated based on surface morphology and roughness. By changing even one part of the analysis protocol (such as plane-fitting on a higher order, or flattening the image to eliminate surface curvature) a completely different outcome could result. The best conclusion that can be drawn is that the surface of each spore contains a great deal of information and variability. This variability is compounded when considering several spores of one species that do not exhibit completely consistent properties. The existence of a quantitatively typical or characteristic surface morphology remains elusive.

Power Spectral Density Analysis Results

Figures 59 through 62 show the two-dimensional isotropic PSD versus wavelength. All plots are generally tapered, which is characteristic of a flat, isotropic surface lacking ordered features. Figure 63 shows a comparison between one spore from each species (*B. cereus* spore 2, *B. thuringiensis* spore 4, *B. anthracis* spore 2, and *B. globigii* spore 2). Any differences in terms of power spectral density are obscured in the smaller wavelengths of the figures that correspond to the scale of the spore surface features.

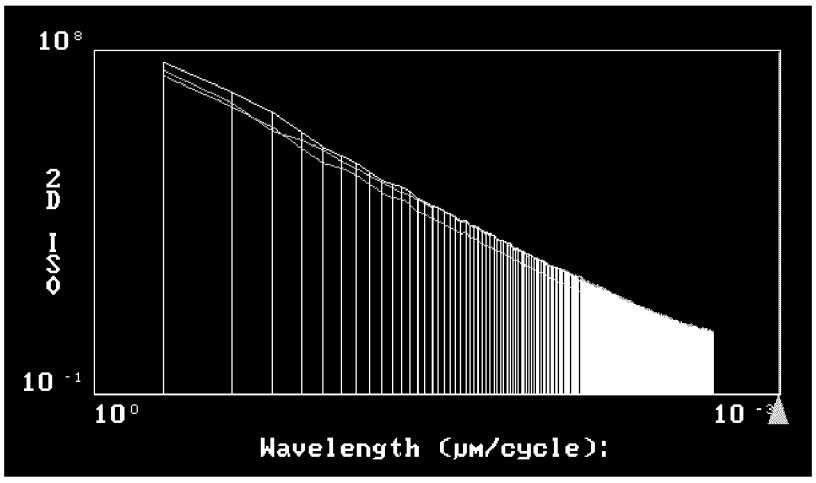

Figure 59. Power Spectral Density for *B. cereus*
(Spores 1-5, 500nm^2 scan size)

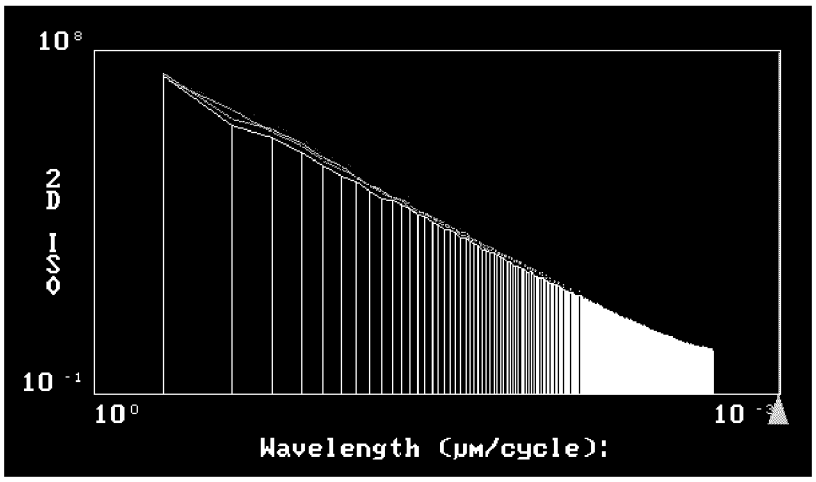

Figure 60. Power Spectral Density for *B. thuringiensis*
(Spores 1-5, 500nm^2 scan size)

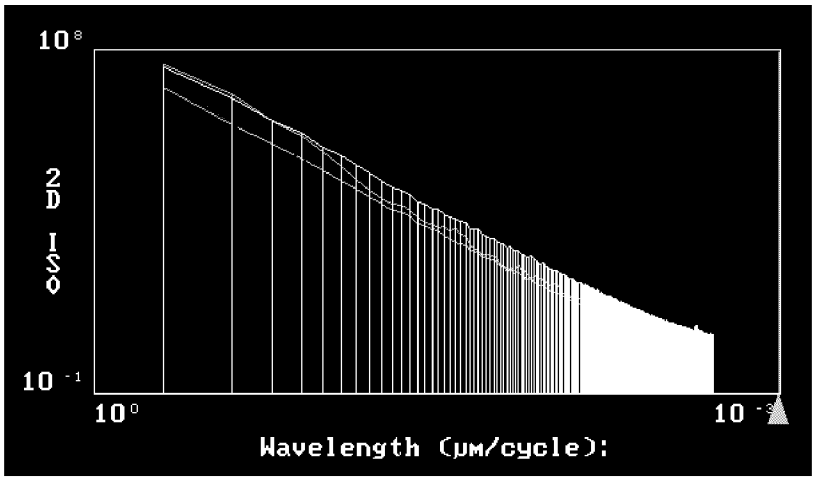

Figure 61. Power Spectral Density for *B. anthracis*
(Spores 1-5, 500nm^2 scan size)

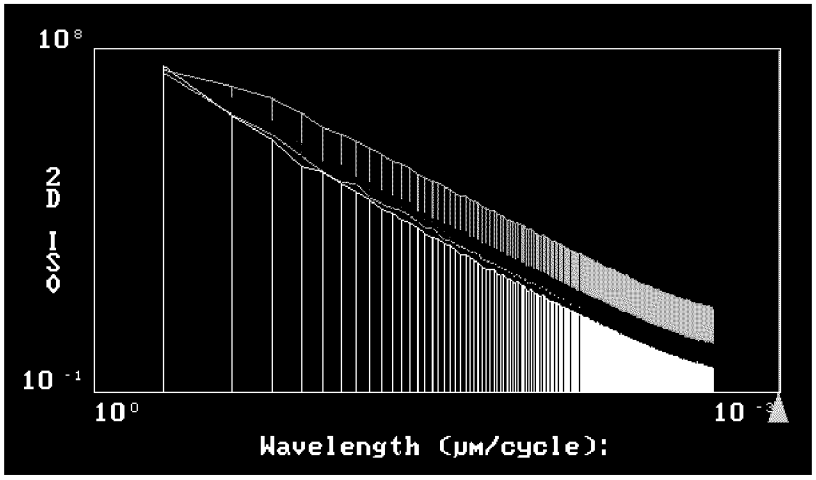

Figure 62. Power Spectral Density for *B. globigii*
(Spores 1-5, 500nm^2 scan size)

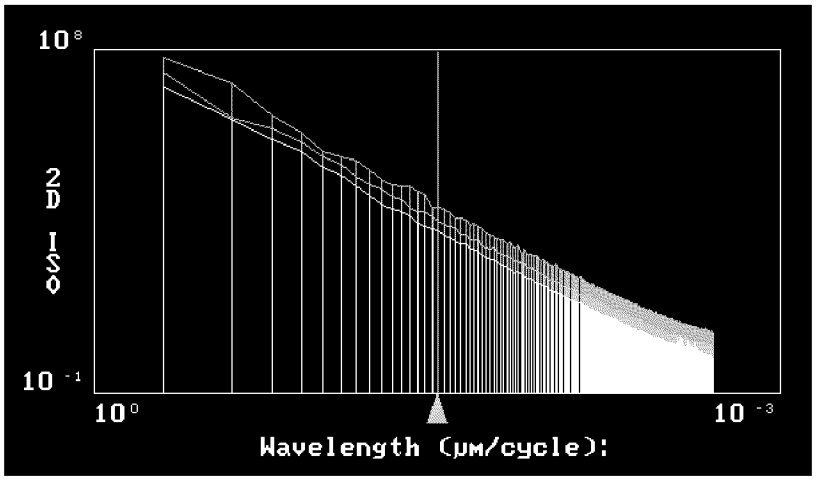

Figure 63. Power Spectral Density Comparison
(yellow for *B. anthracis*, red for *B. cereus*, blue for *B. globigii*, and green for *B. thuringiensis*)

Bearing Analysis Results

The results of the bearing analysis are presented in Figures 64 through 67. The figures are surface height histograms. The histograms are derived from the $500nm^2$ images from all thirty-seven spores. It should be noted that the depth scales are not uniform throughout the figures. The depth on the vertical axis refers to the depth of a point below the plane of the highest point on the image.

It is clear that each species does not have a characteristic height profile. There is significant variation of vertical features on the surfaces of spores within the same species. The spikes in some of the histograms indicate a distinct vertical feature. The flatter surfaces are clearly represented by the narrow histograms (*B. thuringiensis* spore 10). The more curved surfaces have a broader histogram (*B. globigii* spore 9). The general lack of a Gaussian shape in the histograms most likely indicates that the area of the original image did not span the entire width of the spore. Section analysis of the spores did show that the top surface of the spore was evenly curved.

It is important to realize that the histograms represent only approximately one third of the top surface area of a spore. Consequently, the histograms may not be completely representative of the entire spore surface. Rather, they may reflect anomalies more readily than (or out of proportion to) the typical surface morphology. However, this is also an example the variability inherent to each spore's surface.

Prior to analysis, each image was plane-fitted, but not flattened. Thus, the natural curvature of the spore surface is represented in the histograms.

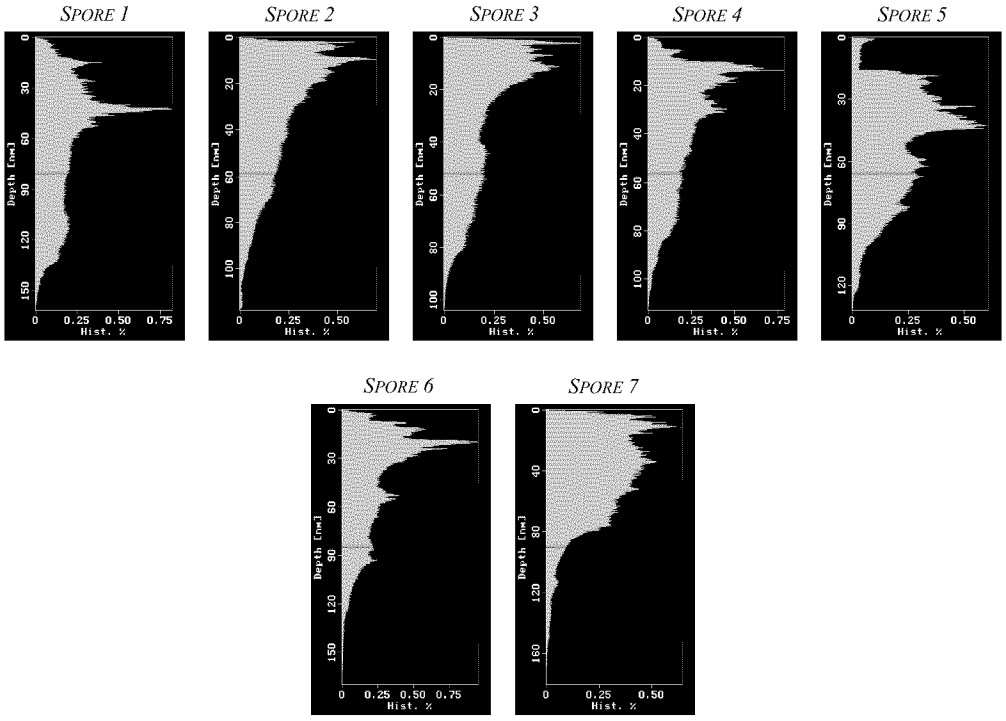

Figure 64. *B. cereus* Bearing Analysis

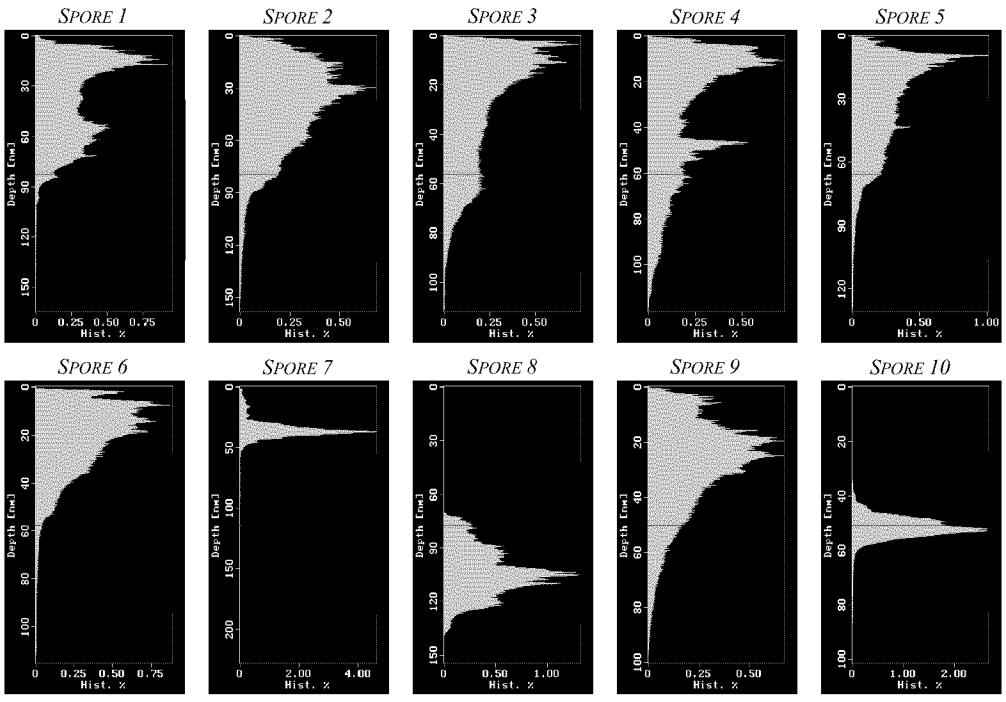

Figure 65. *B. thuringiensis* Bearing Analysis

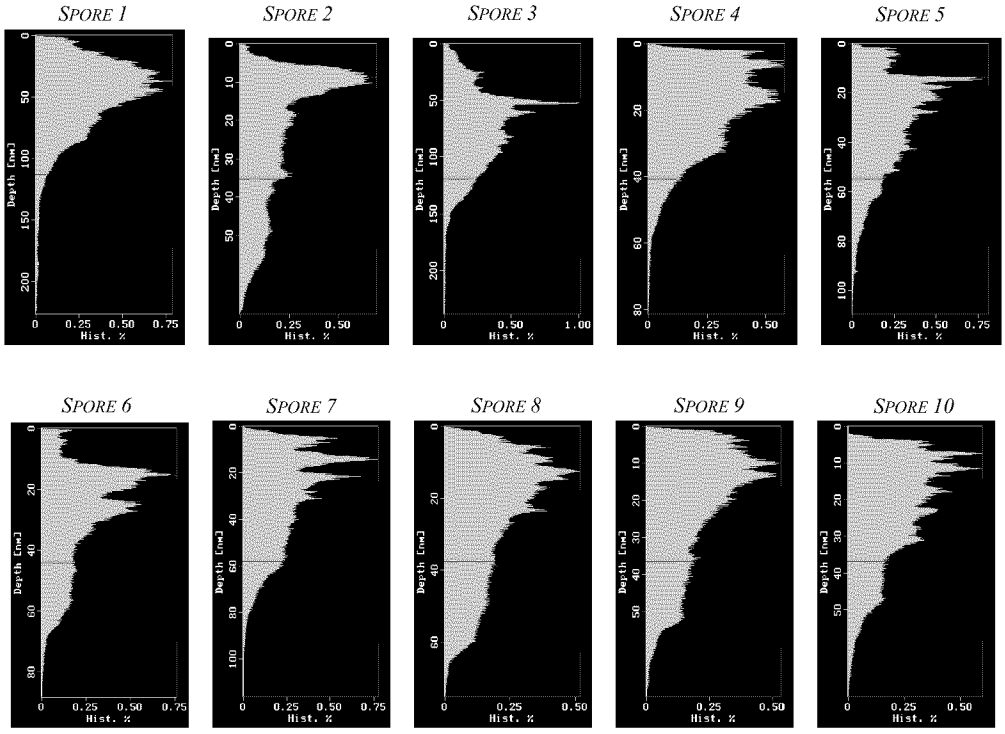

Figure 66. *B. anthracis* Bearing Analysis

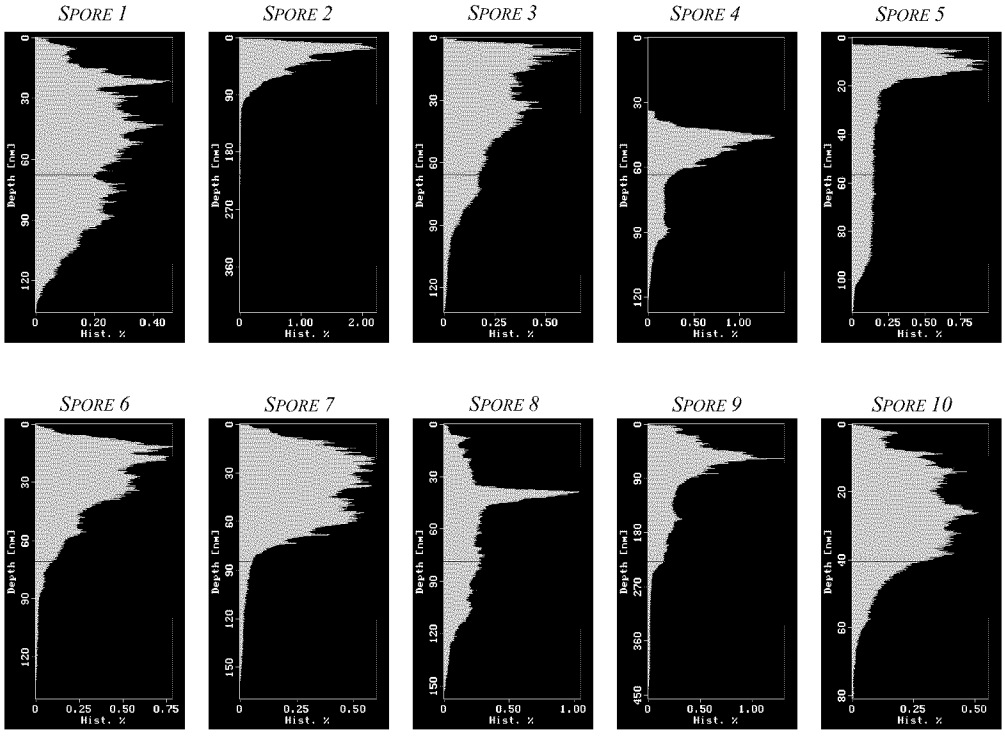

Figure 67. *B. globigii* Bearing Analysis

V. Discussion

Overview

It is clear from the atomic force microscopy images presented in Chapter 4 that the *Bacillus* spore has an information rich surface. Connecting the features observed on the spore surfaces with the limited knowledge found in the literature was difficult. Although the phase images provided a detailed view of the surface, attributing the phase contrasts to physical or biochemical structures was not possible. Altogether, this work is a first step in understanding the surface morphology and biochemical properties of spores studied by atomic force microscopy.

Linking Observations to Theory

Past work on the surface structure of *Bacillus* spores has been done primarily with electron microscopy of spore sections. These sections do not yield much information about surface morphology. Other electron microscopy images of gross spore structure are not presented with sufficient magnification to discern particular details of the surface morphology. Also, techniques of fixation and sample preparation likely alter the natural surfaces to a significant degree. Thus, there is not a solid reference to compare the images presented in this work.

Although the biochemical structure of the outer spore integument has been studied, it has not been definitively established. The exosporium has been shown as a site for esterase activity and is regarded as a site for the production of autolytic enzymes that

degrade the mother cell (Ohye and Murrell, 1973, 1189). This implies a certain amount of biochemical machinery that might be present on the spore surface. However, it is not possible to identify these structures in the images that resulted from this work.

The irregular morphology observed of the spore surfaces could be due to inclusions beneath the exosporium, adsorbed biomolecules, or bona fide surface features (such as an outgrowth or an appendage). For the most part, it appears that the structure is due to features underlying the exosporium. The presence of these features has been documented in the literature (as they are easily visible in sections). The exosporium is commonly described as being "distended by underlying deposits of planar inclusions" (Beaman 1972:1198).

The analysis of parasporal crystals observed in *B. thuringiensis* spores allowed for a solid link to be forged between theory and observation. The structure of the insecticidal crystals has been well established. Observations of the geometry of the parasporal crystals measured from *B. thuringiensis* spore images could be correlated with the cubic structure of the Cry2 toxin produced during sporulation.

Overall, this thesis effort has produced a great deal of new information, rather than reproducing work that has been published previously. Atomic force microscopy has allowed an unprecedented analysis of the biochemical properties and morphology of the natural spore surface unperturbed by dyes, fixatives, or the harsh environment of a vacuum.

Implications of Experimental Method

Overall, the experimental method established that a relatively simple protocol could be employed to image bacterial spores using atomic force microscopy. The use of TappingMode provided significantly more information than contact mode. As the probe makes only intermittent contact with the surface, lateral and shear forces are reduced (Nagao and Dvorak 1999:3289). No surface damage was observed, indicating the spore surface is sufficiently rugged for this type of analysis.

The results do not indicate that the imaging method allowed for sub-molecular resolution of the sample surface. This is possible with intermittent contact mode under certain conditions. The ultimate resolution obtained in this work was not experimentally measured. The $500nm^2$ images suggest that close features could be distinguished at 10-50nm (lateral not vertical). Different scans produced different levels of resolution

Interpreting Phase Images

It is clear from the results that the phase data provided clearer images than the height data. However understanding and interpreting the phase images is more complicated. The phase image is generated from the phase lag of the cantilever oscillation while scanning the sample surface relative to the signal sent to the cantilever's piezoelectric driver.

The phase images should be considered as not just representative of surface properties, but of surface-probe interaction. Phase contrast is affected by several probe properties: the magnitude of the tapping force; stiffness of the cantilever; probe/sample contact area; and drive frequencies (Nagao and Dvorak 1999:3296). Even under harder

tapping forces, only a small fraction of the power delivered to the tapping cantilever is dissipated in the tip – sample interactions (Bar and others 2000:L15). Forces acting on a tip vary non-linearly as a function of tip-sample distance (Bar and others, 2000:L198).

Phase lags are produced by variations in surface material properties such as adhesion, friction, and viscoelasticity (Babcock and Prater, 1995). Phase images do not generally include height information (Nagao and Dvorak 1999:3294). Primarily, phase images map stiffness variations on a surface. A stiffer region has a more positive shift and appears brighter (Magonov and others 1997:L387). Adhesive properties such as capillary forces from the thin layer of water on the sample surface can also lead to a phase lag (Schmitz and others, 1997:191).

It was not possible to identify the cause of the phase contrasts observed on the surfaces of the spores imaged in this work. This would require a detailed mapping of the localized interactive forces between the surface and the probe. Or, the use of functionalized probes could be used to more readily map changes in biochemistry.

Recommendations for Future Work

The results of this work, if nothing else, illustrate the potential of atomic force microscopy to break new ground in bacterial spore research. Recommendations for follow-on research fall into three categories: (1) more sophisticated analysis of existing images; (2) broadening the current methodology; and (3) developing new and better methods to image spore surfaces using atomic force microscopy.

First, hundreds of images of spore surfaces were generated as part of this work. The analysis and interpretation of these images presented here does not completely

capture all of the information available from the digital images. A more refined study would be possible by applying techniques of pattern recognition to each image.

Several options exist to broaden the scope of the current methodology. One of the AFM capabilities not used here was the ability of the AFM to quantitatively map the interaction forces between the cantilever tip and the sample surface. Studying this interaction could yield significantly more information about the exterior surface structure of a bacterial spore. It could be especially useful in the study of mechanisms of bacterial adhesion.

By developing a more extensive atmospheric chamber, the changes that spores undergo as a result of atmospheric disinfectant (such as chlorine dioxide gas) could yield real-time detailed information on the effects of such chemicals and methods to optimize their use.

Several weaknesses inherent in this study should be addressed. First, a calibration grid that can effect calibration on the scale of 10-50nm should be used. Only a 10 micron grid was available for this work which proved inadequate for calibration of the scale of spores. Second, a scanner that works on a smaller scale might be more effective and provide more detailed information. Third, the reduction in humidity used a crude set-up that was not monitored. Humidity control should have taken place in order to ensure identical conditions for each spore. Although no changes were observed in the spore surface features as a result of N_2 gas exposure, this should be tested. The introduction of a more inert gas may have been better. Finally, this work should be correlated with another form of microscopy.

One of the most promising directions for future work is the development of a protocol for examining spores in TappingMode in aqueous conditions using a liquid cell. This AFM configuration has been proven to produce high-resolution images that could even surpass those obtained in this work. Further, using a liquid cell would allow images to be obtained as spores germinate, documenting the morphological changes over time. This could also allow studying the effects of various chemicals (such as fixatives or dyes) or antibiotics on the surface morphology of spores.

Conclusions

Of the three objectives sought by this research, two were achieved. An effective protocol was developed that allowed the examination of the surface structure of bacterial spores without any chemical or physical pretreatment. Second, this protocol allowed a detailed study of spore surface morphology with far more detail than was expected.

Atomic force microscopy allowed a detailed characterization of bacterial spore surface morphology. However, analysis of the images on three scales failed to discern surface features that could be considered distinctive of a given species or that could be used to distinguish spores of different species. Nonetheless, this does not imply that surface characteristics are not present that could discriminate one species of spore from another. Rather, this work suggests that further analysis could reveal the subtle distinctions exposed by this experimental method.

However, the methodology developed as part of this work enabled spores to be examined in a manner that allowed a detailed study of the spore surface morphology. The atomic force microscope allowed information to be collected in a variety of ways. The

information gathered was consistent and provided several methods for analysis of the spore surface properties.

Initially, it is not surprising that distinctions could not be made between the *Bacillus* species examined here based solely on spore surface morphology. The differences among the species are primarily found on extrachromosomal DNA. The genes governing sporulation should be fairly consistent among the species.

However, the diverse surface properties exhibited by the spores, such as hydrophobicity and adhesion, suggest that differences do exist. This work represents the first step in linking the behavior of the spores to specific biochemical structures inherent to the spore surfaces.

Finally, a greater understanding of the surface properties of *Bacillus* spores has far-reaching consequences. These range from improved disinfection technologies, better materials for medical applications, and perhaps even a simpler, more reliable, and faster detector of biological pathogens. All of these are desired in order to combat the effects of that simple structure of bacterial dormancy – the spore.

Appendix: The Geometry of a Cubic Unit Cell Cleaved Along the (111) Plane

The cubic unit cell cleaved along the (111) plane is shown in Figure 68. The theoretical angle that is produced by cleaving the plane was determined by applying the Pythagorean theorem and Law of Cosines. The resulting angle corresponds to the geometry of the parasporal crystals in *B. thuringiensis* spores 7, 8, and 10. The derivation of this angle is shown graphically in Figures 69 through 73.

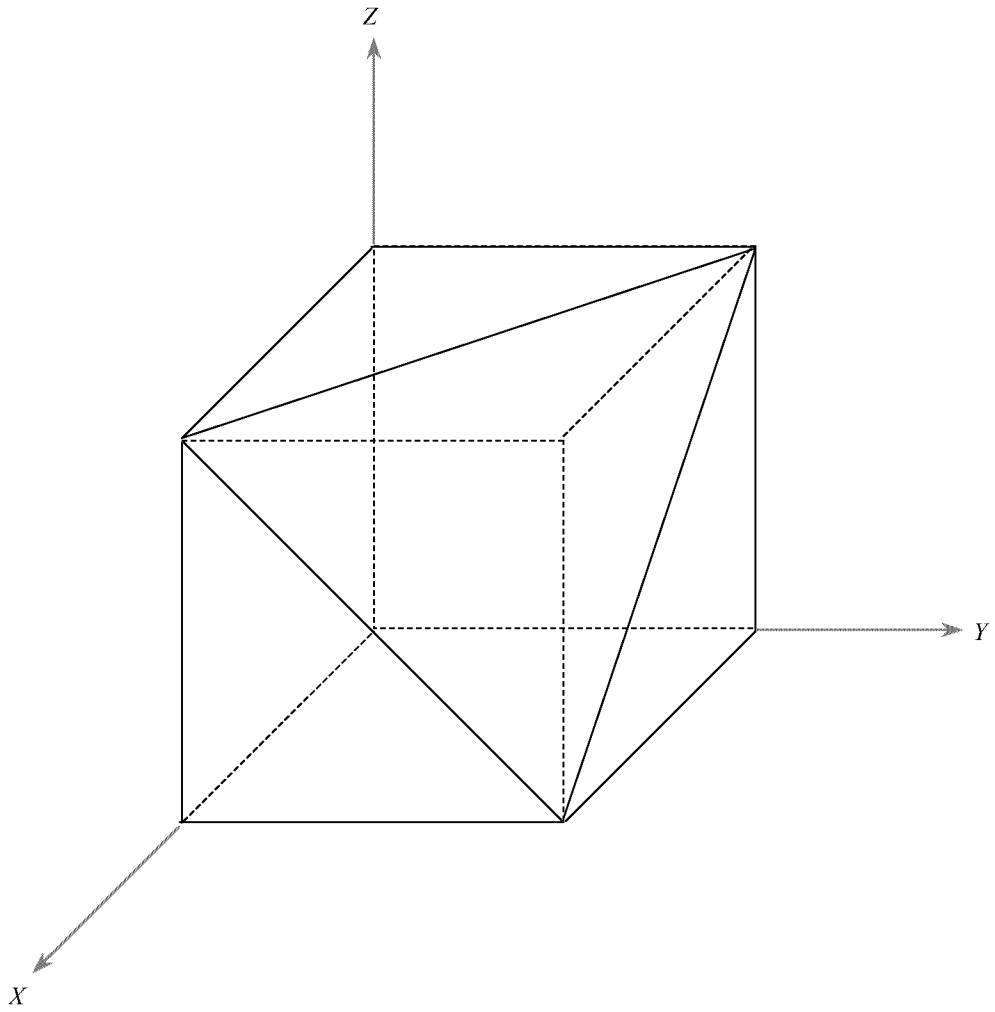

Figure 68. Cubic Unit Cell Cleaved Along the (111) Plane

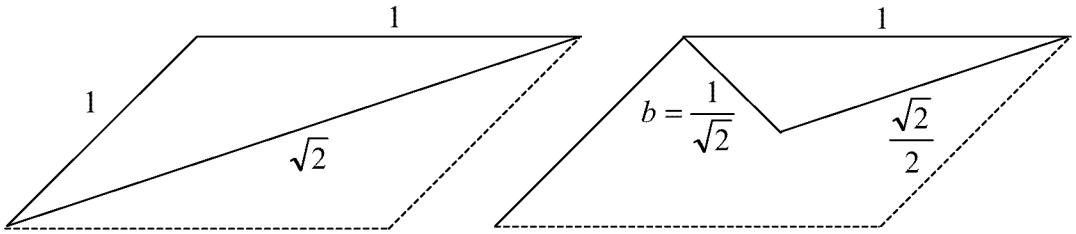

Figure 69. Derivation of Length of Side *b*

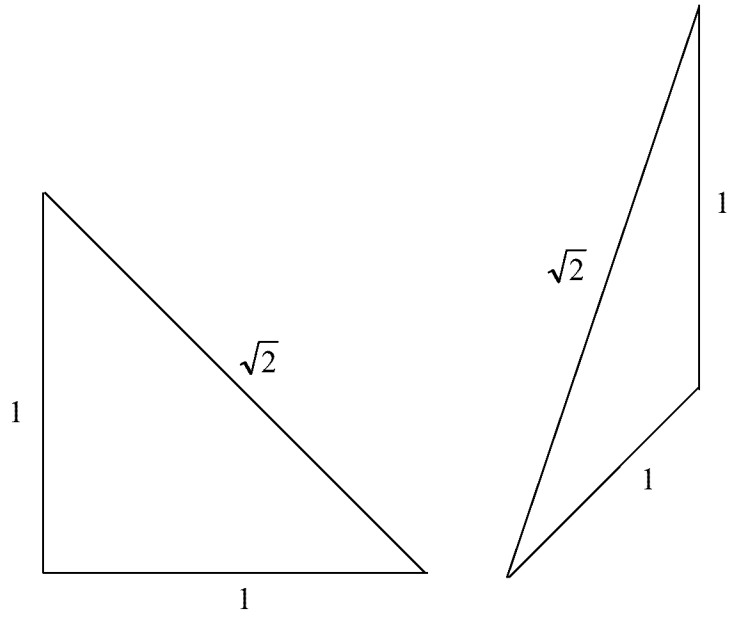

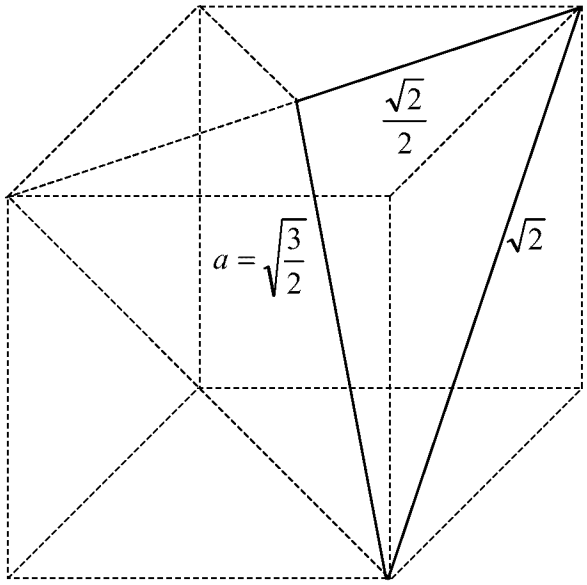

Figure 70. Derivation of Length of Side *a*

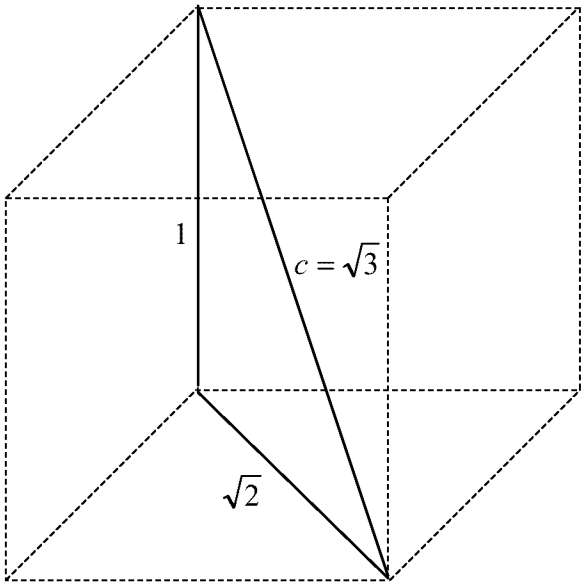

Figure 71. Derivation of Length of Side *c*

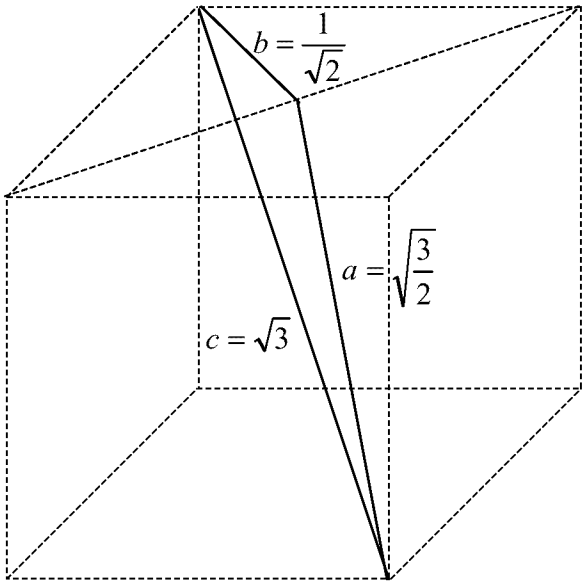

Figure 72. Triangle Used For Law of Cosines Calculation

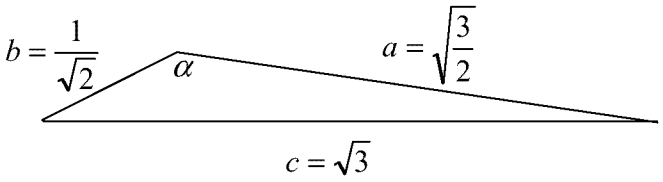

$$\cos\alpha = \frac{a^2 + b^2 - c^2}{2ab}$$

$$\alpha = 144.7^\circ$$

Figure 73. Law of Cosines Calculation

Figure 74 shows the theoretical geometry of a cross section of the parasporal crystal analogous to that presented in Figure 43 of Chapter 4. The angle that is used for comparison is 144.7°.

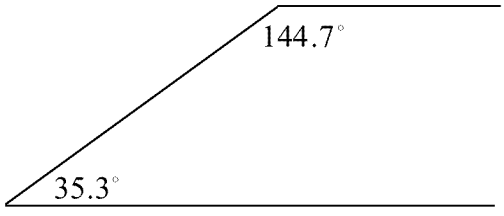

Figure 74. Theoretical Cross-Sectional Geometry of Parasporal Crystal

Bibliography

A-Hassan, E., W. F. Heinz, M. D. Antonik, N. P. D'Costa, S. Nageswaran, C.-A. Schoenenberger and J. H. Hoh. "Relative Microelastic Mapping of Living Cells by Atomic Force Microscopy," *Biophysical Journal*, 74:1564-1578 (1998).

Agaisse, H. and D. Lereclus. "How Does *Bacillus thuringiensis* Produce So Much Insecticidal Crystal Protein?," *Journal of Bacteriology*, 177:6027-6032 (November 1995).

Albrecht, T. R., S. Akamine, T. E. Carver and C. F. Quate. "Microfabrication of Cantilever Styli for the Atomic Force Microscope," *Journal of Vacuum Science and Technology A*, 8:3386-3396 (July/August 1990).

Allison, D. P., L. A. Bottomley, T. Thundat, G. M. Brown, R. P. Woychik, J. J. Schrick, K. B. Jacobson and R. J. Warmack. "Immobilization of DNA For Scanning Probe Microscopy," *Proceedings of the National Academy of Sciences*, 89:10129-10133 (November 1992).

Andersen, G. L., J. M. Simchock and K. H. Wilson. "Identification of a Region of Genetic Variability Among *Bacillus anthracis* Strains and Related Species," *Journal of Bacteriology*, 178:377-384 (1996).

Arnoldi, M., C. M. Kacher, E. Bäuerlein, M. Radmacher and M. Fritz. "Elastic Properties of the Cell Wall of *Magnetospirillum grypiswaldense* Investigated by Atomic Force Microscopy," *Applied Physics A*, 66:S613-S617 (1998).

Aronson, A. I. "Insecticidal Toxins," in *Bacillus subtilis and Other Gram-Positive Bacteria: Biochemistry, Physiology, and Molecular Genetics*. Ed. A. L. Sonenshein. Washington, D.C.: American Society for Microbiology, 1993.

"ASME B46.1-1995: Surface Texture (An American National Standard)," New York: The American Society of Mechanical Engineers, 1996.

Ash, C. J. A. Farrow, M. Dorsch, E. Stackebrandt, and M. D. Collins. "Comparative analysis of *Bacillus anthracis*, *Bacillus cereus*, and related species on the basis of reverse transcriptase sequencing of 16S rRNA," *International Journal of Systematic Bacteriology*, 41:343-436 (1991a)

Ash, C. and M. D. Collins. "Comparative Analysis of 23S Ribosomal RNA Gene Sequences of *Bacillus anthracis* and Emetic *Bacillus cereus* Determined by PCR-Direct Sequencing," *FEMS Microbiology Letters*, 94:75-80 (1992).

Ash, C., J. A. E. Farrow, S. Wallbanks and M. D. Collins. "Phylogenetic Heterogeneity of the Genus *Bacillus* Revealed by Comparative Analysis of Small-Subunit-Ribosomal RNA Sequences," *Letters in Applied Microbiology*, 13:202-206 (1991b).

Atrih, A., P. Zöllner, G. Allmaier, M. P. Williamson and S. J. Foster. "Peptidoglycan Structural Dynamics during Germination of *Bacillus subtilis* 168 Endospores," *Journal of Bacteriology*, 180:4603-4612 (September 1998).

Auerbach, I. D., C. Sorensen, H. G. Hansma and P. A. Holden. "Physical Morphology and Surface Properties of Unsaturated *Pseudomonas putida* Biofilms," *Journal of Bacteriology*, 182:3809-3815 (July 2000).

Babcock, K. L. and C. B. Prater. "Phase Imaging: Beyond Topography," *Digital Instruments Application Notes*, (1995).

"Bacteria Collection Catalog," Excerpt from unpublished article. n. pag. http//www.atcc.org. 2001.

Baker, A. A., W. Helbert, J. Sugiyama and M. J. Miles. "High-Resolution Atomic Force Microscopy of Native *Valonia* Cellulose I Microscrystals," *Journal of Structural Biology*, 119:129-138 (1997).

----. "Surface Structure of Native Cellulose Microcrystals by AFM," *Applied Physics A*, 66:S559-S563 (1998).

Baker, A. A. and M. J. Miles. "Molecular Imaging of Cellulose," *BIOforum International*, 2:96-100 (1997).

Baker, A. A., M. J. Miles and W. Helbert. "Internal Structure of the Starch Granule Revealed by AFM," *Carbohydrate Research*, 330:249-256 (2001).

Bar, G., R. Brandsch, M. Bruch, L. Delineaue and M.-H. Whangbo. "Examination of the relationship between phase shift and energy dissipation in tapping mode atomic force microscopy by frequency-sweep and force-probe measurements," *Surface Science*, 444:L11-L16 (2000).

Baselt, D. R., G. U. Lee and R. J. Colton. "Biosensor based on force microscope technology," *Journal of Vacuum Science and Technology B*, 14:789-793 (March/April 1996).

Barnaby, W. *The Plague Makers*. New York: Continuum, 2000.

Bath, J., L. J. Wu, J. Errington and J. C. Wang. "Role of *Bacillus subtilis* SpoIIIE in DNA Transport Across the Mother Cell-Prespore Division Septum," *Science*, 290:995-997 (3 November 2000).

Beaman, T. C., J. T. Greenamyre, T. R. Corner, H. S. Pankratz and P. Gerhardt. "Bacterial Spore Heat Resistance Correlated with Water Content, Wet Density, and Protoplast/Sporoplast Volume Ratio," *J. Bacteriol.*, 150:870-877 (May 1982).

Beaman, T. C., H. S. Pankratz and P. Gerhardt. "Ultrastructure of the Exosporium and Underlying Inclusions in Spores of *Bacillus megaterium* Strains," *Journal of Bacteriology*, 109:1198-1209 (March 1972).

Beverly, M. B., K. J. Voorhees, T. L. Hadfield and R. B. Cody. "Electron Monochromoter Mass Spectrometry for Analysis of Whole Bacteria and Bacterial Spores," *Anal. Chem.*, 72:2428-2432 (1 June 2000).

Bhushan, B. "Introduction," in *Handbook of Micro/Nano Tribology*. Ed. B. Bhushan. Boca Raton, Florida: CRC Press, 1995.

Binnig, G., C. F. Quate and C. Gerber. "Atomic Force Microscope," *Physical Review Letters*, 56:930-933 (1986).

Black, G. E., A. P. Snyder and K. S. Heroux. "Chemotaxonomic Differentiation Between the *Bacillus cereus* Group and *Bacillus subtilis* by Phospholipid Extracts Analyzed with Electrospray Ionization Tandem Mass Spectrometry," *Journal of Microbiological Methods*, 28:187-199 (1997).

Boyle-Vavra, S., J. Hahm, S. J. Sibener and R. S. Daum. "Structural and Topological Differences between a Glycopeptide-Intermediate Clinical Strain and Glycopeptide-Susceptible Strains of *Staphylococcus aureus* Revealed by Atomic Force Microscopy," *Antimicrobial Agents and Chemotherapy*, 44:3456-3460 (December 2000).

Bradley, D. E. and J. G. Franklin. "Electron Microscope Survey of the Surface Configuration of Spores of the Genus *Bacillus*," *Journal of Bacteriology*, 76:618-630 (1958).

Bradley, D. E. and D. J. Williams. "An Electron Microscope Study of the Spores of Some Species of the Genus *Bacillus* Using Carbon Replicas," *Journal of General Microbiology*, 17:75-79 (1957).

Braga, P. C. and D. Ricci. "Atomic Force Microscopy: Application to Investigation of *Escherichia coli* Morphology Before and After Exposure to Cefodizime," *Antimicrobial Agents and Chemotherapy*, 42:18-22 (January 1998).

Cacciafesta, P., K. R. Hallam, A. C. Watkinson, G. C. Allen, M. J. Miles and K. D. Jandt. "Visualisation of Human Plasma Fibrinogen Adsorbed on Titanium Implant Surfaces With Different Roughness," *Surface Science*, 491:405-420 (2001).

Cacciafesta, P., A. D. L. Humphris, K. D. Jandt and M. J. Miles. "Human Plasma Fibrinogen Adsorption on Ultraflat Titanium Oxide Surfaces Studies with Atomic Force Microscopy," *Langmuir*, (2000).

Carlson, C. R., D. A. Caugant and A.-B. Kolstø. "Genotypic Diversity Among *Bacillus cereus* and *Bacillus thuringiensis* Strains," *Applied and Environmental Microbiology*, 60:1719-1725 (June 1994).

Carlson, C. R., A. Grønstad, and A.-B. Kolstø. "Physical Maps of the Genomes of Three *Bacillus cereus* Strains," *Journal of Bacteriology*, 174:3750-3756 (1992).

Carlson, C. R., T. Johansen, M.-M. Lecadet and A.-B. Kolstø. "Genomic Organization of the Entomopathogenic Bacterium *Bacillus thuringiensis* subsp. *berliner* 1715," *Microbiology*, 142:1625-1634 (1996).

Castleman, K. R. *Digital Image Processing*. Englewood Cliffs, New Jersey: Prentice-Hall, Inc., 1996.

Chamberlain, A. K., C. E. MacPhee, J. Zurdo, L. A. Morozova-Roche, H. A. O. Hill, C. M. Dobson and J. Davis, J. "Ultrastructural Organization of Amyloid Fibrils by Atomic Force Microscopy," *Biophysical Journal*, 79:3282-3293 (December 2000).

Charlton, S., A. J. G. Moir, L. Baillie and A. Moir. "Characterization of the Exosporium of *Bacillus cereus*," *Journal of Applied Microbiology*, 87:241-245 (1999).

Cohen, S., I. Mendelson, Z. Altboum, D. Kobiler, E. Elhanany, T. Bino, M. Leitner, I. Inbar, H. Rosenberg, Y. Gozes and Barak. "Attenuated Nontoxigenic and Nonencapsulated Recombinant *Bacillus anthracis* Spore Vaccines Protect Against Anthrax," *Infection and Immunity*, 68:4549-4558 (August 2000).

Command Reference Manual. Version 4.31ce MN-REF-COM-4.31ce, Rev. A-20OCT97. Digital Instruments, 1999.

Daffonchio, D., S. Borin, G. Frova, R. Gallo, E. Mori, R. Fani and C. Sorlini. "A Randomly Amplified Polymorphic DNA Marker Specific for the *Bacillus cereus* Group Is Diagnostic for *Bacillus anthracis*," *Applied and Environmental Microbiology*, 65:1298-1303 (March 1999).

Daffonchio, D., A. Cherif and S. Borin. "Homoduplex and Heteroduplex Polymorphisms of the Amplified Ribosomal 16S-23S Internal Transcribed Spacers Describe Genetic Relationships in the "*Bacillus cereus* Group"," *Applied and Environmental Microbiology*, 66:5460-5468 (December 2000).

Dagnall, H. *Exploring Surface Texture*. Leicester, England: Rank Taylor Hobsob, 1980.

De Souza Pereira, R. and O. Teschke. "Observation of Structures on *Saccharomyces cerevisiae* Cell Wall by Atomic Force Microscopy," *Probe Microscopy*, 1:277-282 (1997).

Desrosier, J. P. and J. C. Lara. "Synthesis of the Exosporium During Sporulation of *Bacillus cereus*," *Journal of General Microbiology*, 130:935-940 (1984).

Digital Instruments Scanning Probe Microscopy Training Notebook. Digital Instruments, 1998.

Doi, R. H. "Sporulation and Germination," in *Bacillus*. Ed. C. R. Harwood. New York: Plenum Press, 1989.

Doyle, R. J., F. Nedjat-Haiem and J. S. Singh. "Hydrophobic Characteristics of *Bacillus* Spores," *Current Microbiology*, 10:329-332 (1984).

Drake, B., C. B. Prater, A. L. Weisenhorn, S. A. C. Gould, T. R. Albrecht, C. F. Quate, D. S. Cannell, H. G. Hansma and P. K. Hansma. "Imaging Crystals, Polymers, and Processes in Water with the Atomic Force Microscope," *Science*, 243:1586-1589 (1989).

Driks, A. "*Bacillus subtilis* Spore Coat," *Microbiology and Molecular Biology Reviews*, 63:1-20 (March 1999).

Driks, A. and P. Setlow. "Morphogenesis and Properties of the Bacterial Spore," in *Prokaryotic Development*. Ed. B. Y. V and L. J. Shimkets. Washington, D.C.: American Society of Microbiology, 2000.

Drobniewski, F. A. "*Bacillus cereus* and Related Species," *Clinical Microbiology Reviews*, 6:324-338 (October 1993).

Dufrêne, Y. F. "Direct Characterization of the Physicochemical Properties of Fungal Spores Using Functionalized AFM Probes," *Biophysical Journal*, 78:3286-3291 (June 2000).

Dufrêne, Y. F., C. J. Boonaert, P. A. Gerin, M. Asther and P. G. Rouxhet. "Direct Probing of the Surface Ultrastructure and Molecular Interactions of Dormant and Germinating Spores of *Phanerochaete chrysosporium*," *Journal of Bacteriology*, 181:5350-5354 (September 1999).

Dufrêne, Y. F., W. R. Barger, J.-B. D. Green and G. U. Lee. "Nanometer-Scale Surface Properties of Mixed Phospholipid Monolayers and Bilayers," *Langmuir*, 13:4779-4784 (1997).

Ellar, D. J. and D. G. Lundgren. "Fine Structure of Sporulation in *Bacillus cereus* Grown in a Chemically Defined Medium," *Journal of Bacteriology*, 92:1748-1764 (December 1966).

Enserink, M. "Taking Anthraz's Genetic Fingerprint," *Science*, 294:1810-1812 (30 November 2001).

Euzeby, J. P. "List of Bacterial Names with Standing in Nomenclature," Excerpt from unpublished article. n. pag. http//www.bacterio.cict.fr. 10 September 2001.

Fang, H. H. P., K.-Y. Chan and L.-C. Xu. "Quantification of Bacterial Adhesion Forces Using Atomic Force Microscopy (AFM)," *Journal of Microbiological Methods*, 40:89-97 (2000).

Fawcett, P., P. Eichenberger, R. Losick and P. Youngman. "The Transcriptional Profile of Early to Middle Sporulation in *Bacillus subtilis*," *Proceedings of the National Academy of Sciences*, 97:8063-8068 (July 5 2000).

Gergely, C., J.-C. Voegel, P. Schaaf, B. Senger, M. Maaloum, J. K. H. Hörber and J. Hemmerlé. "Unbinding Process of Adsorbed Proteins Under External Stress Studied by Atomic Force Microscopy Spectroscopy," *Proceedings of the National Academy of Sciences*, 97:10802-10807 (26 September 2000).

Gerhardt, P. "Fine Structure of the *Bacillus thuringiensis* Spore," *Applied and Environmental Microbiology*, 32:438-440 (September 1976).

Gerhardt, P. and E. Ribi. "Ultrastructure of the Exosporium Enveloping Spores of *Bacillus cereus*," *Journal of Bacteriology*, 88:1774-1789 (December 1964).

Goh, M. C., M. F. Paige, M. A. Gale, I. Yadegari, M. Edirisinghe and J. Strzelczyk. "Fibril formation in collagen," *Physica A*, 239:95-102 (1997).

Gordon, R. E., W. C. Haynes and C. H.-N. Pang. *Agriculture Handbook No. 427: The Genus Bacillus*. Washington, D.C.: Agricultural Research Service, United States Department of Agriculture, 1973.

Granum, P. E. "*Bacillus cereus*," in *Food Microbiology: Fundamentals and Fronteirs*. Ed. M. P. Doyle, L. R. Beuchat and T. J. Montville. Washington, D.C.: ASM Press, 2001.

Hachisuka, Y., K. Kojima and T. Sato. "Fine Filaments on the Outside of the Exosporium of *Bacillus anthracis* Spores," *Journal of Bacteriology*, 91:2382-2384 (June 1966).

Hachisuka, Y. and S. Kozuka. "A New Test of Differentiation of *Bacillus cereus* and *Bacillus anthracis* Based on the Existence of Spore Appendages," *Microbiol. Immunol.*, 25:1201-1207 (1981).

Hachisuka, Y., S. Kozuka and M. Tsujikawa. "Exosporia and Appendages of Spores of *Bacillus* Species," *Microbiol. Immunol.*, 28:619-624 (1984).

Hallett, P., L. Tskhovrebova, J. Trinnick, G. Offer and M. J. Miles. "Improvements in Atomic Force Microscopy Protocols for Imaging Fibrous Proteins," *Journal of Vacuum Science and Technology*, 14:1444-1448 (March/April 1996).

Hansma, H. G. "Varieties of Imaging With Scanning Probe Microscopes," *Proceedings of the National Academy of Sciences*, 96:14678-14680 (21 December 1999).

Hansma, H. G. and J. H. Hoh. "Biomolecular Imaging with the Atomic Force Microscope," *Annu. Rev. Biophys. Biomol. Struct.*, 23:115-139 (1994).

Hansma, H. G., J. Vesenka, C. Siegerist, G. Kelderman, H. Morrett, R. L. Sinsheimer, V. Elings, C. Bustamante and P. K. Hansma. "Reproducible Imaging and Dissection of Plasmid DNA Under Liquid with the Atomic Force Microscope," *Science*, 256:1180-1184 (22 May 1992).

Harwood, C. R. "Introduction to the Biotechnology of *Bacillus*," in *Bacillus*. Ed. C. R. Harwood. New York: Plenum Press, 1989.

Hathout, Y., P. A. Demirev, Y.-P. Ho, J. L. Bundy, V. Ryzhov, L. Sapp, J. Stutler, J. Jackman and C. Fenselau. "Identification of *Bacillus* Spores by Matrix-Assisted Laser Desorption Ionization-Mass Spectrometry," *Applied and Environmental Microbiology*, 65:4313-4319 (October 1999).

Heinz, W. F. and J. H. Hoh. "Relative Surface Charge Density Mapping with the Atomic Force Microscope," *Biophysical Journal*, 76:528-538 (1999a).

Heinz, W. F. and J. H. Hoh. "Spatially Resolved Force Spectroscopy of Biological Surfaces Using the Atomic Force Microscope," *TIBTECH*, 17:143-150 (April 1999b).

Helgason, E., D. A. Caugant, I. Olsen and A.-B. Kolstø. "Genetic Structure of Population of *Bacillus cereus* and *B. thuringiensis* Isolates Associated with Periodontitis and Other Human Infections," *Journal of Clinical Microbiology*, 38:1615-1622 (April 2000a).

Helgason, E., O. A. Økstad, D. A. Caugant, H. A. Johansen, A. Fouet, M. Mock, I. Hegna and A.-B. Kolstø. "*Bacillus anthracis*, *Bacillus cereus*, and *Bacillus thuringiensis* - One Species on the Basis of Genetic Evidence," *Applied and Environmental Microbiology*, 66:2627-2630 (June 2000b).

Hemmerlé, J., S. M. Altmann, M. Maaloum, J. K. H. Hörber, L. Heinrich, J.-C. Voegel and P. Schaaf. "Direct Observation of the Anchoring Process During the Adsorption of Fibrinogen on a Solid Surface by Force-Spectroscopy Mode Atomic Force Microscopy," *Proceedings of the National Academy of Sciences*, 96:6705-6710 (1999).

Howland, R. and L. Benatar. "A Practical Guide to Scanning Probe Microscopy," Excerpt from unpublished article. n. pag. http//www.tmmicro.com (March, 2000).

Husmark, U. *Adhesion Mechanisms of Bacterial Spores to Solid Surfaces*. PhD dissertation. Chalmers University of Technology, Goteborg, Sweden, 1993.

Husmark, U. and U. Ronner. "Forces Involved in Adhesion of *Bacillus cereus* Spores to Solid Surfaces Under Different Environmental Conditions," *Journal of Applied Microbiology*, 69:557-562 (1990).

----. "The Influence of Hydrophobic, Electrostatic, and Morphologic Properties on the Adhesion of *Bacillus* Spores," *Biofouling*, 5:335-344 (1992).

Iacono-Connors, L. C., C. S. Schmaljohn and J. M. Dalrymple. "Expression of the *Bacillus anthracis* Protective Antigen Gene by Baculovirus and Vaccinia Virus Recombinants," *Infection and Immunity*, 58:366-372 (February 1990).

Jackson, P. J., K. K. Hill, M. T. Laker, L. O. Ticknor and P. Keik. "Genetic Comparison of *Bacillus anthracis* and its Close Relatives Using Amplified Fragment Length Polymorphism and Polymerase Chain Reaction Analysis," *Journal of Applied Microbiology*, 87:263-269 (1999).

Jackson, P. J., M. E. Hugh-Jones, D. M. Adair, G. Green, K. K. Hill, C. R. Kuske, L. M. Grinberg, F. A. Abramova and P. Keim. "PCR Analysis of Tissue Samples From the 1979 Sverdlovsk Anthrax Victims: The Presence of Multiple *Bacillus anthracis* Strains in Different Victims," *Proceedings of the National Academy of Sciences*, 95:1224-1229 (February 1998).

Jandt, K. D. "Atomic Force Microscopy of Biomaterials Surfaces and Interfaces," *Surface Science*, 491:303-332 (2001).

Jass, J., T. Tjärnhage and G. Puu. "From Liposomes to Supported, Planar Bilayer Structures on Hydrophilic and Hydrophobic Surfaces: An Atomic Force Microscopy Study," *Biophysical Journal*, 79:3153-3163 (2000).

Johnson, J. L. "Bacterial Classification III: Nucleic Acids in Bacterial Classification," in *Bergey's Manual of Systematic Bacteriology*. Ed. N. R. Krieg and J. G. Holt. Baltimore: Williams & Wilkins, 1984.

Jones, D. "Bacterial Classification IV: Genetic Methods," in *Bergey's Manual of Systematic Bacteriology*. Ed. N. R. Krieg and J. G. Holt. Baltimore: Williams & Wilkins, 1984.

Jones, D. and N. R. Krieg. "Bacterial Classification V: Serology and Chemotaxonomy," in *Bergey's Manual of Systematic Bacteriology*. Ed. N. R. Krieg and J. G. Holt. Baltimore: Williams & Wilkins, 1984.

Karrasch, S., R. Hegerl, J. H. Hoh, W. Baumeister and A. Engel. "Atomic Force Microscopy Produces Faithful High-Resolution Images of Protein Surfaces in an Aqueous Environment," *Proceedings of the National Academy of Sciences*, 91:836-838 (1994).

Keim, P., A. Kalif, J. Schupp, K. Hill, S. E. Travis, K. Richmond, D. M. Adair, M. Hugh-Jones, C. R. Kuske and P. Jackson. "Molecular Evolution and Diversity in *Bacillus anthracis* as Detected by Amplified Fragment Length Polymorphism Markers," *Journal of Bacteriology*, 179:818-824 (1997).

Keim, P., A. M. Klevytska, L. B. Price, J. M. Schupp, G. Zinser, K. L. Smith, M. E. Hugh-Jones, R. T. Okinaka, K. K. Hill and P. J. Jackson. "Molecular Diversity in *Bacillus anthracis*," *Journal of Applied Microbiology*, 87:215-217 (1999).

Kiel, J. L., J. E. Parker, J. L. Alls, J. Kalns, E. A. Holwitt, L. J. V. Stribling, P. Morales and J. G. Bruno. "Rapid Recovery and Identification of Anthrax Bacteria from the Environment," *Fifth Biennial Conference of the Society for Tropical Veterinary Medicine*. 240-252. Key West, Florida: New York Academy of Sciences, 2000.

Kolb, H.-A., O. Enders and R. Schauer. "Morphology of Native and Reconstituted Biological Membranes and Their Components Analyzed with Atomic Force Microscopy," *Applied Physics A*, 68:247-254 (1999).

Kolstø, A.-B., A. Grønstad, and H. Oppegaard. "Physical Map of the *Bacillus cereus* Chromosome," *Journal of Bacteriology*, 172:3821-3825 (1990).

Koshikawa, T., M. Yamazaki, M. Yoshimi, S. Ogawa, A. Yamada, K. Watabe and M. Torii. "Surface Hydrophobicity of Spores of *Bacillus* spp.," *Journal of General Microbiology*, 135:2717-2722 (1989).

Kotra, L. P., N. A. Amro, G.-Y. Liu and S. Mobashery. "Visualizing Bacteria at High Resolution," *ASM News*, 66:675-681 (2000).

Kozuka, S. and K. Tochikubo. "Properties and Origin of Filamentous Appendages on Spores of *Bacillus cereus*," *Microbiol. Immunol.*, 29:21-37 (1985).

Le Grimellac, C., E. Lesniewska, M.-C. Giocondi, E. Finot, V. Vié and J.-P. Goudonnet. "Imaging of the Surface of Living Cells by Low-Force Contact-Mode Atomic Fore Microscopy," *Biophysical Journal*, 75:695-703 (1998).

Lechner, S., R. Mayr, K. P. Francis, B. M. Prüß, T. Kaplan, E. Wiebner-Gunkel, G. S. A. B. Stewart and S. Scherer. "*Bacillus weihenstephanensis* sp. nov. is a New Psychrotolerant Species of the *Bacillus cereus* Group," *International Journal of Systematic Bacteriology*, 48:1373-1382 (1998).

Léonard, C., O. Zekri and J. Mahillon. "Integrated Physical and Genetic Mapping of *Bacillus cereus* and Other Gram-Positive Bacteria Based on IS*231*A Transposition Vectors," *Infection and Immunity*, 66:2163-2169 (May 1998).

Leuschner, R. G. K. and P. J. Lillford. "Investigation of Bacterial Spore Structure by High Resolution Solid-State Nuclear Magnetic Resonance Spectroscopy and Transmission Electron Microscopy," *International Journal of Food Microbiology*, 63:35-50 (2001).

Liang, X. and D. Yu. "Identification of *Bacillus anthracis* Strains in China," *Journal of Applied Microbiology*, 87:200-203 (1999).

Logan, N. A., J. A. Carman, J. Melling and R. C. W. Berkeley. "Identification of *Bacillus anthracis* by API Tests," *Journal of Medical Microbiology*, 20:75-85 (1985).

Lopez-Meza, J. E. and J. E. Ibarra. "Characterization of a Novel Strain of *Bacillus thuringiensis*," *Applied and Environmental Microbiology*, 62:1306-1310 (April 1996).

Lower, S. K., M. F. Hochella Jr and T. J. Beveridge. "Bacterial Recognition of Mineral Surfaces: Nanoscale Interactions Between *Shewanella* and α-FeOOH," *Science*, 292:1360-1363 (18 May 2001).

Magonov, S. N., V. Elings and M.-H. Whangbo. "Phase imaging and stiffness in tapping-mode atomic force microscopy," *Surface Science*, 375:L385-L391 (1997).

Mäntyen, V. and K. Lindström. "A Rapid PCR-Based DNA Test for Enterotoxic *Bacillus cereus*," *Applied and Environmental Microbiology*, 64:1634-1639 (May 1998).

Marahiel, M. A., and P. Zuber. "Sporulation and Cell Differentiation: Sporulation in *Bacillus subtilis* Is a Multi-step Process That Can Be Dissected Genetically; The Formation of Endospores," in *Biology of the Prokaryotes*. Ed. J. W. Lengeler, G. Drews and H. G. Schlegel. Stuttgart: Georg Thiene Verlag, (1999).

Marshall, B. J. and W. G. Murrell. "Biophysical Analysis of the Spore," *Journal of Applied Bacteriology*, 33:103-129 (1970).

Matz, L. L., T. C. Beaman and P. Gerhardt. "Chemical Composition of Exosporium from Spores of *Bacillus cereus*," *Journal of Bacteriology*, 101:196-201 (January 1970).

McClung, L. S. *General Bacteriology Laboratory Manual*. Philadelphia: W. B. Saunders Company, 1952.

McKiernan, A. E., T. V. Ratto and M. L. Longo. "Domain Growth, Shapes, and Topology in Cationic Lipid Bilayers on Mica by Fluorescence and Atomic Force Microscopy," *Biophysical Journal*, 79:2605-2615 (2000).

McMaster, T. J., M. Berry, A. P. Corfield and M. J. Miles. "Atomic Force Microscopy of the Submolecular Architecture of Hydrated Ocular Mucins," *Biophysical Journal*, 77:533-541 (1999).

McMaster, T. J., M. O. Winfield, A. A. Baker, A. Karp and M. J. Miles. "Chromosome Classification by Atomic Force Microscopy," *Journal of Vacuum Science and Technology*, 14:1438-1443 (March/April 1996).

McMaster, T. J., M. J. Miles, P. R. Shewry and A. S. Tatham. "In Situ Surface Adsorption of Protein C Hordein Using Atomic Force Microscopy," *Langmuir*, 16:1463-1468 (22 February 2000).

Mechaber, W. L., D. B. Marshall, R. A. Mechaber, R. T. Jobe and F. S. Chew. "Mapping Leaf Surface Landscapes," *Proceedings of the National Academy of Sciences*, 93:4600-4603 (May 1996).

Meyer, G. and N. M. Amer. "Novel Optical Approach to Atomic Force Microscopy," *Applied Physics Letters*, 53:1045-1047 (19 September 1988).

Miles, M. "Scanning Probe Microscopy: Probing the Future," *Science*, 277:1845-1846 (19 September 1997).

Mizuki, E., M. Ohba, T. Ichimatsu, S.-H. Hwang, K. Higuchi, H. Saito and T. Akao. "Unique Appendages Associated With Spores of *Bacillus cereus* Isolates," *J. Basic Microbiol.*, 38:33-39 (1998).

Moberly, B. J., F. Shafa and P. Gerhardt. "Structural Details of Anthrax Spores During Stages of Transformation into Vegetative Cells," *Journal of Bacteriology*, 92:220-228 (July 1966).

Möller, C., M. Allen, V. Elings, A. Engel and D. J. Müller. "Tapping-Mode Atomic Force Microscopy Produces Faithful High-Resolution Images of Protein Surfaces," *Biophysical Journal*, 77:1150-1158 (August 1999).

Morris, V. J., A. R. Kirby and A. P. Gunning. *Atomic Force Microscopy for Biologists*. London: Imperial College Press, 1999.

Mueller, H., H.-J. Butt and B. Ernst. "Force Measurements on Myelin Basic Protein Adsorbed to Mica and Lipid Bilayer Surfaces Done with the Atomic Force Microscope," *Biophysical Journal*, 76:1072-1079 (1999).

Müller, D. J., W. Baumeister and A. Engel. "Conformational Change of the Hexagonally Packed Intermediate Layer of *Deinococcus radiodurans* Monitored by Atomic Force Microscopy," *Journal of Bacteriology*, 178:3025-3030 (June 1996).

Müller, D. J., W. Baumeister and A. Engel. "Controlled Unzipping of a Bacterial Surface Layer With Atomic Force Microscopy," *Proceedings of the National Academy of Sciences*, 96:13170-13174 (9 November 1999a).

Müller, D. J., D. Fotiadis, S. Scheuring, S. A. Müller and A. Engel. "Electrostatically Balanced Subnanometer Imaging of Biological Specimens by Atomic Force Microscope," *Biophysical Journal*, 76:1101-1111 (1999b).

Multimode™ SPM Instruction Manual. Version 4.31ce MN-MMSPM-4.31ce-27OCT97. Digital Instruments, 1997.

Murray, M. N., H. G. Hansma, M. Bezanilla, T. Sano, D. F. Olgletree, W. Kolbe, C. L. Smith, C. R. Cantor, S. Spengler, P. K. Hansma and M. Salmeron. "Atomic Force Microscopy of Biochemically Tagged DNA," *Proceedings of the National Academy of Sciences*, 90:3811-3814 (May 1993).

Murrell, W. G. "Chemical Composition of Spores and Spore Structures," in *The Bacterial Spore*, Ed. G. W. Gould and A. Hurst. New York:Academic Press, 1969.

Nagao, E. and J. A. Dvorak. "Phase Imaging by Atomic Force Microscopy: Analysis of Living Homoiothermic Vertebrate Cells," *Biophysical Journal*, 76:3289-3297 (June 1999).

Nakamura, L. K. "Taxonomic Relationship of Black-Pigmented *Bacillus subtilis* Strains and a Proposal for *Bacillus atrophaeus* sp. nov.," *International Journal of Systematic Bacteriology*, 39:295-300 (1989).

"The 1986 Nobel Prize in Physics," Excerpt from unpublished article. n. pag. http//www.nobel.se/physics/laureates/1986/press.html. 16 June 2000.

Ohye, D. F. and W. G. Murrell. "Exosporium and Spore Coat Formation in *Bacillus cereus* T," *Journal of Bacteriology*, 115:1179-1190 (September 1973).

Okinaka, R. T., C. K, O. Hampton, A. R. Hoffmaster, K. K. Hill, P. Keim, T. M. Koehler, G. Lamke, S. Kumano, J. Mahillon, D. Manter, Y. Martinez, D. Ricke, R. Svensson and P. J. Jackson. "Sequence and Organization of pXO1, the Large *Bacillus anthracis* Plasmid Harboring the Anthrax Toxin Genes," *Journal of Bacteriology*, 181:6509-6515 (1999).

Osada, T., S. Takezawa, A. Itoh, H. Arakawa, M. Ichikawa and A. Ikai. "The Distribution of Sugar Chains on the Vomeronasal Epithelium Observed with an Atomic Force Microscope," *Chemical Senses*, 64:1-6 (1999).

Paige, M. F. and M. C. Goh. "Ultrastructure and assembly of segmental long-spacing collagen studied by atomic force microscopy," *Micron*, 32:355-361 (2001).

Paige, M. F., J. K. Rainey and M. C. Goh. "A Study of Fibrous Long-Spacing Collagen Ultrastructure and Assembly by Atomic Force Microscopy," *Micron*, 32:341-353 (2001).

Paige, M. F., J. K. Rainey and M. C. Goh. "Fibrous Long Spacing Collagen Ultrastructure Elucidated by Atomic Force Microscopy," *Biophysical Journal*, 74:3211-3216 (June 1998).

Patra, G., J. Vaissaire, M. Weber-Levy, C. Le Doujet and M. Mock. "Molecular Characterization of *Bacillus* Strains Involved in Outbreaks of Anthrax in France in 1997," *Journal of Clinical Microbiology*, 36:3412-3414 (1998).

Pignataro, B., C. Steinem, H.-J. Galla, H. Fuchs and A. Janshoff. "Specific Adhesion of Vesicles Monitored by Scanning Force Microscopy and Quartz Crystal Microbalance," *Biophysical Journal*, 78:487-498 (January 2000).

Popham, D. L., J. Helin, C. E. Costello and P. Setlow. "Analysis of the Peptidoglycan Structure of *Bacillus subtilis* Endospores," *Journal of Bacteriology*, 178:6451-6458 (November 1996a).

Popham, D. L., J. Helin, C. E. Costello and P. Setlow. "Muramic Lactam in Peptidoglycan of *Bacillus subtilis* Spores is Required for Spore Outgrowth but not for Spore Dehydration or Heat Resistance," *Proceedings of the National Academy of Sciences*, 93:15405-15410 (December 1996b).

Popham, D. L., J. Meador-Parton, C. E. Costello and P. Setlow. "Spore Peptidoglycan Structure in a *cwlD dacB* Double Mutant of *Bacillus subtilis*," *Journal of Bacteriology*, 181:6205-6209 (October 1999).

Popham, D. L. and P. Setlow. "The Cortical Peptidoglycan from Spores of *Bacillus megaterium* and *Bacillus subtilis* Is Not Highly Cross-Linked," *Journal of Bacteriology*, 175:2767-2769 (May 1993).

Priest, F. G., M. Goodfellow and C. Todd. "A Numerical Classification of the Genus *Bacillus*," *Journal of General Microbiology*, 134:1847-1882 (1988).

Priscu, J. C., E. E. Adams, W. B. Lyons, M. A. Voytek, D. W. Mogk, R. L. Brown, C. P. McKay, C. D. Takacs, K. A. Welch, C. F. Wolf, J. D. Kirshtein and R. Avci. "Geomicrobiology of Subglacial Ice Above Lake Vostok, Antarctica," *Science*, 286:2141-2144 (10 December 1999).

Radmacher, M., M. Fritz, H. G. Hansma and P. K. Hansma. "Direct Observation of Enzyme Activity with the Atomic Force Microscope," *Science*, 265:1577-1579 (9 September 1994).

Radmacher, M., R. W. Tillmann, M. Fritz and H. E. Gaub. "From Molecules to Cells: Imaging Soft Samples with the Atomic Force Microscope," *Science*, 257:1900-1905 (25 September 1992).

Ragkouski, K., M. A. Cowan and P. Setlow. "Analysis of Nucleoid Morphology during Germination and Outgrowth of Spores of *Bacillus* Species," *Journal of Bacteriology*, 182:5556-5562 (October 2000).

Ramisse, V., G. Patra, J. Vaissaire and M. Mock. "The Ba813 Chromosomal DNA Sequence Effectively Traces the Whole *Bacillus anthracis* Community," Journal of Applied Microbiology, 87:224-228 (1999).

Regaldo, A. "The Scientists Probing Terror Anthrax Trace Microbe's Family Tree," *The Wall Street Journal*, 8 November 2001:1.

Regis, E. *The Biology of Doom*. New York: Henry Holt and Company, 1999.

Revenko, I., F. Sommer, D. T. Minh, R. Garrone and J.-M. Franc. "Atomic Force Microscopy Study of Collagen Fibre Structure," *Biology of the Cell*, 80:67-69 (1994).

Rosovitz, M. J., M. I. Voskuil and G. H. Chambliss. "Bacillus," in *Topey & Wilson's Microbiology and Microbial Infections*. Ed. L. Collier, A. Balows and M. Sussman. New York: Oxford University Press, 1998.

Rotsch, C., K. Jacobsen and M. Radmacher. "Dimensional and Mechanical Dynamics of Active and Stable Edges in Motile Fibroblasts Investigated by Using Atomic Force Microscopy," *Proceedings of the National Academy of Sciences*, 96:921-926 (February 1999).

Sagvolden, G. "Protein Adhesion Force Dynamics and Single Adhesion Events," *Biophysical Journal*, 77:526-532 (1999).

Schmitz, I., M. Schreiner, G. Friedbacher and M. Grasserbauer. "Phase imaging as an extension to tapping mode AFM for th identification of material properties on humidity-sensitive surfaces," *Applied Surface Science*, 115:190-198 (1997).

Schneider, J., Y. F. Dufrêne, W. R. Barger, Jr. and G. U. Lee. "Atomic Force Microscope Image Contrast Mechanisms on Supported Lipid Bilayers," *Biophysical Journal*, 79:1107-1118 (2000).

Schnepf, E., N. Crickmore, J. Van Rie, D. Lereclus, J. Baum, J. Feitelson, D. R. Zeigler and D. H. Dean. "*Bacillus thuringiensis* and Its Pesticidal Crystal Proteins," *Microbiology and Molecular Biology Reviews*, 62:775-806 (September 1998).

Setlow, P. and E. A. Johnson. "Spores and Their Significance," in *Food Microbiology: Fundamentals and Fronteirs*. Ed. M. P. Doyle, L. R. Beuchat and T. J. Montville. Washington, D.C.: ASM Press, 2001.

Sharp, R. J., M. D. Scawen and T. Atkinson. "Fermentation and Downstream Processing of *Bacillus*," in *Bacillus*. Ed. C. R. Harwood. New York: Plenum Press, 1989.

Shibata-Seki, T., W. Watanabe and J. Masai. "Imaging of Cells with Atomic Force Microscopy Operated at a "Tapping" Mode," *Journal of Vacuum Science and Technology B*, 12:1530-1534 (May/June 1994).

Shlyakhtenko, L. S., A. A. Gall, J. J. Weimer, D. D. Hawn and Y. L. Lyubchenko. "Atomic Force Microscopy Imaging of DNA Covalently Immobilized on a Functionalized Mica Substrate," *Biophysical Journal*, 77:568-576 (1999).

Sit, P. S. and R. E. Marchant. "Surface-dependent Differences in Fibrin Assembly Visualized by Atomic Force Microscopy," *Surface Science*, 491:421-432 (2001).

Smirnova, T. A., L. I. Kulinich, M. Y. Galperin and R. R. Azizbekyan. "Subspecies-Specific Haemagglutination Patterns of Fimbriated *Bacillus thuringiensis* Spores," *FEMS Microbiology Letters*, 90:1-4 (1991).

Smith, K. L., V. DeVos, H. Bryden, L. B. Price, M. E. Hugh-Jones and P. Keim. "*Bacillus anthracis* Diversity in Kruger National Park," *Journal of Clinical Microbiology*, 38:3780-3784 (October 2000).

Smith, N. R., R. E. Gordon and F. E. Clark. *Agriculture Monograph No. 16: Aerobic Sporeforming Bacteria*. Washington, D.C.: United States Department of Agriculture, 1952.

Sneath, P. H. A. "Bacterial Classification II: Numerical Taxonomy," in *Bergey's Manual of Systematic Bacteriology*. Ed. N. R. Krieg and J. G. Holt. Baltimore: Williams & Wilkins, 1984.

----, "Endospore-forming Gram-Positive Rods and Cocci," in *Bergey's Manual of Systematic Bacteriology*. Ed. P. H. A. Sneath, N. S. Mair, M. E. Sharpe and J. G. Holt. Baltimore: Williams & Wilkins, (1986).

Sokolov, I. Y., M. Firtel and G. S. Henderson. "*In situ* high-resolution atomic force microscope imaging of biological surfaces," *Journal of Vacuum Science and Technology A*, 14:674-678 (May/June 1996).

Staley, J. T. and N. R. Krieg. "Bacterial Classification I: Classification of Prokaryotic Organisms: An Overview," in *Bergey's Manual of Systematic Bacteriology*. Ed. N. R. Krieg and J. G. Holt. Baltimore: Williams & Wilkins, 1984.

Stedman, R. L., E. Kravitz, M. Anmuth and J. Harding. "Autoinhibition of Bacterial Endospore Germination," *Science*, 124:403-405 (31 August 1956).

Stein, C. D. "Studies and Observations on the Laboratory Diagnosis of Anthrax," *Vet. Med. [Chicago]*, 38:130-139 (1943)

Sussman, A. S. and H. O. Halvorson. *Spores: Their dormancy and germination*. New York: Harper & Row, 1966.

Taatjes, D. J., A. S. Quinn and E. G. Bovill. "Imaging of Collagen Type III in Fluid by Atomic Force Microscopy," *Microscopy Research and Technioque*, 44:347-352 (1999).

Tamayo, J. and M. Miles. "Human Chromosome Structure Studied by Scanning Force Microscopy After an Enzymatic Digestion of the Covering Cell Material," *Ultramicroscopy*, 82:245-251 (2000).

Ticknor, L. O., A.-B. Kolsto, K. K. Hill, P. Keim, M. T. Laker, M. Tonks and P. J. Jackson. "Fluorescent Amplified Fragment Length Polymorphism Analysis of Norwegian *Bacillus cereus* and *Bacillus thuringiensis* Soil Isolates," *Applied and Environmental Microbiology*, 67:4863-4873 (October 2001).

Turnbull, P. C. B. "Definitive identification of *Bacillus anthracis* - a review," *Journal of Applied Microbiology*, 87:237-240 (1999).

Turnbull, P. C. B., R. A. Hutson, M. J. Ward, M. N. Jones, C. P. Quinn, N. J. Finnie, C. J. Duggleby, J. M. Kramer and J. Melling. "*Bacillus anthracis* But Not Always Anthrax," *Journal of Applied Bacteriology*, 72:21-28 (1992).

Umeda, A., M. Saito and K. Amako. "Surface Characteristics of Gram-Negative and Gram-Positive Bacteria in an Atomic Force Microscope Image," *Microbiol. Immunol.*, 42:159-164 (1998).

van der Mei, H. C., H. J. Busscher, R. Bos, J. de Vries, C. J. Boonaert and Y. F. Dufrêne. "Direct Probing by Atomic Force Microscopy of the Cell Surface Softness of a Fibrillated and Nonfibrillated Oral Streptococcal Strain," *Biophysical Journal*, 78:2668-2674 (May 2000).

van Noort, S. J. T., K. O. van der Werf, B. G. de Grooth and J. Greve. "High Speed Atomic Force Microscopy of Biomolecules by Image Tracking," *Biophysical Journal*, 77:2295-2303 (1999).

Warth, A. D., D. F. Ohye and W. G. Murrell. "The Composition and Structure of Bacterial Spores," *The Journal of Cell Biology*, 16:579-592 (1963).

Weimer, B. C., M. K. Walsh, C. Beer, R. Koka and X. Wang. "Solid-Phase Capture of Proteins, Spores, and Bacteria," *Applied and Environmental Microbiology*, 67:1300-1307 (March 2001).

Willemsen, O. H., M. M. E. Snel, A. Cambi, J. Greve, B. G. de Grooth and C. G. Figdor. "Biomolocular Interactions Measured by Atomic Force Microscopy," *Biophysical Journal*, 79:3267-3281 (2000).

Willett, H. P. "Bacillus," in *Zinsser Microbiology*. Ed. W. K. Joklik, H. P. Willett, D. B. Amos and C. M. Wilfert. Norwalk, CT: Appleton & Lange, 1992a.

----. "Physiology of Bacterial Growth," in *Zinsser Microbiology*. Ed. W. K. Joklik, H. P. Willett, D. B. Amos and C. M. Wilfert. Norwalk, CT: Appleton & Lange, 1992b.

Xu, W., P. J. Mulhern, B. L. Blackford, M. H. Jericho, M. Firtel and T. J. Beveridge. "Modeling and Measuring the Elastic Properties of an Archaeal Surface, the Sheath of *Methanospirillum hungatei*, and the Implication for Methane Production," *Journal of Bacteriology*, 178:3106-3112 (June 1996).

Yamada, S., E. Ohashi, N. Agata and K. Venkateswaran. "Cloning and Nucleotide Sequence Analysis of *gyrB* of *Bacillus cereus*, *B. thuringiensis*, *B. mycoides*, and *B. anthracis* and Their Application to the Detection of *B. cereus* in Rice," *Applied and Environmental Microbiology*, 65:1483-1490 (April 1999).

Yao, X., M. Jericho, D. Pink and T. Beveridge. "Thickness and Elasticity of Gram-Negaive Murein Sacculi Measured by Atomic Force Microscopy," *Journal of Bacteriology*, 181:6865-6875 (November 1999).

Zeigler, D. R. *Bacillus thuringiensis & Bacillus cereus Catalog of Strains*. Columbus, Ohio: Department of Biochemistry, The Ohio State University, 1999.

Vita

Captain Ruth Zolock graduated from Carnegie Mellon University with a Bachelor of Science Degree in Materials Science and Engineering with an additional major in Engineering and Public Policy in May 1993. In January 1994, she enlisted in the United States Marine Corps. She completed Recruit Training at Parris Island, South Carolina followed by Avionics Communication Technician training at Millington Naval Air Station in Tennessee and Cherry Point Marine Corps Air Station in North Carolina. Lance Corporal Zolock was then stationed with MALS-29, Marine Corps Air Station New River. There, she was accepted for the Enlisted Commissioning Program.

Following completion of Officer Candidate School in Quantico, Virginia, she was commissioned a Second Lieutenant in the United States Marine Corps on 18 August 1995. After initial training at The Basic School in Quantico, Virginia and a further school at Camp Johnson, North Carolina, she was assigned to Truck Company, 3D Marine Division, Okinawa, Japan as a Motor Transport Officer. Over the next year she served as a Platoon Commander and Company Executive Officer.

In June 1997, then Second Lieutenant Zolock was reassigned to the Recruit Training Regiment, Parris Island, South Carolina. Over the next three years she served as a Series Commander, Recruit Processing Company Executive Officer, Support Battalion Operations Officer, and the Commanding Officer of Company N.

In August 2000, Captain Zolock entered the Department of Systems and Engineering Management, Air Force Institute of Technology. Upon graduation she will be assigned to Marine Corps Base Quantico, Virginia as an Environmental Engineer.

REPORT DOCUMENTATION PAGE

Form Approved
OMB No. 074-0188

1. REPORT DATE *(DD-MM-YYYY)*	2. REPORT TYPE	3. DATES COVERED *(From – To)*
26-03-2002	**Master's Thesis**	May 2001 – Mar 2002

4. TITLE AND SUBTITLE

CHARACTERIZATION OF THE SURFACE MORPHOLOGY OF *BACILLUS* SPORES BY ATOMIC FORCE MICROSCOPY

5a. CONTRACT NUMBER

5b. GRANT NUMBER

5c. PROGRAM ELEMENT NUMBER

6. AUTHOR(S)

Zolock, Ruth A., Captain, USMC

5d. PROJECT NUMBER

5e. TASK NUMBER

5f. WORK UNIT NUMBER

7. PERFORMING ORGANIZATION NAMES(S) AND ADDRESS(S)
Air Force Institute of Technology
Graduate School of Engineering and Management (AFIT/EN)
2950 P Street, Building 640
WPAFB OH 45433-7765

8. PERFORMING ORGANIZATION REPORT NUMBER

AFIT/GEE/ENV/02M-17

9. SPONSORING/MONITORING AGENCY NAME(S) AND ADDRESS(ES)
Biomechanisms and Modeling Branch
Human Effectiveness Directorate Det 5
Air Force Research Laboratories
Attn: Dr. Eric Holwitt DSN: 240-3583
Brooks Air Force Base, Texas, 78235 e-mail: Eric.Holwitt@hedb.brooks.af.mil

10. SPONSOR/MONITOR'S ACRONYM(S)

11. SPONSOR/MONITOR'S REPORT NUMBER(S)

12. DISTRIBUTION/AVAILABILITY STATEMENT

APPROVED FOR PUBLIC RELEASE; DISTRIBUTION UNLIMITED.

13. SUPPLEMENTARY NOTES

14. ABSTRACT

The surface morphology of *Bacillus* spores was resolved by atomic force microscopy in order to determine if characteristic surface features could be used to distinguish between closely related species. Four strains were studied: *Bacillus anthracis* Sterne strain, *Bacillus thuringiensis* var. *kurstaki*, *Bacillus cereus* strain 569, and *Bacillus globigii* var. *niger*. The spores were separated from a nutrient agar culture by filtering and centrifugation, suspended in deionized water, and immobilized on a graphite substrate by spin-coating. Atomic force microscopy was done in intermittent contact mode, in air, under reduced humidity. Height images showed that the spores had an irregular topography of subtle grooves, bumps, and steps across their upper surface. Phase images showed a superficial grain structure. Although some similarities were observed among spores of the same species, there was also significant variability within each species. The four species were not distinguished by observed surface morphology. Surface texture analysis (roughness, power spectral density, and bearing) did not establish definitive differences between species. Overall, atomic force microscopy revealed a spore surface morphology rich with information. It appears, however, that further analysis and a larger sample size could provide sufficient information to allow identification and differentiation between *B. anthracis* and its close relatives.

15. SUBJECT TERMS

Bacillus anthracis, *Bacillus cereus*, *Bacillus thuringiensis*, *Bacillus globigii*, Spores, Atomic Force Microscopy

16. SECURITY CLASSIFICATION OF:			17. LIMITATION OF ABSTRACT	18. NUMBER OF PAGES	19a. NAME OF RESPONSIBLE PERSON
a. REPORT	b. ABSTRACT	c. THIS PAGE			Dr. Charles A. Bleckmann (ENV)
U	U	U	UU	184	**19b. TELEPHONE NUMBER** *(Include area code)* (937) 255-6565, ext 4721; e-mail: Charles.Bleckmann@afit.edu

Standard Form 298 (Rev. 8-98)
Prescribed by ANSI Std. Z39-18